

SOIL MOISTURE VARIABILITY AND HYDROLOGICAL IMPACT ASSESSMENT OF LAND COVER CHANGE

Thesis

Submitted in partial fulfillment of the requirements for the degree of

DOCTOR OF PHILOSOPHY

by

DIWAN MOHAIDEEN M M



**DEPARTMENT OF APPLIED MECHANICS AND HYDRAULICS
NATIONAL INSTITUTE OF TECHNOLOGY KARNATAKA
SURATHKAL, MANGALURU – 575 025
JUNE 2020**

DECLARATION
By the Ph.D. Research Scholar

I hereby *declare* that the Research Thesis entitled **Soil Moisture Variability and Hydrological Impact Assessment of Land Cover Change** which is being submitted to the **National Institute of Technology Karnataka, Surathkal** in partial fulfilment of the requirements for the award of the Degree of **Doctor of Philosophy** in **Applied Mechanics and Hydraulics Department** is a *bonafide report of the research work* carried out by me. The material contained in this Research Synopsis has not been submitted to any University or Institution for the award of any degree.

145058 AM14F01, DIWAN MOHAIDEEN M M
(Register Number, Name & Signature of the Research Scholar)
Department of Applied Mechanics and Hydraulics

Place: NITK-Surathkal
Date:

CERTIFICATE

This is to *certify* that the Research Thesis entitled **Soil Moisture Variability and Hydrological Impact Assessment of Land Cover Change** submitted by DIWAN MOHAIDEEN M M (Register Number: 145058 AM14F01) as the record of the research work carried out by him, *is accepted as the Research Thesis submission* in partial fulfilment of the requirements for the award of degree of **Doctor of Philosophy.**

Dr. K. Varija
Associate Professor
Research Guide
(Name and Signature with Date and Seal)

Chairman - DRPC
(Signature with Date and Seal)

ACKNOWLEDGEMENT

I am deeply indebted to my doctoral advisor **Dr. K. Varija**, Applied Mechanics and Hydraulics Department, NITK Surathkal, for giving me an opportunity to work with her. I express my sincere gratitude to my supervisor for her constant support throughout my study, including personal affairs, during my tough time apart from the academics.

I am very much grateful to former Head of the Department (HoD) **Prof. G.S. Dwarakish**, **Prof. A. Mahesha** and current HoD **Prof. Amba shetty** for providing necessary support and facilities for my research work. I express my sincere appreciation to the Research Progress Assessment Committee (RPAC) members, **Prof. H. D. Shashikala**, Department of Physics and **Prof. A. Mahesha**, Applied Mechanics and Hydraulics Department for their valuable insights and encouragements during the entire period of my research work. I thank all the faculty members of the Applied Mechanics and Hydraulics department for their support. I would like to acknowledge the financial support provided by **Ministry of Human Resources Development**, Government of India.

I express my sincere gratitude to my undergraduate project supervisor **Dr. T. Nasar** for motivating me and showing direction towards my higher studies after my under graduation studies. He never failed to give his love and support whenever I required till date. I am very much grateful to **Dr. C. Rajesekaran**, Department of Civil Engineering, for his love and constant support during my stay at NITK. I express my sincere gratitude to my well-wisher Anna, **Dr. K. S. Kasivisvanathan**, for his lovely support and encouragement during my research work.

I am fortunate to have loveable friends at NITK across the departments. I express my sincere gratitude for their loveable and moral support during my hard time at NITK, especially to **Mr. Sinan**, **Mr. Pragadeesh**, **Mr. Mohan**, **Dr. Saravanaprakash**, **Mr.**

Abhishek, Mr. Kumaran, Mr. Rajesh, Mr. Rajapandi, Mr. Venkateshwarlu, Mr. Karthik, and Mr. Bheemappa.

My sincere thanks to supporting staff of Applied mechanics and Hydraulics Department Mr. Jagadish, Mr. Balakrishna, Mr. Anil, Mrs. Prathima, Mr. Harish for all their support during my research work. The timely support rendered by administrative staff of NITK is gratefully acknowledged.

I am thankful to all research scholars and graduate students of Applied Mechanics and Hydraulics Department, who created a memorable experience during the period of my research. They helped me with their technical and moral support for the completion of the thesis. My special thanks to Dr. Amit Patil, Dr. Santhosh, Mr. sylus, Mr. Amruth, Dr. Gana sri, Dr. Jagalingam, Dr. Sujay, Dr. Sreedhar, Dr. Geetha, Dr. Harish, Dr. Amogh, Dr. Rishikesh, Mr. Praveen, Mr. Surajith, Mrs. Chaitanya, Mrs. Usha, Mrs. Nithya, Mrs. Suman, Mr. Arun, Mrs. Anjali, Mr. Pandu, Mr. Vineeth, Mr. Niranjana, Mr. Parthasarathy, Mr. Tom, Mr. Athul, Ms. Dinu, Mr. Dinesh, Ms. Pujitha, Ms. Sharanya and Ms. Chinmayee.

Most importantly, I render my deep sense of regards to my lovely parents and my elder sister for their unconditional love and constant support at various stages of my life. At this moment of contentment, I would like to thank all my teachers who taught me at various levels from my schooling.

Above all, Alhamdulillah (all praise be to Allah). O Almighty, I ask you for beneficial knowledge and seek refuge with you from knowledge that is of no benefit.

- DIWAN MOHAIDEEN M M

ABSTRACT

Water availability in a region depends on how precipitation over the region is transformed into various forms after reaching ground such as evaporation losses, runoff, infiltration, soil moisture, and ground water storage etc. Land Use / Land Cover (LU/LC) changes adversely affect the aforementioned components. Particularly, the effects of LU/LC changes on catchment hydrological responses, especially vegetative cover (forest, scrubs and cropland), affect the evapotranspiration. Further, rapid urbanization due to LU/LC changes leads to extent of impervious surface and thereby, impacts the infiltration rates as well as recharge. The LU/LC change impact on the hydrologic system is region specific, and each region is characterized by its own hydrology, terrain, climate and also anthropogenic factors. Therefore, a detailed assessment of LU/LC change impacts on hydrology is required, specifically at the region with seasonally limited water availability. It is emphasized by many researchers that the physically-based, distributed hydrological models along with remote sensing capabilities are more suitable for assessing the LU/LC change impacts on the hydrologic system. Further, Soil moisture, being a critical state variable, its knowledge is of paramount importance in several hydrological applications (e.g., runoff modeling and flood forecasting, agricultural monitoring and drought monitoring). The magnitude of soil moisture variability often under estimated and the spatial pattern of soil moisture is not consistent, and it is largely varying across the site and climate with the influence of heterogeneity in LU/LC, topography, soil properties, precipitation and evapotranspiration. Hence, the characterization of soil moisture variability is essential. The work reported in this thesis aims at understanding the soil moisture variability and land cover change impacts in an agricultural dominant semi-arid basin.

The Variable Infiltration Capacity (VIC) model, a physically based, semi distributed hydrological model was used to simulate the hydrologic responses of the basin for different LU/LC scenarios (the year 2000 and 2010) with multiple soil layers

parameterization (three soil layers: 0 – 10 cm, 10 – 45 cm and 45 – 100 cm). The total drainage area of the basin was discretized into number of model grids (5.5 km resolution: totally 1694 grids), and the input parameterization of the model was made at each grid level. The major input parameters to the model are meteorological forcing (Precipitation, T_{max} , T_{min}), soil characteristics, land surface vegetation classes (vegetation parameter & library) and topography. This study demonstrated a methodological frame work for improved vegetation parameterization to the model simulation. Moderate Resolution Imaging Spectroradiometer (MODIS)-derived 8-day Leaf Area Index (LAI) time-series data was used to sub-group agricultural dominant areas into major crop groups and corresponding monthly vegetation phenology in terms of LAI, albedo, height, root distribution were arrived. This exercise enabled improved definition of vegetation parameterization for the study area, incorporating the region specific conditions. Firstly, the model was calibrated and validated using the observed stream flow data collected at two different locations for the period 1994 – 2001. The model parameter values were adopted for each model grid (about 5.5 km) based on the saturated hydraulic conductivity at that grid by trial and error method. To assess the hydrological impacts of LU/LC change on the flow regime of the basin, the model was run using the two LU/LC conditions separately with the same observed meteorological forcing and soil data.

The changes attributed to LU/LC at basin level indicate that the surface runoff and baseflow decreased by 18.86 and 5.83% respectively. The evapotranspiration increased by 7.8%, mainly because of the agricultural crops. The variability in hydrological components and the spatial variation of each component attributed to LU/LC was further assessed at the basin grid level. The majority of the basin grids showed an increase in evapotranspiration (80 % of basin grids) and subsequent decrease in runoff and baseflow (79 and 85% of basin grids, respectively) with respect to LU/LC change. Further, the spatio-temporal variation of soil moisture was assessed using the model simulated soil moisture along with three different satellite derived surface soil moisture products (SM-CCI, SM-TRMM and SM-AMSRE). It was found from the analysis that the impacts of LU/LC changes on soil moisture were more evident in the deeper layers (45 cm and 100 cm). The soil moisture decreased by

an average of 14.43 and 18.21% (percentage change), particularly in dry periods at second and third layers, respectively.

Further, the modeled soil moisture along with three different satellite surface soil moisture products were investigated for its spatio-temporal variability in the basin. The soil moisture in the top layer (up to 10 cm) showed high temporal variations. However, the mean soil moisture was found almost constant during the summer and winter seasons. The basin showed high variability in soil moisture during the intermediate wetness condition. Further, the spatial variability of the soil moisture during the wetting period (June-August) was high compared to drying period (December – February). Based on the analysis performed in this study, 29 (out of total model grids - 1694) representative grid locations were identified in the basin. These locations could be effectively considered for installing observational network mainly for monitoring soil moisture in near real-time.

Keywords: Hydrologic modelling,, Soil moisture, VIC model, Land Use Land Cover, Leaf Area index, Temporal Stability Analysis, Upper Bhima

TABLE OF CONTENT		Page No.
ACKNOWLEDGEMENT		i
ABSTRACT		iii
LIST OF TABLES		viii
LIST OF FIGURES		ix
ABBREVIATION		xiv
NOTATION		xvi
1	INTRODUCTION	1
	1.1 GENERAL	1
	1.2 CLIMATE AND LAND USE/LAND COVER CHANGE	2
	1.3 SOIL MOISTURE: TERMS AND MEASUREMENTS	2
	1.4 ORGANIZATION OF THE THESIS	5
2	LITERATURE REVIEW	7
	2.1 GENERAL	7
	2.2 RAINFALL-RUNOFF MODELLING: A BREIF OVERVIEW	8
	2.3 IMPACTS OF LU/LC CHANGE OF HYDROLOGIC SYSTEM	9
	2.4 SOIL MOISTURE ESTIMATION	14
	2.5 SOIL MOISTURE VARIABILITY	17
	2.6 THE VIC MODEL	21
	2.7 SUMMARY AND OBJECTIVES OF THE STUDY	23
3	STUDY AREA AND DATA SOURCES	27
	3.1 STUDY AREA DISCRPTION	27
	3.1.1 Physiography	27
	3.1.2 Rainfall and Temperature	27
	3.1.3 Soils	29

	3.1.4 Land Use/Land Cover	30
	3.1.5 Flow	31
	3.2 DATA SOURCES	32
	3.2.1 LU/LC classification of satellite images	33
	3.2.2 MODIS-derived data	34
	3.2.3 Satellite-derived soil moisture data	36
4	MODEL SET UP AND INPUT PARAMETERIZATION	39
	4.1 VIC MODEL	39
	4.2 ROUTING MODEL	43
	4.3 VIC MODEL INPUT PARAMETERIZATION	45
	4.3.1 Basin delineation	45
	4.3.2 Preparation of model grids	48
	4.3.3 Global parameter file	48
	4.3.4 Soil parameter file	48
	4.3.5 Meteorological forcing file	51
	4.3.6 Improved vegetation parameterization	52
	4.3.7 Elevation band file	58
	4.4 ROUTING MODEL INPUT PARAMETERIZATION	59
	4.4.1 Flow direction file	60
	4.4.2 Flow fraction file	60
	4.4.3 Station location and UH file	61
5	MODEL PERFORMANCE AND HYDROLOGICAL IMPACTS OF LU/LC CHANGE	63
	5.1 MODEL CALIBRATION AND VALIDATION	63

	5.2	MODEL PERFORMANCE	64
	5.2.1	Inter comparison of ET estimation	66
	5.2.2	Validation of soil moisture	68
	5.3	LU/LC CHANGE AND WATER BALANCE	70
	5.3.1	Impacts of LU/LC change on soil moisture	76
6		SPATIO-TEMPORAL ANALYSIS OF SOIL MOISTURE	79
	6.1	GENERAL	79
	6.2	TEMPORAL VARIATION OF SOIL MOISTURE	79
	6.3	SPATIAL MEAN AND VARIANCE	87
	6.4	TEMPORAL STABILITY ANALYSIS	89
	6.5	REPRESENTATIVE GRID LOCATIONS	93
7		SUMMARY AND CONCLUSIONS	97
	7.1	GENERAL	97
	7.2	SUMMARY	98
	7.3	CONCLUSIONS	99
	7.4	LIMITATIONS	101
	7.5	SCOPES FOR THE FUTURE WORK	101
		REFERENCES	103
		LIST OF PUBLICATIONS	
		CURRICULUM VITAE	

LIST OF TABLES

Table No.	Tittle	Page
3.1	Datasets used in the study	32
3.2	Accuracy assessment for LU/LC classification	34

4.1	Soil parameter	50
4.2	Soil hydraulic properties based on soil texture	51
4.3	Rooting depth information adopted for vegetation parameter with LU/LC 2000	56
4.4	Rooting depth information adopted for vegetation parameter with LU/LC 2010	56
4.1	Calibration parameter, range and calibrated value	64
5.2	Average monthly statistics for water balance components during period (1996 – 2000)	72
5.3	Annual sums of water balance components during the period (1996 – 2000)	72
5.4	Change in water balance component with respect to change in LU/LC	74
5.5	Average monthly statistics for soil moisture at multiple layers during the period (1996-2005)	77
5.6	Grids showing maximum change in soil moisture with respect to LU/LC change	78
6.1	R^2 and RMSE between the benchmark time series and time series at each grid	94
6.2	Representative grids and its location	94

LIST OF FIGURES

Figure No.	Title	Page
1.1	Characteristic soil moisture level and units	3
1.2	Support scale of soil moisture observation	4
2.1	Schematic representation of the VIC and Routing model	21

3.1	Location of the study area along with DEM and drainage network	28
3.2	Spatial distribution of average annual rainfall over the basin	29
3.3	Distribution of soil types and texture characteristics in the Upper Bhima: a) Soil type b) Topsoil texture c) Subsoil texture	30
3.4	LULC map along with its percentage area: a) LULC for the year 2000 b) LULC for the year 2010 c) LULC percentage area in the Upper Bhima	31
3.5	Typical LAI: [a] 19 July 2000 [b] 20 July 2010	35
3.6	Typical Albedo: [a] 19 July 2000 [b] 20 July 2010	35
3.7	Spatial distribution of the MODIS-derived ET over the basin (on 2 June 2001)	36
4.1	Terrain pre-processing for basin delineation	47
4.2	Model grids generation	47
4.3	Typical soil parameter file to the model (Initial ten grids are shown)	49
4.4	Schematic representation of the workflow for vegetation parameterization	52
4.5	Temporal LAI profile of vegetation classes in the Upper Bhima for the year 2000-01	53
4.6	Temporal LAI profile of vegetation classes in the Upper Bhima for the year 2010-11	54
4.7	Spatial location of LAI groups for the year 2000-01	54
4.8	Spatial location of LAI groups for the year 2000-01	55

4.9	Typical vegetation parameter file for the LULC 2000 (Initial five grids are shown)	55
4.10	Typical vegetation library file	57
4.11	Classification of the basin elevation	58
4.12	Typical Elevation band file (Initial 20 grids are shown)	59
4.13	Typical routing control file	59
4.14	Flow directions of the basin grids	60
4.15	Basin grid flow fraction	61
4.16	Typical station location file [a] and [b] UH file	61
5.1	Observed and simulated discharge during calibration: a) Takli b) Wadakbal	65
5.2	Observed and simulated discharge during validation: a) Takli b) Wadakbal	65
5.3	Comparison of 8-days ET estimation from VIC, MODIS and FAO-56PM during the period June 2001 – May 2005.	67
5.4	Comparison of basin average ET during the period 2001-05: a) 8-day b) month-wise	68
5.5	Validation of model simulated soil moisture with field observed soil moisture at [a] 10 cm and [b] 45 cm soil depth	69
5.6	Correlation coefficient of VIC-soil moisture with SM-DM15	70
5.7	Spatial variation of estimated annual water balance components for the water year 2000 – 01 using both LULC period 2000 (a) and 2010 (b)	73
5.8	Spatial variation of observed annual rainfall for the water year 2000 -01 along with basin grids and grid showing a maximum change in water balance	75

6.1	Schematic representation of the workflow	80
6.2	Time series of spatial mean soil moisture	81
6.3	Typical spatial correlation coefficient matrix between the soil moisture during different time step for the modelled and satellite soil moisture data in the year 1996-97 [a] VIC-Layer1 [b] VIC-Layer 2 [c] VIC-Layer 3 (LULC-2000, lower triangle; LULC-2010, upper triangle) [d] satellite soil moisture	82
6.4	Spatial correlation coefficient matrix between the soil moisture during different time step for the modelled and satellite soil moisture data in the year 1998-99 [a] VIC-Layer1 [b] VIC-Layer 2 [c] VIC-Layer 3 (LU/LC-2000, lower triangle; LU/LC-2010, upper triangle) [d] satellite soil moisture	83
6.5	Spatial correlation coefficient matrix between the soil moisture during different time step for the modelled and satellite soil moisture data in the year 2000-01 [a] VIC-Layer1 [b] VIC-Layer 2 [c] VIC-Layer 3 (LU/LC-2000, lower triangle; LU/LC-2010, upper triangle) [d] satellite soil moisture	84
6.6	Spatial correlation coefficient matrix between the soil moisture during different time step for the modelled and satellite soil moisture data in the year 2002-03 [a] VIC-Layer1 [b] VIC-Layer 2 [c] VIC-Layer 3 (LU/LC-2000, lower triangle; LU/LC-2010, upper triangle) [d] satellite soil moisture	85

6.7	Spatial correlation coefficient matrix between the soil moisture during different time step for the modelled and satellite soil moisture data in the year 2004-05 [a] VIC-Layer1 [b] VIC-Layer 2 [c] VIC-Layer 3 (LU/LC-2000, lower triangle; LU/LC-2010, upper triangle) [d] satellite soil moisture	86
6.8	Relationship between $\overline{\theta}_t$ and σ_t^2 of modelled and satellite soil moisture. Left side column shows VIC-lulc2000, middle VIC-lulc2010 and right satellite soil moisture. The red and black lines indicate the means of $\overline{\theta}_t$ and σ_t^2 , respectively	88
6.9	The Spatial maps of MRDs. Left side column shows VIC-lulc2000, middle VIC-lulc2010 and right satellite soil moisture	90
6.10	The Spatial maps of standard deviation of MRDs. Left side column shows VIC-lulc2000, middle VIC-lulc2010 and right satellite soil moisture	91
6.11	Rank ordered mean relative difference for [a] VIC-lulc2000 [b] VIC-lulc2010 [c] SM-CCI [d] SM-TRMM [e] SM-AMSRE (Error bar indicates ± 1 std. deviation)	92
6.12	Spatial maps of “Representative” locations along with the MRDs of third layer	93

ABBREVIATIONS

ALOS	- Advanced Land Observing Satellite
AMSR-E	- Advanced Microwaves Scanning Radiometer – Earth Observing System
AOI	- Area of Interest
ASCAT	- Advanced Scatterometer
ASCII	- American Standard Code for Information Interchange
CCI	- Climate Change Initiative
CLUE-S	- Conversion of Land Use and its Effects at Small regional extent
CWC	- Central Water Commission
DEM	- Digital Elevation Model
EMI	- Electro Magnetic Induction
ENVISAT	- Environmental Satellite
ERS	- European Remote Sensing
ERT	- Electrical Resistivity Tomography
ESA	- European Space Agency
ESTAR	- Electronically Scanned Thinned Array Radiometer
ETM ⁺	- Enhanced Thematic Mapper plus
GCM	- General Circulation model
GIS	- Geographic Information System
GPR	- Ground Penetrating Radar
GRACE	- Gravity Recovery and Climate Experiments
HWSD	- Harmonized World Soil Database
IMD	- Indian Meteorological Department
INDIA-WRIS	- India Water Resources Information System
IPCC	- Intergovernmental Panel on Climate Change
JERS	- Japan Earth Resources Satellite
LAI	- Leaf Area Index
LU/LC	- Land Use Land Cover
MetOp	- Meteorological Operational satellite
MODIS	- Moderate Resolution Imaging Spectroradiometer

NRSC	- National Remote Sensing Centre
NSE	- Nash-Sutcliffe Efficiency
PALS	- Passive and Active L-band System
PBMR	- Pushbroom Microwave Radiometer
RADARSAT	- Radar satellite
RFI	- Radio Frequency Interference
RMSE	- Root Mean Square Error
RTM	- Radiative Transfer Model
SAR	- Synthetic Aperture Radars
SCS-CN	- Soil Conservation Service Curve Number
SMAP	- Soil Moisture Active Passive mission
SMMR	- Scanning Multichannel Microwave Radiometry
SMOS	- Soil Moisture Ocean Salinity
SRES	- Special Report on Emissions Scenarios
SRTM	- Shuttle Radar Topographic Mission
SWAT	- Soil Water Assessment Tool
TDR	- Time Domain Reflectometry
TRMM	- Tropical Rainfall Measuring Mission
USDA	- United States Department of Agriculture
VIC	- Variable Infiltration Capacity
WaSim	- Water Flow and Balance Simulation Model

NOTATION

A_S	-	Fraction of the bare soil that is saturated
a_c	-	Minimum canopy resistance
a_0	-	Architectural resistance
a_w	-	Aerodynamic resistance
b_i	-	Infiltration curve shape parameter
C_n	-	Fraction coverage for n^{th} vegetation
d	-	Soil depth
D_{smax}	-	Maximum subsurface flow
D_m	-	Fraction of D_{smax}
$D(\theta)$	-	Soil water diffusivity
E_c	-	Evapotranspiration from canopy
ET_o	-	Reference evapotranspiration
G	-	Soil heat flux density
i_0	-	Infiltration capacity
i_m	-	Maximum infiltration capacity of soil
K_{sat}	-	Saturated hydraulic conductivity
$K(\theta)$	-	Hydraulic conductivity
MRD	-	Mean Relative difference
N_g	-	Number of grids.
P	-	Precipitation
P^{eff}	-	Effective precipitation
P_t	-	Throughfall
Q_b	-	Baseflow
Q_s	-	Surface runoff
R	-	Runoff
Rh	-	Relative humidity
R_n	-	Net solar radiation at the reference grass surface
SRD	-	standard deviation of relative difference
V	-	Volume of soil

v	-	Volume of water
W_i	-	Intercepted water
W_s	-	Fraction of maximum soil moisture
Δ	-	Saturation slope of vapor pressure curve
θ	-	Volumetric soil moisture
θ_{fc}	-	Field capacity
θ_s	-	Saturation ratio
θ_{sat}	-	Saturated soil moisture
$\partial S / \partial t$	-	Water storage change
θ_t	-	Spatial mean
θ_{wilt}	-	Wilting point
γ	-	Psychrometric constant
σ_t^2	-	Spatial variance

1.1 GENERAL

Water resources management requires the better understanding and quantification of the various hydrological components of the catchment. Water on the earth, continuously moving through water cycle by evaporation, transpiration (evapotranspiration), precipitation, infiltration and runoff reach the ocean. The total quantity of water remains constant in the global water cycle, however, their distribution is continuously changing over the continents, in regional and within the catchment scale (Chow et. al, 1988). The predominant source of water on earth is precipitation, and each of its form confined to its specific conditions. The precipitation (rainfall) transforms into runoff and reaches the outlet of the catchment through very complex processes. It needs to meet the demands from interception, (loss by vegetative surface, throughfall and stem flow) depression storage and infiltration. The infiltrated water makes the availability of soil water content in the vadose zone, and further it reaches ground water. The quantity of runoff generated from a storm depends on intensity, duration, distribution of the rainfall and characteristics of the catchment. To understand this complex processes, hydrological modeling is one of the efficient ways, and it facilitates to study the long term behavior of the hydrologic system.

Hydrologic models are generally represented by mathematical equations, which approximate the natural hydrologic processes that are primarily based on the water and energy balance of a system. The hydrologic system is highly complex in nature, and thorough understanding of their processes is extremely tough. However, to gain the better understanding of these complex processes, the hydrological models have evolved over the time. These models are also useful in generation of synthetic sequence of hydrologic variables for better design and forecast.

1.2 CLIMATE AND LAND USE/LAND COVER CHANGE

In the past few decades, the influence of climate and Land Use Land Cover (LU/LC) changes on hydrology are significantly increasing and becoming more vulnerable in the arid and semi-arid region (Vorosmarty et al. 2010). Further, Climate affects the basic constituents of hydrological cycle mainly evaporation, precipitation, atmospheric water content and soil moisture (Wang et al. 2008). In addition to climate, LU/LC adversely affects the natural hydrologic system and its components mainly runoff, evapotranspiration (ET), subsurface flow and infiltration. Hence, understanding the variability in the hydrologic response of a river basin attributed to climate/LU/LC change is vital for the effective planning and management of water resources (Nijssen et al. 2001; Wang et al. 2008; Chawla and Mujumdar 2015). Climate change impacts on water resources are likely to affect the environmental flows (dry season) and flood flows (wet season), thus causing frequent extreme floods and droughts in urban and rural areas (Gosain et al. 2011). The effects of LU/LC changes on catchment hydrological responses, especially forest cover, affect the evapotranspiration. Further, rapid urbanization due to LU/LC changes leads to extent of impervious surface and thereby, impacts the infiltration rates as well as recharge

1.3 SOIL MOISTURE: TERMS AND MEASUREMENTS

In general, the amount of water content stored in the unsaturated zone or vadose zone is called soil moisture, however, its precise definition may vary based on the context and how it is defined (relative, absolute/indirect terms and also based on the reference storage) (Seneviratene et al. 2010).

Volumetric soil moisture (θ), it is expressed as the ratio of the volume of water (v) to the given soil volume (V).

$$\theta = \frac{\text{Volume of water (V)}}{\text{Soil volume(V)}} \quad (1.1)$$

The maximum soil water content for a given soil volume is referred as saturated soil moisture, (θ_{sat}), and it is related to soil porosity. Further, the saturation ratio, (θ_s), can be defined as:

$$\theta_s = \frac{\theta}{\theta_{sat}} \quad (\text{varies between } 0 \text{ to } 1) \quad (1.2)$$

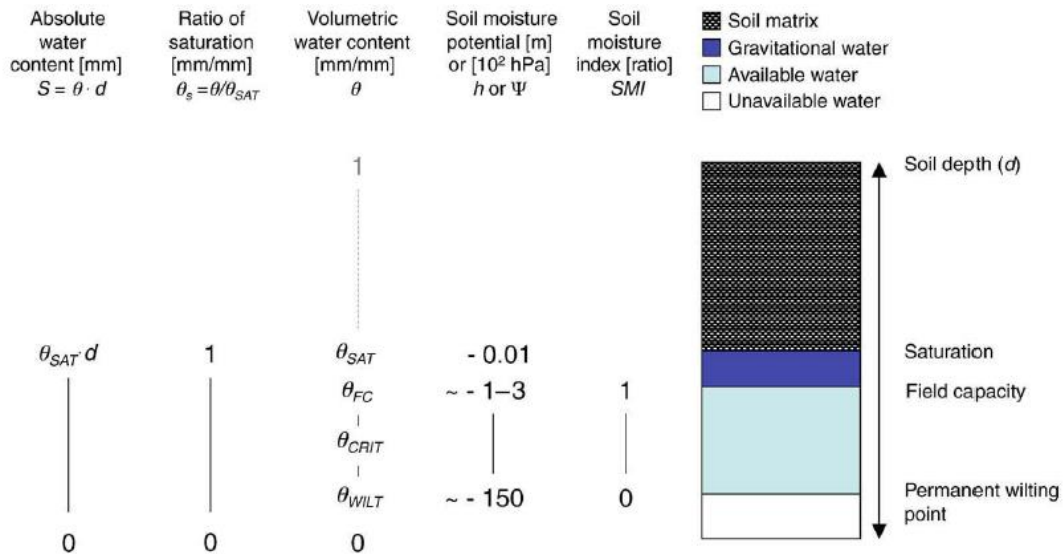
The maximum available water to the plant is generally between field capacity (θ_{fc}) and permanent wilting point (θ_{wilt}). The moisture content above the field capacity obviously drains by the gravity, and below the wilting point, it has a strong bonding with soil matrix that cannot be accessible to the plants. With this, the definition of soil moisture index (SMI) was proposed by Betts (2004):

$$SMI = \frac{\theta - \theta_{wilt}}{\theta_{fc} - \theta_{wilt}} \quad (\text{ranges from } 0 \text{ to } 1) \quad (1.3)$$

In the above equations (1.1) to (1.3), soil moisture is expressed as a relative terms. Further, it can also be defined as an absolute term, S , (in mm).

$$S = \theta \cdot d \quad (1.4)$$

Where, d denotes given soil depth.



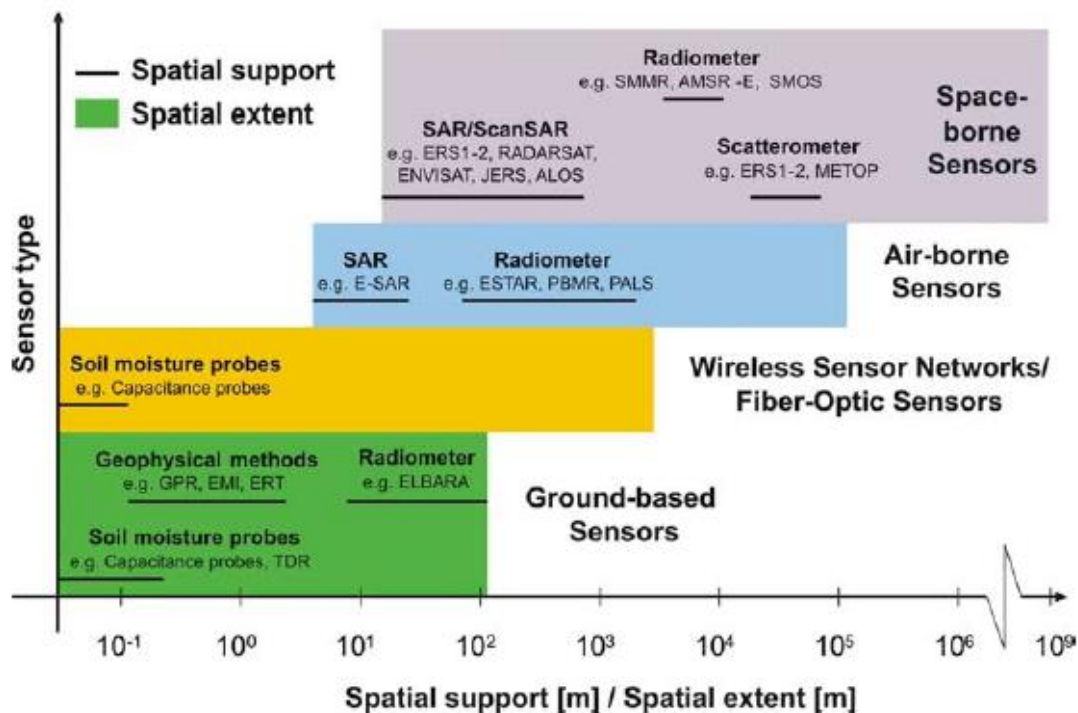
Source: Seneviratne et al. (2010)

Figure 1.1 Characteristic soil moisture level and units

The saturation soil moisture (θ_{sat}), field capacity (θ_{fc}) and wilting point (θ_{wilt}) can be defined through soil moisture potential of approximately (-1)hPa, (-100) to (-300) hPa and (-15,000 hPa) respectively, and its corresponding suction heads are 1cm, 1-3m

and 150m respectively (Seneviratne et. al, 2010). The schematics of characteristic soil moisture level and units are shown in Figure 1.1.

Soil moisture measurement techniques include: (i) ground based, direct (gravimetric) and indirect method and (ii) remote sensing approaches (air-borne and space-borne sensors). Further, soil moisture is also modeled from land surface/hydrological model (Nijssen et al., 2001). The ground based indirect methods are capacitance sensor, time domain reflectometry (TDR), cosmos sensor (Zreda et al. 2008) and other geophysical methods (electromagnetic induction, ground penetrating radar (GPR) and electrical resistivity tomography (ERT)) etc.



Source: Vereecken et. al, 2008

Figure 1.2 Support Scale of soil moisture observation

Further, remote sensing approaches include microwave remote sensing based on radiometers, scatterometer and synthetic aperture radars (SAR). Many microwave remote sensing missions provide soil moisture retrieval including advanced scatterometer (ASCAT, from meteorological operational satellite (MetOp)), Scanning Multichannel Microwave Radiometry (SMMR), Advanced Microwaves Scanning Radiometer (AMSR-E), Soil Moisture Ocean Salinity Mission (SMOS) (Kerr et al.

2001) and Soil Moisture Active Passive mission (SMAP) (Chan et al. 2016). A detailed review on different soil moisture measurements is presented in the chapter 2. The support scale for different soil moisture measurement techniques are shown in Figure 1.2.

Further, Soil moisture exhibits high spatio-temporal variation, and its information is vital for agricultural monitoring (Porporato et al., 2002), weather forecasting (Drusch, 2007; Dharssi et al., 2011; Rosnay et al., 2014), land slide modelling (Brocca et al., 2012a), drought assessment (Enenkel et al., 2016; Sánchez et al., 2016) and flood forecasting (Koster et al., 2010; Brocca et al., 2010;).

1.4 ORGANIZATION OF THE THESIS

The structure of the thesis is organized in seven chapters as listed below.

Chapter 1 presents a general background on hydrological processes, the factors (climate and LU/LC) affecting the natural hydrologic system and a brief description on soil moisture and its measurements.

Chapter 2 discusses the state of art of the research that deals with hydrological modelling, LU/LC change impacts on the hydrologic system, soil moisture estimation (ground, satellite measurements and modeling) and spatio-temporal variability of soil moisture. Further, it summarises the need of the present study. In the light of discussions, the objectives are formulated and presented in this chapter.

Chapter 3 describes the study area, the data required for the present study and preprocessing of the required data.

Chapter 4 explains the model set up and various input parameterization to the model.

Chapter 5 evaluates the model performance, and presents a detailed assessment of LU/LC change impacts on the flow regime of the study region.

Chapter 6 analyses the spatio-temporal variability of soil moisture, and identifies the representative locations for soil moisture measurements in the study region.

Chapter 7 summarizes the work with the specific conclusions, and highlights the limitations and scope for future work.

2.1 GENERAL

The global available quantity of water is constant but their occurrence and distribution is varying with respect to space and time (Chow et al, 1988). Precipitation is the predominant source of the water, which is transformed into various forms after reaching ground such as evaporation losses, runoff, infiltration, soil moisture, and ground water storage. In order to assess the impact of various scenarios for better water management, modeling the hydrological processes is essential. The necessity for such modeling increases with increase in economic implications pertaining to the water demand. The primary interest in water availability studies is generally estimating the runoff, and it is critical for water resources management. Further, climate and LU/LC changes adversely affect the above mentioned natural hydrological processes. Particularly, the effects of LU/LC changes on catchment hydrological responses, especially vegetative cover (forest, scrubs and cropland), affect the evapotranspiration. Further, rapid urbanization due to LU/LC changes leads to extent of impervious surface and thereby, impacts the infiltration rates as well as recharge (Matheussen et al. 2000; Fang et al. 2013). Therefore, several studies were conducted in the past to assess the impact of climate and LU/LC changes on the hydrologic system.

The percentage of soil moisture in the estimated total world water balance is very low (0.0012%) quantities (Chow et el. 1988). However, being a state variable, soil moisture has a significant impact on water and energy exchange at land-atmosphere interface. And also, it plays a crucial role in linking carbon, energy and terrestrial water cycles. Further, soil moisture is largely varying across the site and climate with the influence of static (e.g., soil texture/structure, topography and land cover) and dynamic factors (e.g., precipitation). Therefore, numerous efforts were made in the

past to estimate the soil moisture (in-situ and satellite measurements), and assessing its spatio-temporal variations.

In this chapter, the review of literature mainly focusing on hydrological modeling, LU/LC change impacts on the hydrologic system, soil moisture estimation (ground, satellite measurements and modeling) and spatio-temporal variability of soil moisture are presented.

2.2 RANFALL-RUNOFF MODELLING: A BREIF OVERVIEW

Traditionally, the concepts of rainfall-runoff modeling evolved in response to engineering problems such as design of sewer, drainage and reservoir spill ways. Basically, the design discharge is the interest to solve the above problems. Initially, an empirical method ($Q = CiA$) was developed. This simple rational method uses catchment area (A), rainfall intensity (i) through runoff coefficient (C), and it estimates the peak hydrograph without predicting the entire hydrograph. However, this method is still utilized by many engineers and researchers for design and planning of water resources. Later, the concept of unit hydrograph was proposed (Sherman 1932), in which, various time delays for runoff to reach outlet of the catchment could be represented as time distribution. In this case, with the assumption of linearity, the principle of superposition is valid, and the shape of hydrograph does not change over time. Being simple and easy to apply, unit hydrograph method becomes the most commonly used tool in rainfall-runoff modeling. Further, Horton (1933) developed an empirical method through experiments, and it described the infiltration excess runoff generation. Thus, the infiltration excess model and unit hydrograph together form a functional relationship that separates the baseflow from the surface runoff.

A large number of conceptual and lumped rainfall-runoff models were developed during 1960 to 1970. Probably, the most successful models were Stanford Watershed model (Crawford and Linsley 1966), Sacramento Soil Moisture Accounting Model (Burnash et al. 1973), the HBV model (Bergstrom and Forsman, 1973) and the Tank model (WMO, 1975). In the late 1970s, one of the remark models, TOPMODEL (Beven and Kirkby, 1979) was developed. In which topography uses a dominant

control on flow routing through upland catchments. Further, advent of computers helped in developing more sophisticated, complex and physically-based distributed hydrological models, in order to address the demand includes: (i) forecasting the impacts of land-use change, (ii) the impacts of spatially variable inputs/outputs, (iii) studying the movement of sediments and pollutants and (iv) hydrologic response of ungauged basin. Due to increasing interest in understanding the climate variability and LU/LC changes over a large geographical domain, the hydrologist and water managers were developed the macro-scale hydrological models. For instance, the model developed by Vörösmarty et al. (1989), Variable Infiltration Capacity (VIC) model (Liang et al. 1994) and the Macro-PDM (Arnell 1999).

The distributed hydrological modeling is effective, and pre-calibrated models can be used for generating design flows for ungauged watersheds (Micovic and Quick, 1999). With the advancement in remote sensing, satellite derived data of various hydro-meteorological variables improved the rainfall-runoff modelling applications, particularly in Climate and LU/LC change impact studies (Martheussen et al. 2000; Zhang and schilling, 2006; Defries and Eshleman 2004) and Soil moisture studies (Sheffield et al. 2004; Hu et al. 2010; Wang et al. 2015; Wagner et al. 2007).

2.3 IMPACTS OF LU/LC CHANGE ON HYDROLOGIC SYSTEM

The biophysical and socio-economical drivers are largely accountable for the LU/LC change. The biophysical drivers are slope, elevation, climatic variables and soil type, while socio-economic drivers are primarily economic, social, technological, demographic and political factors (Dwarakish and Ganasri 2015; Garg et al. 2017). Understanding the cause and effect of LULC changes related to hydrology require proper identification of these drivers (Garg et al. 2017). Several methods were developed to evaluate the hydrological impacts due to LU/LC and climate change on the catchment across different regions, which are primarily classified into three categories: (i) time series analysis (statistical approach), (ii) paired catchment approach and (iii) hydrological modeling (empirical/conceptual models and distributed physically-based models) (Li et al. 2009). The paired catchment approach is considered as an effective method for small experimental catchments. Further, it

requires continuous monitoring to collect a large amount of data, which may not be feasible for the large catchments (Lorup et al. 1998; Li et al. 2009). Lorup et al. (1998) assessed the long-term impacts of LULC on six catchments (drainage area ranges from 197 to 1036 km²) in Zimbabwe, using combined statistical test and lumped conceptual hydrological model. They showed that is a viable method for non-experimental, medium-sized catchments. However, these techniques are poor in explaining the physical mechanism. Thus, the physically-based distributed hydrological models can be more suitable for LU/LC change impacts studies (Li et al. 2009). The input parameters of the physically-based distributed models are directly representing land surface characteristics and provide suitable frameworks for assessing the impact of changes on hydrology driven by LU/LC (Wang et al. 2010; Yang et al. 2014; Chen et al. 2016).

Several investigations have been carried out for understanding the individual effect (climate or LU/LC) (Christensen and Lettenmaier, 2007; Wagner et al. 2013; Garg et al. 2017), isolated and integrated effect (Wilk and Hughes 2002; Aggarwal et al. 2012; Chawla and Mujumdar 2015; Yin et al. 2017). However, this section of the chapter is primarily focusing on the studies related to LU/LC change impacts on hydrologic system. LU/LC change impact assessment on water resources are generally carried out based on scenario analysis, mainly focusing on agricultural management, sediment yield/soil erosion, runoff potential and ground water assessment.

For instance, Sharma et al. (2001) prioritized the watersheds in the catchment on the basis of runoff generated for suggesting soil and water conservation measures, and evaluated the hydrologic responses of the suggested measures on the runoff under alternative land use practices. The information related to hydro geomorphology, land use, soil and slope and other relevant information were integrated with Geographic Information System (GIS) tool to identifying the problem, and recommending soil and water conservation measures. Soil Conservation Service Curve Number (SCS-CN) method was utilized for generating the runoff. They have found a decrease in runoff (42.88%) after the conservation measures. Further, Mishra et al. (2007) prioritized the control measures for watershed management by quantifying the effects of LU/LC on

catchment runoff and sediment yield. They have analyzed the effects of LU/LC pattern on runoff and sediment yield from the different sub-watershed in the catchment. Soil Water Assessment Tool (SWAT) model was utilized to simulate the runoff and sediment yield, and sub-watersheds were prioritized based on the sediment load.

Chen et al. (2009) combined an event-based hydrological model (HEC-HMS) and an empirical land use change model (CLUE-S model) for quantifying the impacts of land use change on storm-runoff generation. HEC-HMS model was applied for two different land use scenarios under designed storm with difference recurrence intervals (10, 50 and 100 years). They have found that runoff increased with response to land use change, and also observed that the runoff increases, while the recurrence interval decreases. Further, Ali et al. (2011) also studied the effects of land use change using HEC-HMS model with different future land use scenario. The study showed runoff and peak discharge projected to increase related to expansion of built-up areas.

Niehoff et al. (2002) applied process-based distributed model (WaSim-ETH) with spatially explicit land use scenarios for an agricultural dominant catchment. Spatially distributed land use scenarios were prepared using a new approach, the Land Use Change modeling Kit (LUCK), and the potential impacts of these scenarios on flood generation were investigated. The convective storm with high rainfall intensity produced high storm-runoff generation with the influence of land use. Verbunt et al. (2005) investigated the hydrologic impacts of hydropower station along with land cover changes in a catchment (drainage area of 4108 km²) using the WaSim-ETH model. Land cover change analysis was performed in a sub-catchment (616 km²) since this particular sub-catchment was not influenced by the hydropower station. The possible land cover scenarios used in this analysis was combined urbanization-afforestation. Further, a theoretical investigation was also carried out based on the hypothetical scenarios of pastures into forests. They have found that urbanization has a strong impact on local flood events, and it was negligible at the downstream. Particularly at the bottom of valley, changes from grassland into forest caused an increase in evapotranspiration, and subsequently reduction in runoff was observed. Further, they found that this reduction in runoff depended on the decrease in soil and

root depths with altitude increase. Merta et al. (2007) assessed the land use change in order to determine the risk areas with rapid runoff process for flood prevention and nature conservation. The study was performed with two sub-catchments of two different scales (7.4 km² and 16.7 km²) with different land use scenarios using two different models (WBS FLAB and WaSim-ETH). With the influence of land use changes, the reduction in rapid runoff and the discharge was observed. The analysis showed that with the reoccurrence intervals of 5 to 50 years, the influence of land use changes was greater for small to medium –sized catchments. Bormann and Elfert (2010) applied the WaSim-ETH model to lowland catchment (2141 km²), and evaluated the model performance related to model sensitivity to land use change and catchment characteristics. Agricultural land use scenarios based on SRES-IPCC scenarios were utilized in the model simulation. They observed that the simulation quality was decreasing with decreasing catchment slope. Therefore, they reported that the WaSim model performed better in sloped catchment than plane ones. However, the hydrological response to land use scenarios was found similar in all catchment.

The SWAT model, being a distributed and watershed to river basin-scale model, it has been applied for several hydrological modeling studies. Further, numerous studies related to LU/LC change impacts on hydrologic system using SWAT model are available in the recent past literatures. For instance, Schilling et al. (2008) evaluated the future LU/LC change impacts of water balance of a large agricultural dominant catchment. In this catchment, the anticipated growth in biofuel industry may lead to LU/LC changes, especially, increase in corn acreage and conversion of cellulosic bioenergy crops of warm/cool grasses. Therefore, they have considered scenarios of: (i) expansion of corn acreage, (ii) expansion of warm season grasses and cool season grasses. They have observed that the scenario of increased corn production will be resulting of decrease in annual ET, subsequently increase in water yield, and losses of nutrients (nitrate and phosphorus) and sediment. Further, they have reported that future LU/LC change of increase in grassland may lead to high ET and less water yield. However, the water quality may improve with less nutrients and sediment load discharge into streams due to perennial grassland. Githui et al. (2009) investigated the LU/LC change impacts on runoff potential of the River Nzoia catchment, Kenya.

LU/LC change scenarios were generated using CLUE-S model. LU/LC of a specific location was identified using logistic regression based on dependent variable (actual LU/LC pattern) and location factor for each LU/LC (population, slope, lithology, elevation, town and distances to rivers). The major changes were observed in agricultural area (39.6 to 64.3%) and forest (12.3 to 7%). During the period 1973 – 2001, LU/LC changes were significant, and it contributed to increase in runoff (30%).

Ghaffari et al. (2010) simulated the impact of LU/LC change for a catchment with drainage area of 4354 km² located at Northwest Iran. Three different period of LU/LC information was utilized to study the influence of LU/LC on the hydrology of the catchment. With response to LU/LC change, the catchment runoff increased by 33%, annual groundwater and streamflow decreased by 22% and 16% respectively. Singh et al. (2015) evaluated the potential of SWAT model in predicting water quality as well as quantity in response to LU/LC change for a coastal watershed in USA. LU/LC of the year 1992 was utilized for the model calibration and validation (the period 1990-1998 for flow and 1994-1998 for water quality parameter) using flow and other water quality parameters (Total Suspended Solids (TSS), nitrate and organic phosphorus). The performance of the model in simulating flow, TSS, nitrate and organic phosphorus was evaluated using the LU/LC of the year 2008 as an input to the model. The performance was found to be good. Further, they have highlighted the importance of utilizing the up-to-date LU/LC data, since the model performance was less with the 1992 LU/LC compared to the LU/LC of the year 2008.

Further, Wagner et al. (2016) integrated dynamically land use model projection with SWAT model, and analyzed impacts of LU/LC on the water resources of a rapidly growing Indian catchment. They utilized the SLEUTH model for future LU/LC projections. The potential impacts of LU/LC changes on the water balance are investigated for the period (2009-2028) along with four different climate conditions. They have reported that LU/LC projection indicates rapid increase in urban area and subsequent decrease in agricultural and semi-natural area. Further, water yield is reported to be increased especially at the onset of monsoon, whereas ET decreased in the dry season. Gashaw et al. (2018) modeled the hydrological impacts of LU/LC change in a watershed located in the Blue Nile basin, Ethiopia. The hydrologic impact

of LU/LC change was studied during the period (1985-2015), and it was predicted for the year 2045. LU/LC map of three different periods (1985, 2000 and 2015) was generated using Landsat images through hybrid classification techniques. The prediction of LU/LC states (the year 2030 and 2045) was prepared using Cellular-Automata Markov (CA-Markov) method. The study showed that expansion in cultivated land and built-up, and reduction in shrubland, forest and grassland during the period (1985-2015). They found increased annual flow (2.2%), surface runoff (9.3%) and water yield (2.4%) and consequently, reduced groundwater flow (7.8%) and ET (0.3%) was observed. Further, they reported that this same scenario is expected to be continuing for the year 2030 and 2045.

2.4 SOIL MOISTURE ESTIMATION

Soil moisture is generally measured by ground measurement techniques, satellite observations, and also modeled from land surface model (Vereecken et al., 2008). However, the accurate estimation of soil moisture is often challenging, particularly at large scales (Al-Shrafany et al., 2014). The direct measurement is gravimetric method in which soil samples are extorted from the field and weighted before and after over drying (at 105° C). However, the gravimetric method has some practical limitation that it requires more man power to do sampling and laboratory test (leads to poor temporal resolution, 1-2 weeks). Nevertheless, this method is still used as reference for calibrating other indirect measurements such as time domain reflectometry (TDR), capacitance sensor, and other hydro geophysical methods such as electromagnetic induction (EMI), ground penetrating radar(GPR) and electrical resistivity tomography (ERT) (Vereecken et. al, 2014). Topp et al. (1980) introduced TDR and developed a method to measure soil moisture. TDR is based on the concept of dielectric permittivity of the soil, and it strongly related to soil water content. The electromagnetic waves are generated by pulse generator, and it is passed along the waveguides of the TDR probe. The velocity of the propagated waves is determined by travel time along the probe with a known length (Robinson et al. 2003). Multiple TDR probes can be connected as a network. However, It has a limitation with cable length (<20 m), thus, the application restricted to small field plots. Capacitance sensor is an

alternative to the TDR, and it is relatively cost-effective and easy to operate (Vereecken et al. 2014).

In order to measure the soil moisture in near real time, wireless sensor network of soil moisture have emerged. For maximum number of sensor nodes, these sensors need to be cost-effective as possible without compromising its accuracy. Therefore, capacitance sensors can be an appropriate option for soil moisture sensor network (Bogena et al. 2007). In the recent past, cosmic-ray probes are used for the soil moisture measurement at small or field scale (Zreda et al., 2008). Cosmic-ray probes count the secondary fast neutrons. Hydrogen atoms present in the soil (mainly as water) moderate the secondary fast neutrons that are on the way back to the surface, which are created by primary cosmic-ray particle in the atmosphere and in the soil. The negative correlation of near surface fast neutron counts (more neutrons escape in dry soil) and soil moisture content which facilitate the use of cosmic-ray probe to sense soil moisture (Vereecken et. al, 2014). Further, the cosmic-ray probes have been successfully applied to measure the soil moisture in different environmental settings including a coastal area (Desilets et al. 2010), a desert location (Franz et al. 2012), an agricultural site (Rivera Villarreyes et al. 2011) and humid forested catchment (Bogena et al. 2013).

Overall, these ground-based measurements have limited spatial coverage, as it is difficult to employ a large numbers in the field mainly due to labour-intensive as well as cost-intensive for the installation (Vereecken et al., 2008). Satellite remote sensing of soil moisture has more advantages over the ground measurements in terms of global coverage and availability of the areal average (Wagner et. al, 2007). In the past years, lots of effort has been taken in the field of soil moisture remote sensing which includes active and passive microwave remote sensing based on scatterometer, radiometers, synthetic aperture radars (SAR) and gravity recovery and climate experiments (GRACE) mission. The passive sensor (radiometer) measures the energy that are naturally emitting from the earth surface as a brightness temperature (T_B). The active sensor (radar) is sending microwave radiation towards the earth surface and captures the backscattering signal. In general, the soil moisture-sensitive frequencies are L- (0.5–1.5 GHz), C-(4–8 GHz), and X- (8–12 GHz) bands in the microwave

region of electromagnetic radiation (Karthikeyan et al. 2017a). The active and passive microwave remote sensing use the soil dielectric constant, which increases with increasing water content to retrieve the soil moisture (Wagner et. al, 2007). Soil moisture retrievals from microwave sensors require an algorithm. These algorithms use radiometer brightness temperature from passive sensor and radar backscatter measurements from active sensor to retrieve the soil moisture. Soil moisture retrieval algorithm primarily based on Radiative Transfer Model (RTM) and dielectric mixing model (Karthikeyan et al. 2017a). Ulaby et al. (1982) formulated the general scheme for radiative transfer equation, and it was assisted by many experiments (Blinn and Quade 1972; Choudhury et al. 1979; Eagleman and Lin 1976).

Further, the assessment of relation between microwave signal and soil moisture under different sensor features, surface characteristics and atmospheric effects leads to the development of τ - ω vegetation model (Mo et al. 1982), which is consider as a baseline for the many RTMs (Karthikeyan et al. 2017a). In active sensor, soil moisture retrieval algorithm calculating dielectric constant of soil from backscatter coefficient. Further, this dielectric constant is used to estimate soil moisture using dielectric mixing models. In the past, many dielectric mixing models have been developed, and these models can be grouped into four categories: physical, empirical, semi-empirical and change detection models (Karthikeyan et al. 2017a). In the last few decades, several efforts have been made for active and passive microwave satellite missions, particularly, the two dedicated missions for soil moisture retrieval, the Soil Moisture Ocean Salinity (SMOS) (Kerr et al. 2001), and the Soil Moisture Active Passive (SMAP) mission (Chan et al. 2016).

As an indirect measurement, the satellite-derived soil moisture is influenced by several factors such as soil roughness, vegetation, atmospheric correction etc. Therefore, comprehensive validation is essential for these products. Soil moisture retrievals from satellite are generally validated using ground-based measurements, and it is not straight forward due to different spatial resolution, measurement uncertainty and observational depths (Brocca et al. 2011). However, A large body of scientific literatures are available towards validating soil moisture retrieval from the satellite using ground-based observation and /or modelled data (Bindlish et al. 2003;

Gruhier et al. 2008; Jackson et al. 2010; Loew and Schlenz 2011; Crow et al. 2012; Rotzer et al. 2014; Dorigo et al. 2015; Chan et al. 2016; Zhang et al. 2017; Chen et al. 2018; Á. González-Zamora et al. 2019).

2.5 SOIL MOISTURE VARIABILITY

In the last four decades, with the development of soil moisture measurements techniques, several studies were carried out for understanding the spatio-temporal variability of soil moisture. Further, a basic concept, temporal stability was introduced by Vachaud et al. (1985), and it leads to several studies towards understanding of soil moisture variability. For instance, A. Gomez-Plaza et al. (2000) studied the soil moisture spatial pattern and temporal stability in a semi-arid environment. They considered three transects (300, 310 and 200 m lengths), and spatial pattern of soil moisture distribution were studied. Soil moisture was measured at 15 cm depth in the selected transects in every 20 m length. It was reported that time stability was observed in spatial pattern, while factors influencing soil moisture were limited to local topography. In contrast, the spatial pattern showed time unstable, while accounting the vegetation factor. This study suggested a two-step sampling procedure for a semi-arid catchment: (i) identification of time-stable location, which can reduce the sampling points and (ii) increasing the sampling frequency. Mohanty et al. (2000) analyzed soil moisture variability at field scale. The soil moisture measurements were made at 0-6 cm depth using portable impedance probes. It was reported that spatio-temporal analysis showed change in the field variance. However, constant field mean was observed. It was also reported that slope position was the major contributor to the temporal variability.

Further, Mohanty and Skaggs (2001) evaluated the time-stable characteristics of soil moisture. The soil moisture measurements from air-borne radiometer (ESTAR) pixel-averaged data (800 m × 800 m) along with ground based data were utilized for this analysis. They found good time-stable feature for a pixel containing sandy loam soil compared to silt loam soil. Further, flat topography with grass/wheat land showed least time-stability, and high spatial variability in soil moisture. Martínez-Fernández et al. (2003) investigated the temporal stability of soil moisture through extensive

field experiments. They found temporal stability of soil moisture is more during dry periods. Further, this study underlined the significance of temporal stability of soil moisture for sampling design to establishing soil moisture observational network. Western et al. (2004) studied the geo-statistical properties of soil moisture pattern from the sites that are having different soil characteristic and contrasting climatic condition in Australia and New Zealand. Soil moisture from top 30 cm was measured using TDR. They analyzed the patterns of correlation structures and variance. They identified differenced in spatial variability, and it is systematically related to mean soil moisture. Further, they inferred that different factors (topography and/or soil properties) for different sites are influencing soil moisture variation in space.

Hebrard et al. (2006) identified the influencing factors for spatio-temporal variability of surface soil moisture in a heterogeneously formed catchment (drainage area: 0.91 km²) located in France. They found soil surface characteristics that are resulting from agricultural practices (soil tillage, chemical weed control and grass covering) were the major influencing factors for spatio-temporal distribution of soil moisture in dry and wet conditions. In contrast to the above mentioned studies (e.g., A. Gomez-Plaza et al. 2000; Mohanty et al. 2000), they found none of the local factor (soil texture, slope, aspect, and soil isolation) was correlated to spatial variability of soil moisture. It was reported that this may be the influence of land management. Brocca et al. (2007) investigated the soil moisture variability through field experiments using statistical properties of soil moisture measurements. They found decreasing trend of variance with increasing mean soil moisture. It was reported that geo-statistical analysis showed spatial organization of soil moisture was inconsistency for flat area. Further, the spatial pattern was found correlated to topographical attributes (slope, distance from drainage channel and the elevation), especially during wetter condition. For the flat area, a negative correlation was found between skewness and mean soil moisture. Furthermore, several studies were carried out for the temporal stability of soil moisture from a different climatic condition (Cosh et al. 2008; Schneider et al. 2008; Goe et al. 2019; Montenegro et al. 2019), hill slope (Gao et al. 2015), different vegetation type (Wang et al. 2015; Zhou et al. 2015; He et al. 2019; Fry and Guber 2019) different scale (Zhou et al. 2007).

Many studies were analyzed the first and second statistical moments (mean and variance) of soil moisture and its mutual relationship. For instance, Pan and Peters-Lidard (2008) studied the mutual relation of mean and variance with the focus on the effects of soil texture in the mutual relation during soil dry-down process. They proposed a nonlinear differential equation, which characterize the soil dry-down process. Further, the study showed that when the mean soil moisture is within the threshold, the variance decreases with decreasing mean, whereas, variance increases with decreasing mean while mean soil moisture exceeding the threshold. It is noted that threshold was between field capacity and wilting point, and it is depends on soil texture. Famiglietti et al. (2008) analyzed the soil moisture variability through extensive field campaign across the scale in the central USA. They have investigated the relationship of coefficient of variation, skewness and standard deviation with mean soil moisture at six different scale extents (ranged from 2.5 m to 50 km). It was reported that in general, variability showed an increase with scale extent. They found that mutual relation of mean soil moisture and standard deviation showed a convex upward relationship. Further, they derived an empirical model based on the behavior of soil moisture variability. This empirical model was used to quantify uncertainty in the mean soil moisture for a fixed number of samples (800 km – 50 km scales), It was also suggested that these empirical relation can also be useful in parameterization of soil moisture variation in land surface/hydrological models at different range of scales.

Rotzer et al. (2014) validated the satellite-derived soil moisture products (SMOS and ASCAT) using hydrological modeling along with temporal stability analysis for a catchment in Germany (drainage area: 4125 km²). They used the WaSim, hydrological model for simulating the surface soil moisture with a resolution of 200 m. Initially, modeled soil moisture was evaluated with field observed values at three different locations in the catchment during the period (2010-2011). Further, these modeled data was considered as a reference for the evaluation of satellite-derived products. Modeled data was averaged to satellite-data pixel resolution (about 25 km), and correlation analysis was carried out. It was reported that high correlation was observed for ASCAT product than SMOS. However, the correlation was found

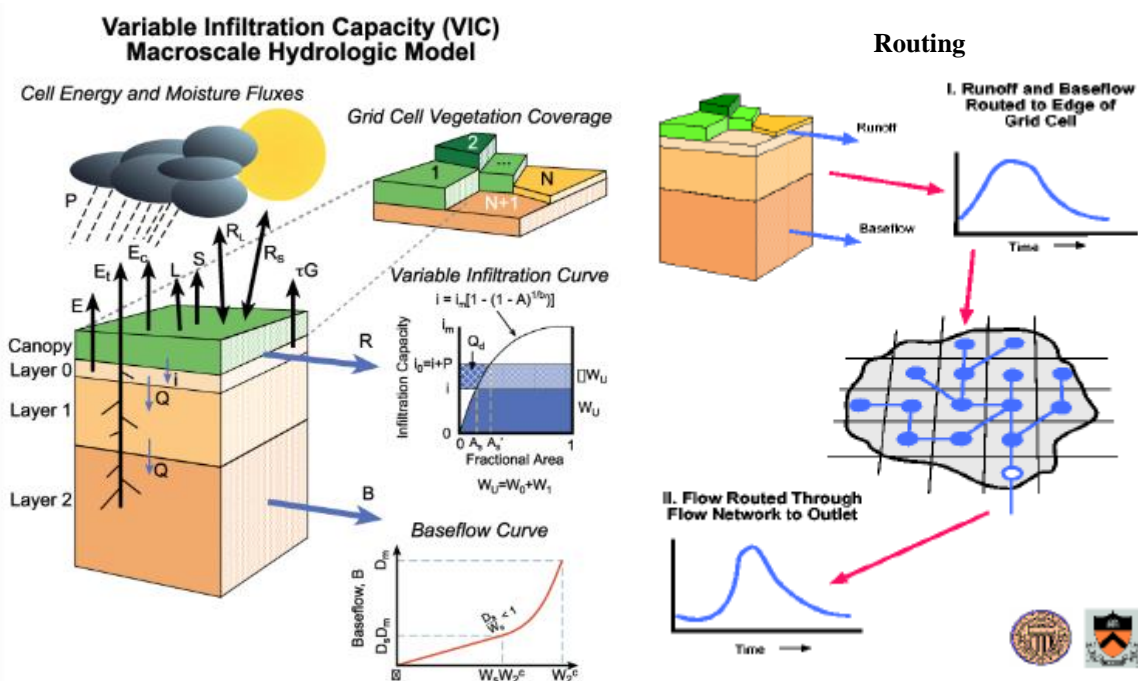
declined in the areas that are having high vegetative cover. Therefore, it is suggesting that soil moisture retrieval from ASCAT mainly depends on vegetation height and topography, thus, influence volumetric scattering and affects the retrieval. They found the Radio Frequency Interference (RFI), and it affected in the SMOS retrieval in some parts of the study area. Furthermore, the temporal stability analysis was carried out for both modeled and satellite products. The rank ordered mean relative difference (MRDs) was analyzed for the modeled and satellite-derived pixels. It was reported that a similar spatial pattern was found for absolute ASCAT values and reference (modeled) data. Nevertheless, relative ASCAT and SMOS soil moisture did not show similar spatial pattern as the reference. The study suggested that temporal stability analysis can be used as a tool for more detailed validation.

Further, Rotzer et al. (2015) compared and evaluated different global soil moisture products (ASCAT, SMOS and ERS-interim products). They used temporal stability analysis to characterize the soil moisture variability, and also studied the mutual relation of mean and variance. Further, the spatial variance decomposed into two components (time variant and invariant). It was reported that in general, spatial soil moisture showed a similar pattern, however high deviation was observed in absolute values. The time series of ASCAT showed higher variability for different climatic conditions within the selected regions compared to other counterpart products, especially ERA-interim product. It was observed that precipitation patterns are largely influencing the mutual relationship of mean and variance for the ERA and ASCAT product, especially during wet period. In SMOS product, sensor and retrieval characteristics are influencing the relation. Their analysis on the decomposition of spatial variance showed high dependence on retrieval algorithm of the individual products. It was reported that change detection algorithm has a large influence of time variant factors (evaporation and precipitation) on the ASCAT product, whereas, ERA and SMOS are influenced by time invariant factors (soil characteristics and topography). Looking into investigation on changing scales, the results showed that no variation was observed in variance with increasing support scale for the different selected region. However, increase in spatial variance was reported for increasing extent scale (250 to 300 km) with all products and all selected region, and this

variation occurred seasonally. In contrast to earlier studies, few studies reported that the analysis of decomposition of soil moisture variability of temporal anomaly showed high variability in wet and dry condition, and it was observed minimum at intermediate wetness condition (Mittelbach and Seneviratne 2012; Hu and Si 2016). Therefore, the soil moisture data of absolute and anomaly behave differently.

2.6 THE VIC MODEL

Initially, Wood et al. (1992) described the VIC model as a single layer model and implemented as a land surface scheme in the GCMs. Further, Liang et al. (1994) updated the model with two layers including varying vegetation and evaporation within a grid. With this update, sub-grid variability in runoff production, evaporation and soil moisture storage was enabled. However, the two layer scheme had a poor mechanism of moisture movement from lower soil layer to upper layer, and thus, model underestimated the evaporation. Therefore, Liang et al. (1996) provided an additional thin layer (10 cm) on the top to allow moisture diffusion between the layers.



Source: <https://vic.readthedocs.io/en/master/Overview/ModelOverview/>

Figure 2.1 Schematic representation of the VIC and Routing model

Figure 2.1 shows the schematic representation of the VIC model with a combined representation of vegetation coverage and three soil layers. The surface of each grid cell is described by $N+1$ land cover tiles, where $n = 1, 2, \dots, N$ represents N different tiles of vegetation, and $n = N+1$ represents bare soil (Gao et al. 2009). Several modifications to the model structure have been made over the period to include complex processes such as snow and cold land processes (Wigmosta et al. 1994; Storck et al. 1998; Bowling et al. 2004), elevation dependent structure for stream flow simulation (Nijssen et al. 2001), frozen soil (Cherkauer and Lettenmaier 1999), lake and wetland (Bowling and Lettenmaier 2010; Cherkauer et al. 2003), representation of reservoir and irrigation (Haddeland et al. 2006, 2007) etc. However, the model is still being considered for further development. With the implementation of separate routing scheme coupled with model (Lohmann et al. 1996, 1998) enabled the usage of model in various hydrological application studies. The detailed descriptions of model structure, parameterization and governing equations are presented in the chapter 4.

The VIC model, being a physically-based, gridded and semi-distributed model, a wide body of literature that used this model has been well established in various applications including stream flow and water budget (Liang et al., 1994; Sivabalan and woods, 1995; Abdullah et al., 1996; Nijssen et al., 1997; Maurer et al., 2001; Li et al. 2007; Wang et al., 2012), drought monitoring (Sheffield et al., 2004; Andreadis and Lettenmaier, 2006; Luo and Wood, 2007; Shukla et al., 2011; Mishra et al., 2014; Shah and Mishra 2015), snow modelling (Cherkauer and Lettenmaier, 2003; Pan et al., 2003; Feng et al. 2008), Data assimilation (Gao et al., 2007; Pan and Wood, 2006; Naha et al., 2016) and soil moisture evaluation (Nijssen et al., 2001; Wu et al., 2007; Gao et al., 2006; Meng and Quiring, 2008). LULC change impact assessment using VIC model is emerging in the recent past (Matheussen et al. 2000; Dadhwal et al. 2010; Garg et al. 2017, 2019), as it is a physically-based, semi-distributed and grid-based model with explicit representation of sub-grid variability in land cover classes. Particularly, Garg et al. 2017 assessed the LU/LC change impacts on flow regime of a large basin (drainage area is about 54,970 km²). They extensively studied the LU/LC impact on water balance of the basin with three different period of LU/LC condition (the year 1985, 1995 and 2005). The calibrated and validate model was used

to simulate the water balance of the basin with different LU/LC condition and other input parameters such as meteorological forcing (minimum and maximum temperature, precipitation and soil data) were kept uniform for the simulation. This study reported a detailed investigation on LU/LC change impacts also at the basin grid level. Further, it is suggested that LU/LC impact on hydrology of the basin needs to be studied finer spatial scale rather than basin as a whole.

2.7 SUMMARY AND OBJECTIVES OF THE STUDY

Our understanding of complex hydrologic system has been improved over the period with the development of hydrological models. LU/LC change adversely affects the natural hydrologic system. Therefore, understanding the hydrologic response to LU/LC change is essential for planning, development and management of water resources. Hydrological models are proven to be an effective tool for the assessment of LU/LC impact on the hydrologic system. A large body of the scientific literature assessed the LU/LC change impacts, mainly at the catchment or river basin scales. A few studies were addressed this issues at sub catchment or finer grid scale. However, the LU/LC change impact on the hydrologic system is region specific, and each region is characterized by its own hydrology, terrain, climate and also anthropogenic factors. Hence, a detailed assessment of LU/LC change impacts on the flow regime of the major river basins in the country is required at finer spatial scale, specifically the region with seasonally limited water availability. It is widely accepted that the physically-based, distributed hydrological models along with remote sensing capabilities are more suitable for assessing the LU/LC change impacts on the hydrologic system.

Soil moisture, being a critical state variable, its knowledge is of paramount importance in several hydrological applications. Each soil moisture estimation method (in situ, satellite and modeling approach) has its own limitations in terms of scales, accuracy and resolution. It is widely recognized that the integration of all these approach is an effective way to utilize the potential of soil moisture in the hydrological applications. Further, Soil moisture shows high variability in both space and time, and the variability mainly influenced by the heterogeneity of topography,

soil properties, LU/LC, precipitation and evapotranspiration. The ground based techniques can provide soil moisture information up to root zone, however, they are limited to small scale application (few meter to field or small catchment) while, satellite based approach can provide measurements on large scale, but limited to few centimeter depth (5-10cm with about 50m course spatial resolution). Understanding the dynamics of soil moisture in surface (5- 20cm) and subsurface (up to root zone) is essential for weather prediction, agricultural and irrigation practices. Further, agricultural and irrigation practices especially semi-arid and arid regions are depend on the root soil moisture dynamics which impact the production and health of the plants. Hence, understanding the soil moisture dynamic is essential especially the agricultural dominant catchment.

In the past, several studies have been conducted for understanding the soil moisture variability. However, the studies that are addressing the soil moisture variability influenced by heterogeneities in LU/LC at multiple depths with finer resolution are limited. Further, finding the optimal locations for mean soil moisture at different depth of a large area can reduce the costs. Thus, identifying the optimal locations to set up soil moisture observational network, particularly to the data scarce region for agricultural monitoring is essential.

As compared to other land surface/hydrological model, the distinguished features of the VIC model are: (i) base flow parameterization from lower soil layer as a nonlinear recession (Zhao et al. 1980), (ii) explicit representation of sub-grid heterogeneity in land cover classes along with bare soil and (iii) sub-grid variability in soil moisture storage capacity. Being a grid based model, it is easy to integrate satellite-derived data, which are usually available in gridded nature. Therefore, being a physically-based, gridded and semi distributed model, it is suitable for assessing the LU/LC change impact and soil moisture variability. However, any model has its own effectiveness depending upon the study objective, degree of complexity of the problem and preferred accuracy.

With the above background, this study is focused on understanding the soil moisture variability and land cover change impacts in the Upper Bhima basin, Maharastra,

India. The Variable Infiltration Capacity (VIC) model, a land surface hydrological model was used to simulate the hydrologic responses of the basin for different LU/LC scenarios with multiple soil layers parameterization (three soil layers: 0 – 10 cm, 10 – 45 cm and 45 – 100 cm). The specific objectives of the study are:

1. To evaluate the potential of VIC model to simulate the hydrological responses of the Upper Bhima basin with improved model vegetation parameterization
2. To assess the impact of Land Use Land Cover changes on the flow regime of the basin at finer spatial scale.
3. To analyse the spatio-temporal dynamics of the soil moisture at multiple soil layers in order to identify the optimal locations for setting up soil moisture observational network in the study region.

STUDY AREA AND DATA SOURCES

In this chapter, a detailed description of the study area and various data sets utilized for this study is presented. The area chosen for this study is Upper Bhima basin and it is located in the western part of the Indian peninsula. The present study used different hydro-meteorological data from field and satellite observations, soil data, topographic details (Digital Elevation Model (DEM)) and Land Use/Land Cover (LU/LC) information. The pre-processing of the required data sets is also explained in detail.

3.1 STUDY AREA DISCRIPTION

3.1.1 Physiography

The River Bhima is a major tributary of Krishna River, which is originating at Bhimashankar (Pune district, Maharashtra) and lies in the Western Ghats on the western part of Indian peninsula. The river flows towards southeast for a long distance of about 860 km through Maharashtra, Telangana and Karnataka states, before joining Krishna River at Raichur in Karnataka. The total drainage area of the Upper Bhima basin (16.5°- 20° N and 73°- 77°E) at the confluence (Sina with river Bhima) near Kudal is about 45,780 km² (Fig. 3.1). The major rivers in the basin (Sina, Nira and Bhima) are originating from the eastern side of the Western Ghats ranges. River Sina is the longest tributary of Bhima, which rises from Harichandra range in Ahmednagar district. River Nira is a right bank tributary and it joins with Bhima Akluj in Solapur district. The elevation ranges from 401 m to 1476 m (Western Ghats ranges in the upper portion), while 90% of the catchment area lies below 700 m (lower part of the basin) and comparatively flat.

3.1.2 Rainfall and Temperature

The catchment experiences semi-arid climate with high spatial and temporal variability in rainfall. The upper portion (Western Ghats ranges) receives more than

3500 mm/year. The Western Ghats are parallel to the coast of Arabian Sea, and the monsoon winds from sea bring abundant moisture, which is shedding their moisture on the western slopes. Hence, the Western Ghats ranges receive a high amount of rainfall. However, in the central part, it decreases less than 500 mm/year (Fig. 3.2). The average annual rainfall is about 640 mm, predominantly in the south-west monsoon (June to September). However, the central portion of the basin receives low rainfall than the east and upper portion of the catchment (Gartley et al. 2009). The average daily maximum temperature during winter (December – February) varies between 29 to 31° C in the lower reaches of the basin. It is lowest in the upper reaches of the basin and it varies between 11 to 16° C. The mean daily maximum temperature during summer (March – May) is about 38 to 40° C. The basin shows less variation in daily mean temperature during south-west monsoon. It varies between 21 to 22° C; however, the mean daily temperature is about 28° C at Puna and 31° C at Solapur.

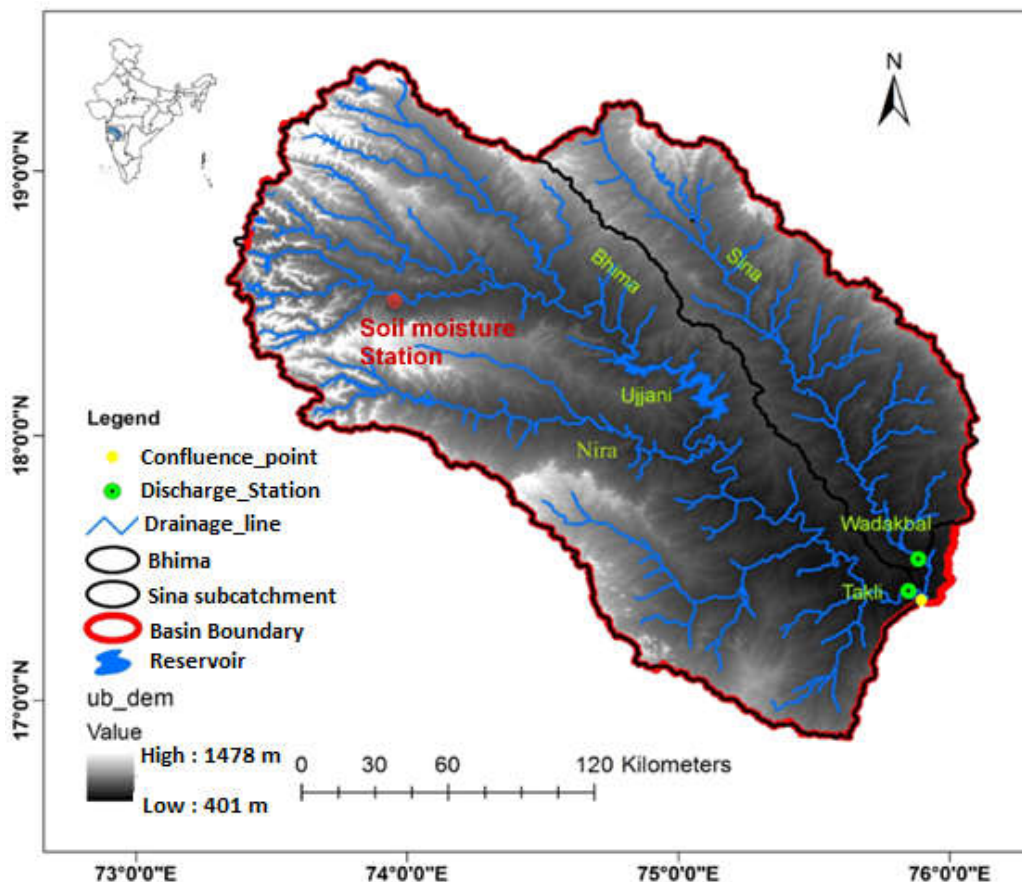
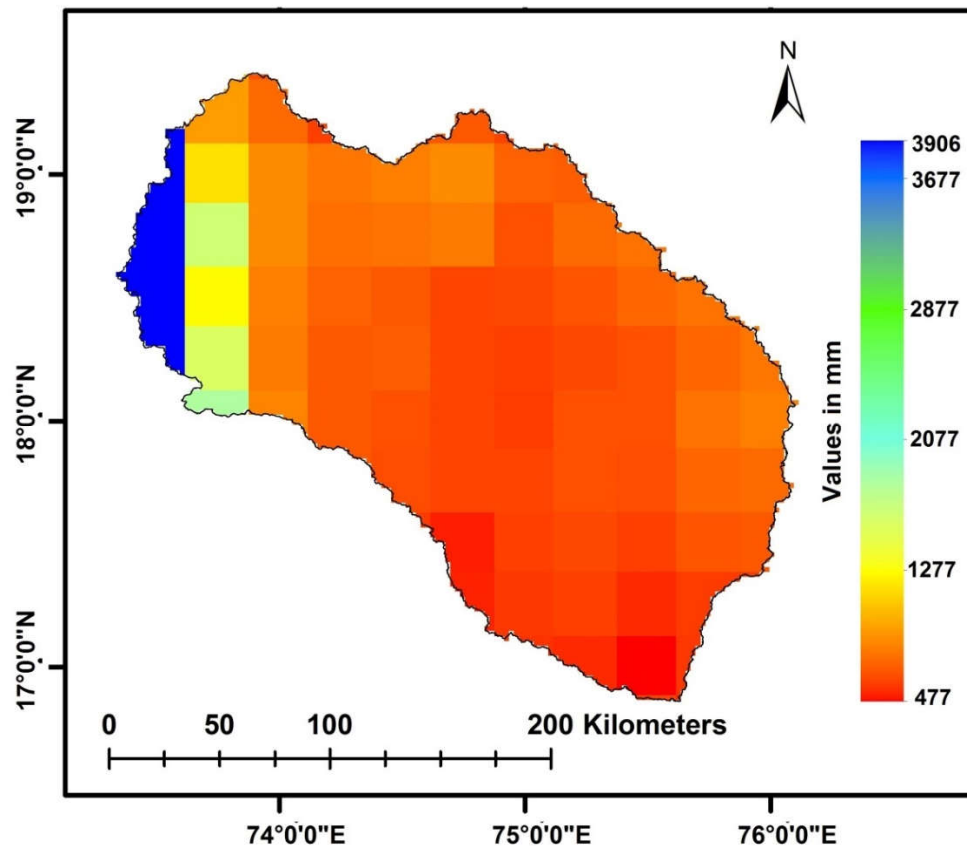


Figure 3.1 Location of the study area along with DEM and drainage network

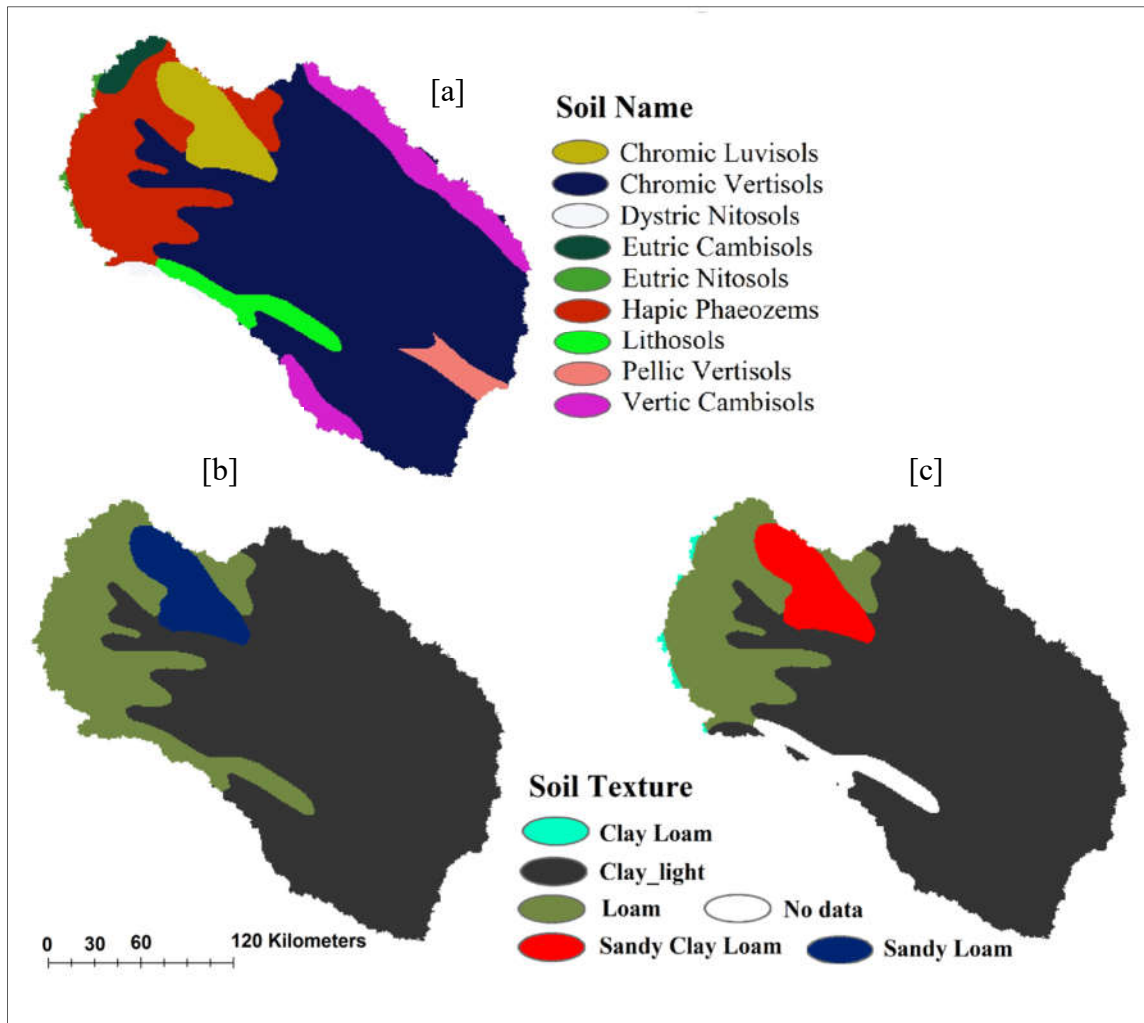


Source: India Meteorological Department

Figure 3.2 Spatial distribution of average annual rainfall over the basin (1980-2010)

3.1.3 Soils

Information on the soil profile is important for simulating the hydrological characteristics of the catchment. The soil in the catchment is predominantly vertisols and 10 different soil types have been identified. The soils, which occupy higher slopes are coarser in texture and shallow in depth (2.5 cm to 30 cm), while soils in lower elements of relief (below 600m) have texture varied from sandy loam to light clay. The alluvial plains are mainly characterized by vertisols, while the Western Ghats and steeper slopes by luvisols (Fig. 3.3). The catchment mostly lies on granite, zeonite and basalts rocks, having a significant stock of groundwater with high variability in both space and time (Immerzeel et al. 2008).



Source: FAO soil database

Figure 3.3 Distribution of soil types and texture characteristics in the Upper Bhima: [a] Soil type [b] Topsoil texture [c] Subsoil texture

3.1.4 Land Use/Land Cover

Land use is a depiction of how the land and socio-economic activity is utilized. The most commonly known land uses are agricultural and urban land use classes. Land cover is generally a description of physical materials at the earth surface, which includes water bodies, trees, barren land, grass etc. Land Use/Land Cover of the Upper Bhima consists of cropland, forest, built-up, scrubs, barren/sparse vegetated land and water bodies (Fig. 3.4). Semi-natural vegetation with the forest is mostly on the higher elevation (900 – 1200 m) in the western side of the basin. Cropland is

predominant, and it is found very dense in proximity to rivers. Urban settlement is predominant in the upper portion of the basin, where the Pune city and its nearby settlements are situated. Agriculture is the primary water consuming sector, and about 70% of the total land area is irrigated for the major crops: sugarcane, millet, sorghum wheat, groundnut, corn, and other horticultural crops (Garg et al. 2012).

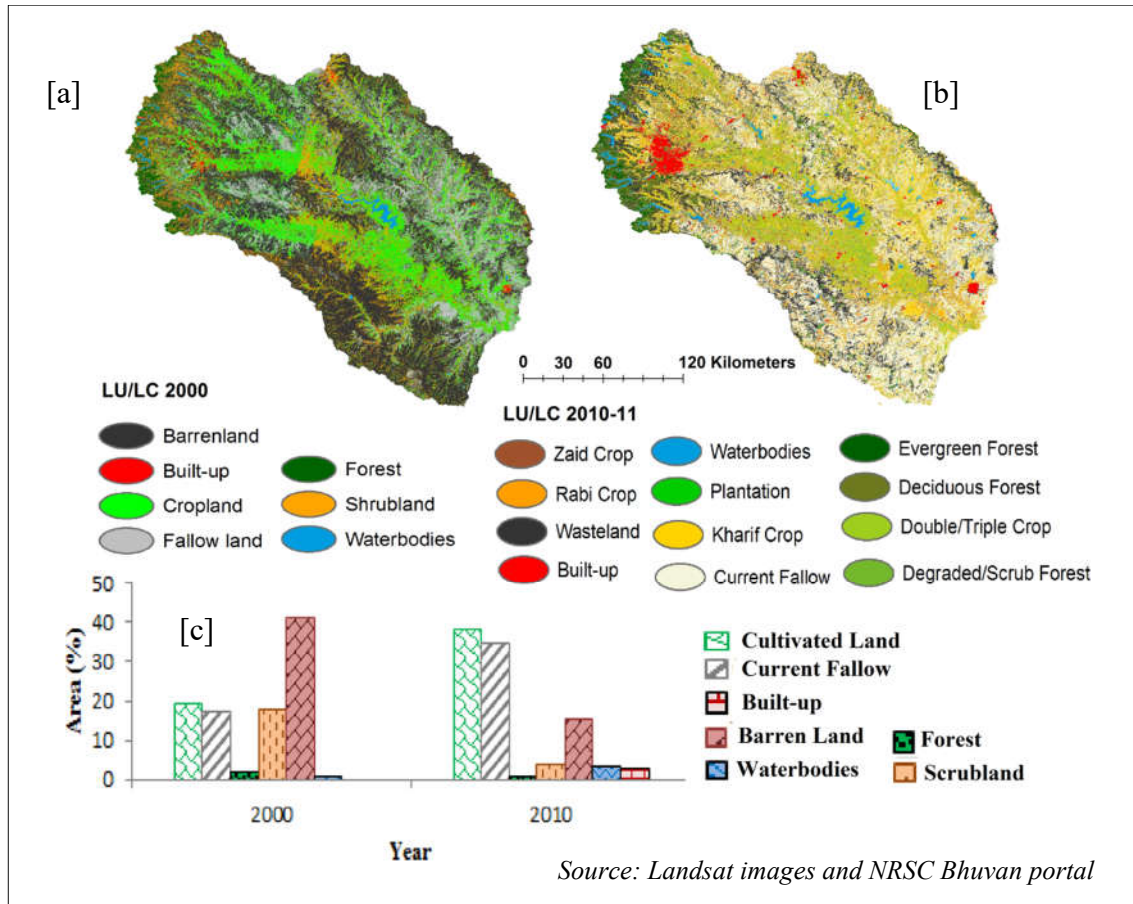


Figure 3.4 LU/LC map along with its percentage area: [a] LU/LC for the year 2000 [b] LU/LC for the year 2010 [c] LU/LC percentage area in the Upper Bhima

3.1.5 Flow

The river flows are ephemeral and feeding the need of many irrigation projects through dams and canal structures (Biggs et al. 2007). The average annual river discharge at different locations ranges from 5.38 to 148.56 m³/sec, whereas discharge at Takli and Wadakbal station is about 148.56 m³/sec and 35.77 m³/sec respectively (available at <http://hydrology-project.gov.in>).

3.2 DATA SOURCES

The meteorological forcing data such as precipitation, minimum temperature (T_{\min}) and maximum temperature (T_{\max}) were obtained from India Meteorological Department (IMD). This gridded daily rainfall data with a spatial resolution of $0.25^\circ \times 0.25^\circ$ (about 25 km) was developed using rain gauges installed at numerous location in the country (Pai et al. 2014). Over this study area, up to 44 rain gauges data were used. The daily temperature data sets (T_{\min} and T_{\max}) with a resolution of $1^\circ \times 1^\circ$ were used and it was developed using various daily temperature values from various observation (Srivastava et al. 2009). Digital elevation model from Shuttle Radar Topographic Mission (SRTM) (NASA JPL2013) with 30 m spatial resolution was used for delineating catchment, stream network and other terrain related information.

The soil data from Food and Agriculture Organization - Harmonized World Soil Database (FAO-HWSD) (G. F. Fischer et al. 2008) with 30-arc seconds comprising of soil properties up to one-meter depth distributed in two layers (topsoil-up to 30 cm; remaining subsoil) were used. The observed daily streamflow data at two locations (Takli and Wadakbal) in the study area was obtained from India Water Resources Information System (INDIA-WRIS). The detailed information regarding the sources of datasets used in this study is listed in Table 3.1.

Table 3.1 Datasets used in the study

Data sets	Source	Scale/Spatial resolution	Period
Rainfall	IMD Gridded rainfall	$0.25^\circ \times 0.25^\circ$	1994 - 2005
Minimum (T_{\min}) and Maximum Temperature (T_{\max})	IMD Gridded temperature	$1^\circ \times 1^\circ$	1994 – 2005
Stream Discharge	CWC Gauging Station	-	1996 – 2001

LULC	NRSC	1:250,000	2010
Soil Map	FAO HWSO V1.2	1:5,000,000	2008
Satellite Imagery	Landsat7 ETM ⁺	30 m	2001
Topography	SRTM GDEM	30 m	2013
LAI	MODIS	1 km and 500 m	2000-01 and 2010-11
Albedo	MODIS	500 m	2000 – 2001 and 2010 - 2011
Evapotranspiration	MODIS	500 m	2001 – 05
Satellite Soil moisture products	AMSRE, TRMM-TMI and ECA- CCI- combined	25 km	1996-2005

3.2.1 LU/LC classification of satellite images

LU/LC maps for two different periods (the year 2000 and 2010) were used for the present study. LU/LC map of the year 2010 - 11 (NRSC, 2011) was obtained from National Remote Sensing Center (NRSC), while for the year 2000; it was prepared from satellite imagery (Landsat 7 Enhanced Thematic Mapper plus (ETM⁺)) using pixel-based supervised classification algorithm (maximum likelihood), framed in the software suit ERDAS IMAGINE[®]. Seven LU/LC classes were identified and accordingly LU/LC map was prepared for the year 2000 (Fig. 3.4a). Care has been taken to perform the classification by ensuring with sufficient training sample (Congalton 1991) using the computer-based algorithm. The accuracy assessment for the classified images was carried out with the reference ground truth points collected from available historical Google Earth imageries for the corresponding period (Table

3.2). It is in a good agreement with an overall efficiency of 93% and kappa statistics of 0.92. Producer’s accuracy (Omission Error) is resulted from the number of correctly classified pixels in each class divided by the total number of references. User’s accuracy (Commission Error) is defined by the number of correctly classified pixels in each class divided by the total number of pixels that are classified in that class.

Table 3.2 Accuracy assessment for LU/LC classification

Class Name	Reference Total	Classified Total	Number Correct	Producer’s accuracy (%)	User’s accuracy (%)
Built-up	100	81	81	81	100
Barren land	101	119	99	98.02	83.19
Crop land	101	121	100	99.01	82.644
Fallow land	98	97	97	98.98	100
Forest	98	98	98	100	100
Scrubland	99	81	77	77.78	95.06
water bodies	101	101	100	99.01	99.01
Totals	698	698	652		

Over all Classification accuracy = 93.41% : Kappa statistics =0.92

3.2.2 MODIS-derived data

Leaf Area Index (LAI) (MOD15A2 - 8day (year 2000) and MCD15A3 - 4day) and Albedo (MCD43A3 – 8day) for the corresponding period of LU/LC map (June 2000 – May 2001 and June 2010 - May 2011) was derived from Moderate Resolution Imaging Spectroradiometer (MODIS) with a spatial resolution of 1000 m (MOD15A2) and 500 m (MCD15A3 and MCD43A3). Typical LAI and albedo values are shown in Figure 3.5 and 3.6 respectively.

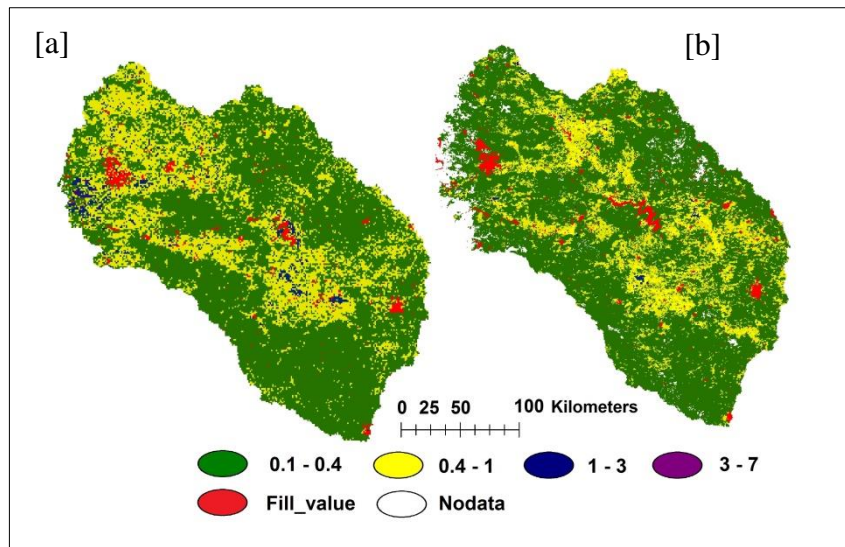


Figure 3.5 Typical LAI: [a] 19 July 2000 [b] 20 July 2010

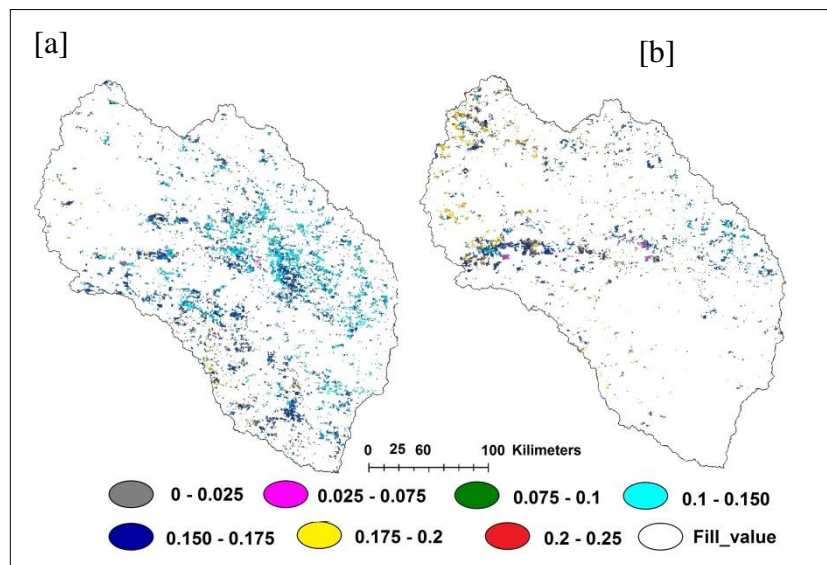


Figure 3.6 Typical Albedo: [a] 19 July 2000 [b] 20 July 2010

MODIS/Terra (MOD16A2, 8-day) derived Evapotranspiration (June 2001 – May 2005) with a spatial resolution of 500m was extracted for the study area. Figure 3.7 shows the typical ET distribution over the basin

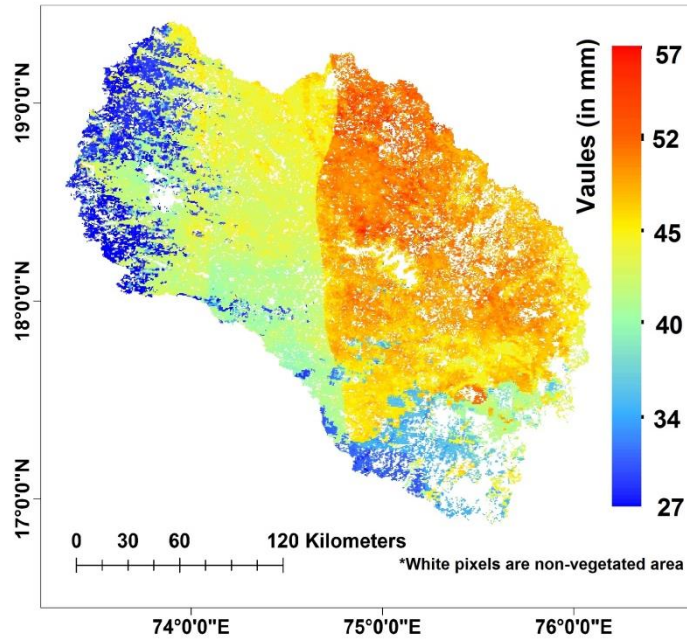


Figure 3.7 Spatial distribution of the MODIS-derived ET over the basin (on 2 June 2001)

3.2.3 Satellite-derived soil moisture data

Microwave soil moisture products from two passive and one combined active/passive sensors were used. The passive sensors are Advanced Microwave Scanning Radiometer for Earth observing system (AMSR-E) and Tropical Rainfall Measuring Mission (TRMM)’s – microwave imager (TMI) (referred as SM-TRMM hereafter). The AMSR-E sensor is dual polarized and having six frequencies (6.92, 10.65, 18.7, 23.8, 36.5, and 89.0 GHz) (Karthikeyan et al., 2017b). The global coverage of AMSR-E is achieved within two day for ascending and descending passes separately.

To obtain the soil moisture data in daily scale from AMSR-E, the following method was adopted:

$$SM(t) = [0.25 \times SM_{des}(t)] + [0.5 \times SM_{asc}(t)] + [0.25 \times SM_{des}(t + 1)] \quad (3.1)$$

Where,

$SM(t)$ – Soil moisture at time, t (in days)

SM_{des} – Descending pass (night time)

SM_{asc} –Ascending pass (day time)

By this way, the soil moisture at time t, on the day time pass is centred by including previous and succeeding night time pass retrievals to obtain soil moisture in a day.

On the other hand, the TMI sensor is also dual polarized and having the frequencies of 10.65, 19.4, 21.3, 37, and 85.5 GHz (Karthikeyan et al., 2017b). The TMI has ascending and descending passes daily at near equatorial orbit. For a particular day, the average of ascending pass and descending pass were considered. The AMSR-E based soil moisture product (0.25° resolution), jointly developed by NASA Goddard Space Flight Centre (GSFC) and Vrije Universiteit Amsterdam was used in this study (referred as SM-AMSRE hereafter). The combined active/passive sensors products were acquired from Climate Change Initiative (CCI) organized by the European Space Agency (ESA) (referred as SM-CCI hereafter). It is a global scale daily long term soil moisture record with a resolution of 0.25°, and it has been derived by combining various active and passive microwave soil moisture sensors.

MODEL SET UP AND INPUT PARAMETERIZATION

As mentioned in the earlier chapters, the present study used the Variable Infiltration Capacity (VIC), a semi distributed hydrological model to characterize the hydrological processes in the study region. In this chapter, a detailed description about the model and its input parameterization is presented. The required inputs for the model are land surface vegetation classes (as a vegetation library & vegetation parameter files), soil characteristics (soil parameter file), topography (as an elevation band file) and meteorological forcing (Precipitation, T_{\max} and T_{\min}). The methodological framework for the improved vegetation parameterization with the region-specific condition to the model simulation is also presented in this chapter.

4.1 VIC MODEL

VIC model (Liang et al. 1994) is a physically-based semi-distributed land surface model, that solves both energy and water balance equations. It is a grid-based model, and in each grid cell, the interaction among land surfaces processes including soil water interaction, evapotranspiration (ET) and runoff generation are performed. The model represents the subsurface into multiple soil layers characterizing soil hydrological properties including saturated hydraulic conductivity (K_{sat}), bulk density, soil moisture diffusion parameter, infiltration capacity and soil layer depth (Geo et al. 2009). In the present study, three layers model (VIC-3L) (Liang et al. 1996) was adopted. As compared to other land surface model, the important features of the VIC model are: (i) modelling sub-grid variability in land surface vegetation classes and soil moisture storage capacity (Gao et al., 2009), (ii) base flow parameterization from lower soil layer as a nonlinear recession (Zhao et al. 1980).

The water balance computation at each time step in the model uses continuity equation as described below (Geo et al. 2009):

$$\frac{\partial S}{\partial t} = P - E - R \quad (4.1)$$

$$\frac{\partial W_i}{\partial t} = P - E_c - P_t \quad (\text{For interception}) \quad (4.2)$$

Where,

$\partial S/\partial t$ - Water storage change

P - Precipitation

R - Runoff

W_i - Intercepted water

E - Evapotranspiration

E_c - Evapotranspiration from canopy

P_t - Throughfall

The units of all the above variables are denoted by millimetre (mm) within the time step (daily). The surface runoff from the upper two soil layers is generated, when precipitation excess to soil moisture storage in the previous time steps surpasses the soil storage capacity (Liang et al. 1996). The spatial heterogeneity of runoff generation is characterized by variable infiltration curve (Zhao et al. 1980). The VIC model estimates the ET as the one of the hydrological fluxes from the water balance computation. The model partitioning the grid-cell ET into canopy layer evaporation (E_c), transpiration from each vegetation class (E_t) and bare soil evaporation (E_l), and the total evaporation for each model grid is area weighted sum of these components. The formulation of total evaporation as follows:

$$E = \sum_{n=1}^N C_n \cdot (E_{c,n} + E_{t,n}) + C_{N+1} \cdot E_l \quad (4.3)$$

Where,

C_n - Fraction coverage for n^{th} vegetation

C_{N+1} - Bare soil fraction and $\sum_{n=1}^{N+1} C_n = 0$

The canopy evaporation is given by

$$E_c = \left(\frac{W_i}{W_{im}} \right)^{2/3} ET_0 \left(\frac{a_w}{a_w + a_0} \right) \quad (4.4)$$

Where,

W_i - Canopy interception (mm)

W_{im} - Amount of maximum water the canopy can intercept (mm)

a_0 - Architectural resistance (s/m)

a_w - Aerodynamic resistance (s/m)

ET_0 - Reference evapotranspiration estimated by the FAO-56 PM method(mm)

Transpiration from vegetation is estimated as:

$$E_c = 1 - \left(\frac{W_i}{W_{im}} \right)^{2/3} ET_0 \left(\frac{a_w}{a_w + a_0 + a_c} \right) \quad (4.5)$$

Where,

a_c - Minimum canopy resistance (s/m)

When the top thin soil layer is not saturated, the bare soil evaporation (E_1) is calculated using Arno model formulation (Franchini and Pacciani 1991), and the infiltration capacity (i) is described by Xianjiang model conceptualization (Zhao et al. 1980).

$$E_1 = E_p \left[\int_0^{A_s} dA + \int_{A_s}^1 \frac{i_0}{i_m \left[1 - (1-A)^{1/b_i} \right]} dA \right]$$

(4.6)

$$i = i_m \left[1 - (1-A)^{1/b_i} \right] \quad (4.7)$$

$$i_m = (1 + b_i) \cdot \theta_s \cdot |d| \quad (4.8)$$

Where,

A_S - Fraction of the bare soil that is saturated

i_0 - Infiltration capacity (corresponding point) (mm)

i_m - Maximum infiltration capacity of soil (mm)

A - Fraction of area for which the infiltration capacity is less than i_m

b_i - Infiltration curve shape parameter

θ_S - Soil porosity

d - Depth of the soil layer (m).

The movement of moisture in the top two layers is characterized by the one-dimensional Richard's equation, assuming that there is no lateral flow (Gao et al. 2009).

$$\frac{\partial \theta}{\partial t} = \frac{\partial}{\partial d} \left[D(\theta) \frac{\partial \theta}{\partial d} \right] + \frac{\partial K(\theta)}{\partial d} \quad (4.9)$$

Where,

θ - Volumetric soil moisture content (mm^3/mm^3)

$D(\theta)$ - Soil water diffusivity (mm^2/day)

$K(\theta)$ - Hydraulic conductivity (mm/day)

Soil moisture for the layer 1 and 2 by considering the atmospheric forcing (Mahrt and Pan 1984):

$$\frac{\partial \theta_i}{\partial t} \cdot d_i = I - E - K(\theta) \Big|_{-d_i} + D(\theta) \frac{\partial \theta}{\partial d} \Big|_{-d_i} \quad (i = 1,2) \quad (4.10)$$

Where,

I - Infiltration rate (mm/day)

d_1 and d_2 - Soil layer depth for layer 1 and 2

For the lower soil layer,

$$\frac{\partial \theta_3}{\partial t} \cdot (d_3 - d_2) = K(\theta) \Big|_{-d_2} + D(\theta) \frac{\partial \theta}{\partial d} \Big|_{-d_2} - E - Q_b \quad (4.11)$$

Where, Q_b - baseflow (in mm). For the bare soil, the term E is zero, and thus there is no evaporation from the lower soil layer. The surface runoff (Q_s) (in mm) is calculated within each time step for the top layers as described by Liang et al. (1996):

$$Q_s = \begin{cases} P - d_2 \cdot (\theta_s - \theta_2) + d_2 \cdot \theta_s \cdot \left[1 - \frac{i_0 + P}{i_m} \right]^{1+b_i}, & P + i_0 \leq i_m \\ P - d_2 \cdot (\theta_s - \theta_2), & P + i_0 \geq i_m \end{cases} \quad (4.12)$$

The baseflow formulation is expressed as (Franchini and Paccianni, 1991):

$$Q_b = \begin{cases} \frac{D_s D_m}{W_s \theta_s} \cdot \theta_3, & 0 \leq \theta_3 \leq W_s \theta_s \\ \frac{D_s D_m}{W_s \theta_s} \cdot \theta_3 + \left[D_m - \frac{D_s D_m}{W_s} \right] \left[\frac{\theta_3 - W_s \theta_s}{\theta_s - W_s \theta_s} \right]^2, & \theta \geq W_s \theta_s \end{cases} \quad (4.13)$$

Where,

D_s - Maximum subsurface flow (mm/day)

D_m - Fraction of D_s

W_s - Fraction of maximum soil moisture

4.2 ROUTING MODEL

The VIC model simulates runoff for each grid and distributes non-uniformly within the grid without horizontal water flow. Thus, a separate routing model has been employed to route each grid surface runoff and base flow out of the grid, then to the river system (Lohmann et al. 1996, 1998). It assumes that runoff is exiting from each

grid in a single flow direction. The total discharge is calculated at the outlet using linearized Saint-Venant equation and the linear transfer function model (within-grid routing) (Lohmann et al. 1996, 1998). For simulating the dynamics of routing process within a grid cell, the discharge is separated by slow and fast component as described by Duband et al. (1993):

$$\frac{dQ^{Sl}(t)}{dt} = -k \cdot Q^{Sl}(t) + b \cdot Q^F(t) \quad (4.14)$$

Where,

$Q^{Sl}(t)$ - Slow flow (base flow); $Q^F(t)$ - Fast flow (surface runoff)

k and b are parameter, and it is assumed to be constant for each catchment over the period of calculation

$$Q(t) = Q^{Sl}(t) + Q^F(t) \quad (4.15)$$

Both the components are connected by:

$$Q^{Sl}(t) = b \int_0^t \exp(-k(t-\tau)) Q^F(\tau) d\tau + Q^{Sl}(0) \exp(-kt) \quad (4.16)$$

Equation (4.14) can be solved with discrete data:

$$Q^{Sl}(t) = \frac{\exp(-k \cdot \Delta t)}{1 + b \cdot \Delta t} Q^{Sl}(t - \Delta t) + \frac{b \cdot \Delta t}{1 + b \cdot \Delta t} Q(t) \quad (4.17)$$

As mentioned by the equation (4.16), the initial condition $Q^{Sl}(0)$ decays via $\exp(-kt)$ assuming the linear relationship between the effective precipitation P^{eff} , and it is used to find an impulse response function by connecting Q^{Sl} and P^{eff} . The effective precipitation and impulse response function can be calculated iteratively by solving the equation:

$$Q^F(t) = b \int_0^{t_{max}} UH^F(\tau) P^{eff}(t-\tau) d\tau \quad (4.18)$$

Where $UH^F(\tau)$ – impulse response function; t_{max} – time decay for all fast processes.

For discrete case, the equation (4.18) becomes (4.19) and (4.21) with length of data $n \cdot \Delta t$ and $t_{max} = (m-1) \cdot \Delta t$. It is solved iteratively starting with measured precipitation.

$$\begin{pmatrix} Q_m^F \\ \vdots \\ Q_n^F \end{pmatrix} = \begin{pmatrix} P_m^{eff} & \dots & P_1^{eff} \\ \vdots & \ddots & \vdots \\ P_n^{eff} & \dots & P_{n-m+1}^{eff} \end{pmatrix} \begin{pmatrix} UH_0^F \\ \vdots \\ UH_{m-1}^F \end{pmatrix} \quad (4.19)$$

Constraint for each of the iteration:

$$\sum_{i=0}^{m-1} UH_i^F = \frac{1}{1 + \frac{b}{k}} \text{ with } UH_i^F \geq 0 \forall i \quad (4.20)$$

$$\begin{pmatrix} Q_m^F \\ \vdots \\ Q_n^F \end{pmatrix} = \begin{pmatrix} UH_{m-1}^F \dots UH_0^F & 0 & \dots & 0 \\ 0 & \ddots & \ddots & \ddots \\ \vdots & \ddots & \ddots & \ddots \\ 0 & \dots & 0 & UH_{m-1}^F \dots UH_0^F \end{pmatrix} \begin{pmatrix} P_1^{eff} \\ \vdots \\ P_n^{eff} \end{pmatrix} \quad (4.21)$$

Again, constraint for each of the iteration:

$$0 = P_i^{eff} \leq \text{precipitation}_i \forall i$$

P_i^{eff} from equation (4.21) is substituted in the equation (4.19) and the deconvolutions are repeated until the convergence.

Linearized Saint-Venant equation for river routing:

$$\frac{\partial Q}{\partial t} = D \frac{\partial^2 Q}{\partial x^2} - C \frac{\partial Q}{\partial x} \quad (4.22)$$

Where, D and C are optimized for each grid cell. The above equation (4.22) is solved with Green's function (Lohmann et al. 1998).

4.3 VIC MODEL INPUT PARAMETERIZATION

4.3.1 Basin delineation

Initially, the study area was delineated using Digital Elevation Model (DEM). Traditionally, the delineation of catchment area and drainage network was manually carried out using topographic/contour maps. With the advancement of remote sensing

and GIS tools, this process becomes much easier with DEM. The processing of DEM was carried out using an ArcGIS extension called Arc Hydro tools. The delineation of catchment and drainage network from DEM involves the following sequential steps (terrain pre-processing) (Fig. 4.1).

Fill sink: If a cell is surrounded by higher elevation cells, it traps water and restricts the flow. This function modifies the elevation values to rectify this issue.

Flow direction: This function defines the flow direction for a grid, and the values in the grids (ranges from 2^0 to 2^7) specify the direction of the deepest descent from that grid.

Flow accumulation: It computes number of upstream grids that drain into the individual input grids

Stream definition: It defines stream flow path based on the threshold area. The flow accumulation grid having the value greater than the threshold will be assigned the value 1 (stream grid). A smaller threshold generates the denser stream network.

Stream segmentation: It generates a grid of stream segments that are having unique identification.

Catchment grid delineation: It creates grids that are having values indicating to which catchment the grid belongs. The values are corresponding to the stream segment which drains that area.

Catchment polygon processing: It converts raster data into the vector format (Polygon features).

Drainage line processing: Conversion of stream segments to drainage line (feature class). And also, each drainage line holds the identifier indicating to which catchment it belongs.

Watershed processing: It delineates the boundary of a basin at an outlet point defined by the user. This function takes the input from previous steps such as flow direction, stream definition and the catchment processing.

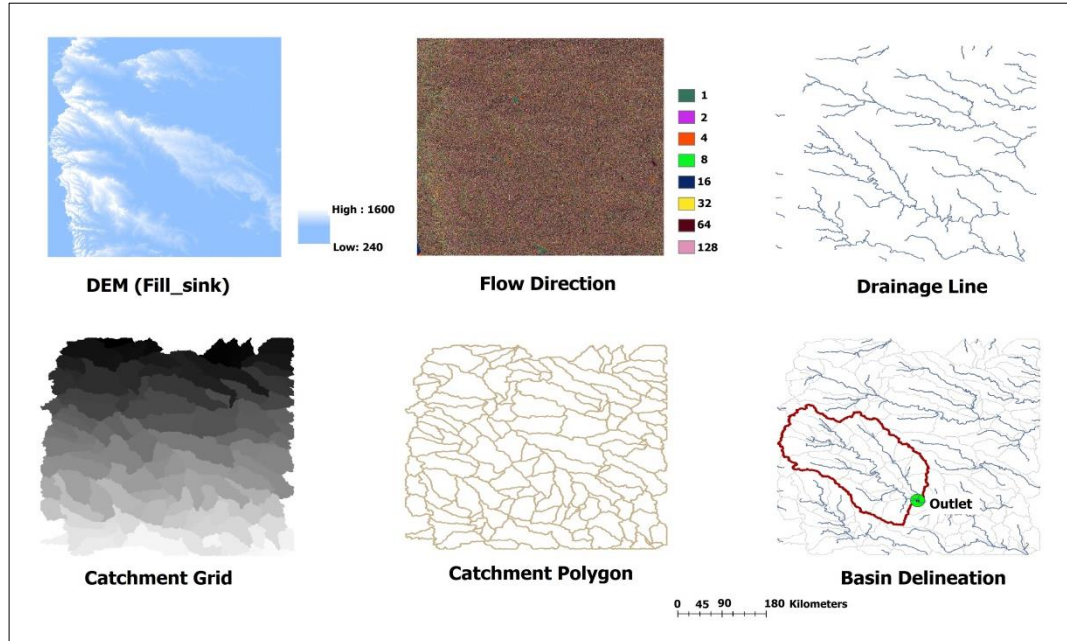


Figure 4.1 Terrain pre-processing for basin delineation

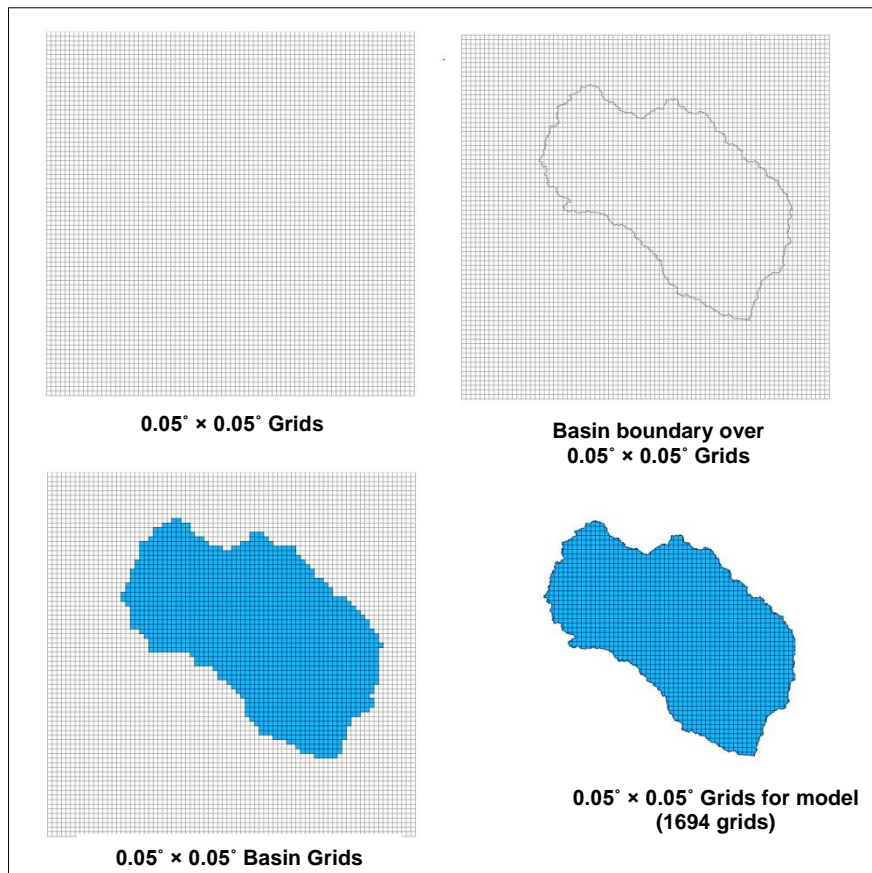


Figure 4.2 Model grids generation

4.3.2 Preparation of model grids

The total drainage area of the basin was discretised into number of grids with a resolution of $0.05^\circ \times 0.05^\circ$ (about 5.5 km). Thus, the model parameterization was made at each grid level. These grids were prepared by using feature class tool in ArcGIS. The approximate boundary extent of the study region, the required size of the grids, number of rows and columns were given as the inputs for the grids generation. The resulted grids were clipped with exact boundary of the study area (Fig. 4.2). Further, the model accepts numbering of grids (indexing) only with descending order along the latitude and ascending order along the longitude. Hence, the grids were numbered accordingly (totally 1694 grids).

4.3.3 Global parameter file

Global parameter file serves as a control file for the model simulations. It defines VIC to the directories of the various input/output files and assigns parameters that govern the model simulation such as modes of operation (water/water and energy balance), length of the simulation and time step etc.

4.3.4 Soil parameter file

Soil parameter file plays a major role in the model simulation. It defines grid cell index (latitude, longitude and grid cell ID), soil hydraulic properties for each grid cell, soil thermal parameters and soil layers depth etc. The soil parameter file is defined as a single ASCII file to the model, with an individual row for each model grid containing various parameters value (Fig. 4.3). The list of various soil parameters for the model simulation and hydraulic properties of different soil are presented in the Table 4.1 and 4.2. The soil parameters were derived from FAO-HWSD global soil map based on USDA soil texture. For each soil, the hydraulic properties (adopted from Cosby et al., 1984; Rawls et al., 1998; Reynolds et al., 2000) were derived by their area-weighted average based on the textural class for each grid. Three soil layer depths (0-10 cm, 10-45 cm and 45-100 cm) were adopted for the model simulation.

Model set up and input parameterization

#Run_cell	Grid_cell	Lat	Long	Infilt	Ds	Dsmax	Ws	c	expt_lyr1	expt_lyr2	expt_lyr3	Ksat_lyr1	Ksat_lyr2							
Ksat_lyr3	Phi_s1	Phi_s2	Phi_s3	Init_moist1	Init_moist2	Init_moist3	Elev	Depth1	Depth2	Depth3	Avg_T	Dp	Bub11	Bub12	Bub13	Qutz1				
Qutz2	Qutz3	Bulk_den1	Bulk_den2	Bulk_den3	Soil_den1	Soil_den2	Soil_den3	Off_gmt	Wcr_FRACT1	Wcr_FRACT2	Wcr_FRACT3	Wcr_FRACT3	Wcr_FRACT3							
Wpwp_Fract1	Wpwp_Fract2	Wpwp_Fract3	Rough_brsoil	Rough_snow	Anul_prec	Res_moist1	Res_Moist2	Res_moist3	Fs_act											
1	1	19.425	73.875	0.1	0.025	8.9	0.65	2	13.6	13.6	13.6	472.8	472.8	472.8	-999	-999	-999	4.06	12.18	20.3
903.32	0.1	0.45	1	25.97	4	-99	-99	-99	-99	-99	-99	1490	1490	1490	2685	2685	2685	5.5	0.2	0.2
0.2	0.14	0.14	0.14	0.001	0.0005	822	0.03	0.03	0.03	0										
1	2	19.425	73.925	0.1	0.025	7.37	0.65	2	13.6	13.6	13.6	472.8	472.8	472.8	-999	-999	-999	4.06	12.18	20.3
828.07	0.1	0.45	1	25.92	4	-99	-99	-99	-99	-99	-99	1490	1490	1490	2685	2685	2685	5.5	0.2	0.2
0.2	0.14	0.14	0.14	0.001	0.0005	642	0.03	0.03	0.03	0										
1	3	19.375	73.775	0.1	0.025	17.51	0.65	2	13.6	13.6	13.6	472.8	472.8	472.8	-999	-999	-999	4.06	12.18	20.3
580.4	0.1	0.45	1	26.03	4	-99	-99	-99	-99	-99	-99	1490	1490	1490	2685	2685	2685	5.5	0.2	0.2
0.2	0.14	0.14	0.14	0.001	0.0005	940.67	0.03	0.03	0.03	0										
1	4	19.375	73.825	0.1	0.025	12.2	0.65	2	13.6	13.6	13.6	472.8	472.8	472.8	-999	-999	-999	4.06	12.18	20.3
916.51	0.1	0.45	1	26	4	-99	-99	-99	-99	-99	-99	1490	1490	1490	2685	2685	2685	5.5	0.2	0.2
0.2	0.14	0.14	0.14	0.001	0.0005	940.67	0.03	0.03	0.03	0										
1	5	19.375	73.875	0.1	0.025	13.43	0.65	2	13.6	13.6	13.6	472.8	472.8	472.8	-999	-999	-999	4.06	12.18	20.3
1140.64	0.1	0.45	1	25.96	4	-99	-99	-99	-99	-99	-99	1490	1490	1490	2685	2685	2685	5.5	0.2	0.2
0.2	0.14	0.14	0.14	0.001	0.0005	818	0.03	0.03	0.03	0										
1	6	19.375	73.925	0.1	0.025	11.14	0.65	2	13.6	13.6	13.6	472.8	472.8	472.8	-999	-999	-999	4.06	12.18	20.3
1020.27	0.1	0.45	1	25.92	4	-99	-99	-99	-99	-99	-99	1490	1490	1490	2685	2685	2685	5.5	0.2	0.2
0.2	0.14	0.14	0.14	0.001	0.0005	695.33	0.03	0.03	0.03	0										
1	7	19.375	73.975	0.1	0.025	9.34	0.65	2	13.6	13.6	13.6	472.8	472.8	472.8	-999	-999	-999	4.06	12.18	20.3
952.7	0.1	0.45	1	25.89	4	-99	-99	-99	-99	-99	-99	1490	1490	1490	2685	2685	2685	5.5	0.2	0.2
0.2	0.14	0.14	0.14	0.001	0.0005	695.33	0.03	0.03	0.03	0										
1	8	19.375	74.025	0.1	0.025	7.08	0.65	2	13.6	13.6	13.6	472.8	472.8	472.8	-999	-999	-999	4.06	12.18	20.3
872.71	0.1	0.45	1	25.85	4	-99	-99	-99	-99	-99	-99	1490	1490	1490	2685	2685	2685	5.5	0.2	0.2
0.2	0.14	0.14	0.14	0.001	0.0005	695.33	0.03	0.03	0.03	0										
1	9	19.325	73.675	0.1	0.025	6.87	0.65	2	13.6	17	19.04	472.8	442.8	424.8	-999	-999	-999	4.06	13.49	23.8
226.97	0.1	0.45	1	26.06	4	-99	-99	-99	-99	-99	-99	1490	1452.5	1430	2685	2685	2685	5.5	0.2	0.22
0.24	0.14	0.18	0.21	0.001	0.0005	910	0.03	0.06	0.08	0										
1	10	19.325	73.725	0.1	0.025	14.46	0.65	2	13.6	14.01	14.25	472.8	469.2	467.04	-999	-999	-999	4.06	12.34	20.72
541.84	0.1	0.45	1	26.03	4	-99	-99	-99	-99	-99	-99	1490	1485.5	1482.8	2685	2685	2685	5.5	0.2	0.21
0.21	0.14	0.15	0.15	0.001	0.0005	910	0.03	0.03	0.03	0										

Figure 4.3 Typical soil parameter file to the model (Initial ten grids are shown)

Table 4.1 Soil Parameters

Parameter	Description
Run_cell	Run (1), Skip (0)
Grid_cell	Grid cell No
Lat	Latitude of the grid
Long	Longitude of the grid
Infilt	Describe the infiltration curve
D_s	Fraction of maximum velocity of the base flow
D_{smax}	Maximum velocity of the base flow (mm/day)
W_s	Fraction of maximum soil moisture
C	Exponent of base flow curve normally 2
Expt	Exponent 'n' in the campell's equation for hydraulic conductivity
Ksat	Saturated hydraulic conductivity
Phi_s	Soil moisture diffusion
Init_moist	Initial moisture content of each layer
Elev	Mean elevation of the grid cell
Depth	Depth of the three soil layer
Avg_T	Average temperature
Dp	Soil damping depth
Bubbling	Bubbling pressure of the soil
Quartz	Quartz content in the soil
Bulk density	Bulk density of the soil layer
Soil density	Soil particle density (normally 2685 Kg/m ³)
Off_gmt	Time zone offset from GMT

Wcr_Fract	Fraction of soil moisture at critical point
Wpwp_Fract	Fraction of soil moisture at wilting point
Rough_baresoil	Surface roughness of bare soil
Rough_snow	Surface roughness of snow
Annual precipitation	Average annual precipitation
Residual moisture	Soil moisture layer residual moisture
Fs_active	Status of include frozen soil algorithm

Table 4.2 Soil hydraulic properties based on soil texture

Soil / property	Clay	Loam	Sandy clay loam	Sandy Loam	Clay Loam
K_{sat} (cm/hr)	3.18	1.97	2.4	5.24	1.77
Bulk density (g/cm ³)	1.39	1.49	1.6	1.57	1.43
Bubbling (cm)	37.3	11.15	28.08	14.66	25.89
Field capacity (cm ³ /cm ³)	0.4	0.29	0.27	0.21	0.34
Wilting point (cm ³ /cm ³)	0.27	0.14	0.17	0.09	0.21
Quartz content	0.25	0.41	0.61	0.69	0.25
Slope of retention curve ‘b’	12.28	5.3	8.66	4.84	8.02
Residual moisture (cm ³ /cm ³)	0.09	0.027	0.068	0.041	0.075

Source: <https://vic.readthedocs.io/en/develop/Documentation/soiltext/>

4.3.5 Meteorological forcing file

The required forcing variables (precipitation, T_{max} and T_{min}) were extracted from IMD meteorological data sets to each model grid in the prescribed format (an ASCII file for each grid contains time series of all forcing) for the model simulation. The model simulation was carried out at daily time step during the study period (1994 – 2005). The directory contains these forcing files, column number and the units of the variable should be specified in the global parameter file.

4.3.6 Improved vegetation parameterization

Land cover classes and their phenological changes play a critical role in the model simulation. MODIS-derived, time series (June 2000–May 2001 and June 2010–May 2011) of both LAI and albedo along with the LU/LC information were used for the model vegetation parameterization. As mentioned in the section 3.2.1, two different periods of LU/LC map (2000 and 2010) were used. In LU/LC 2010 (see Fig. 3.4b), all crop classes were considered as cropland in order to bring the two LU/LC images in the same fashion for further processes. Similarly, other vegetation classes including forest, scrubland and barren/sparse vegetated land were considered for the parameterization.

Iso-clustering: Area of Interest (AOI) corresponds to agriculture/crop classes were generated using the crop classes presented in the LU/LC map. Unsupervised classification (k-mean clustering) was performed with LAI time series (stacked image for the corresponding year) data from agriculture/crop land area for the two periods (2000–2001 and 2010–2011) separately (Fig. 4.4).

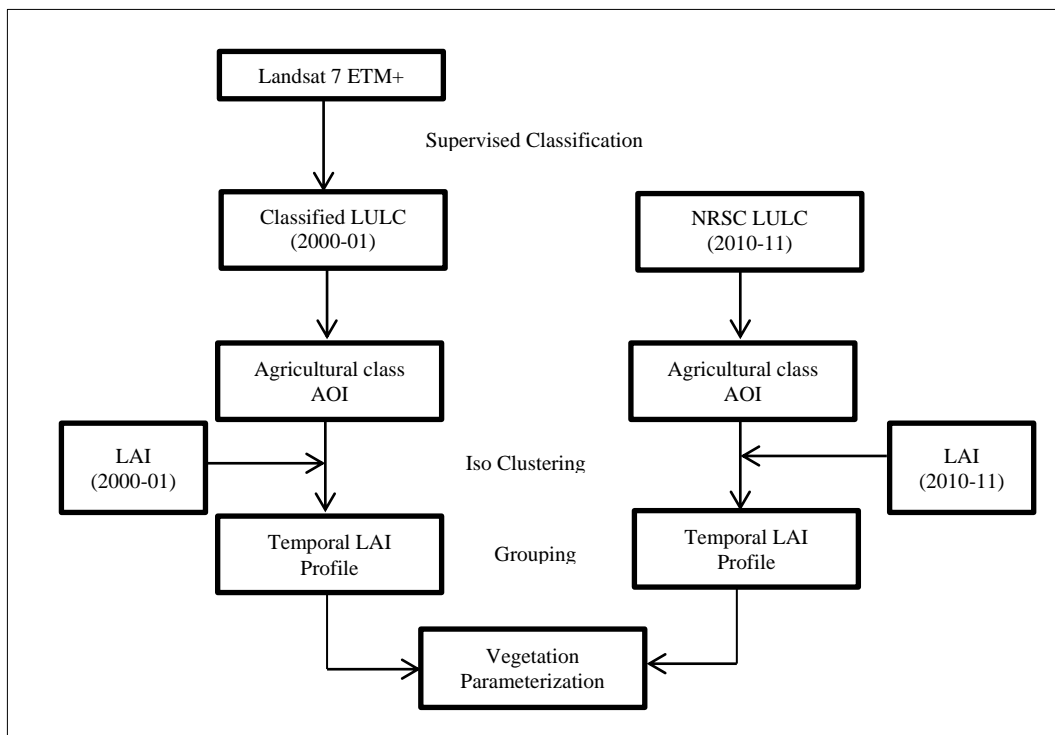


Figure 4.4 Schematic representation of the workflow for vegetation parameterization

The number of classes/clusters was initially chosen as 10 in the algorithm, considering the possible number of vegetation classes present in the agricultural land area according to the LU/LC information. This classification resulted in only nine different classes after the possible iterations (until that 95% or more pixels stay in the same class/cluster between one iteration and the next). These classes were grouped based on the temporal profile (Fig. 4.5 and 4.6). Further, the locations of each group were identified and predominant crop within each group in that particular location/district (available at <https://data.gov.in>) were considered for the model vegetation parameterization (Fig. 4.7 and 4.8).

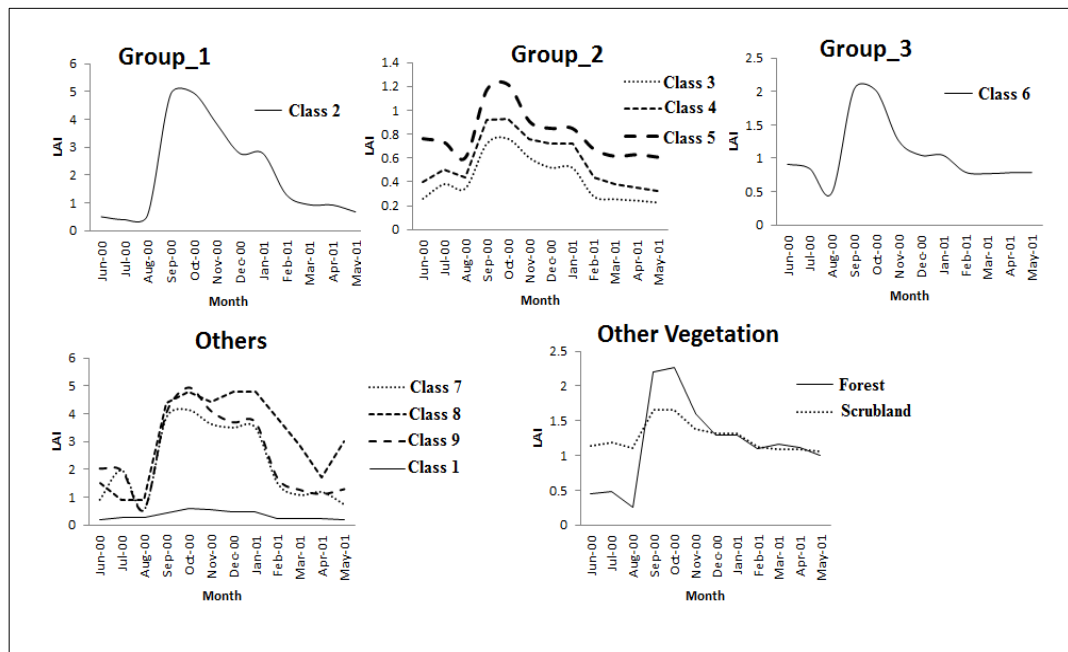


Figure 4.5 Temporal LAI profiles of the vegetation classes for the year 2000-01

The classes 1, 7, 8 and 9 were not considered since their count was less than three pixels in the study area (Fig. 4.5). For other vegetation (forest and scrubland), average LAI values were taken from represented random samples in the study area (Fig. 4.5 and 4.6). These practices enable to come up with the number of land cover classes for the model, and hence improved vegetation parameterization by integrating region-specific condition. The entire vegetation parameterization in the model development is comprised of vegetation parameter and vegetation library file. Vegetation parameter file was prepared by compiling the rooting depth information for each vegetation class

(Table 4.3 and 4.4) and vegetation cover fraction for each grid cell. Thus, vegetation parameter file consists of vegetation cover fraction with its class index for each grid cell and corresponding root depth fraction for each vegetation class (Fig. 4.9). The rooting depth information enables different vegetation to extract soil moisture from upper and deeper soil layers, respectively.

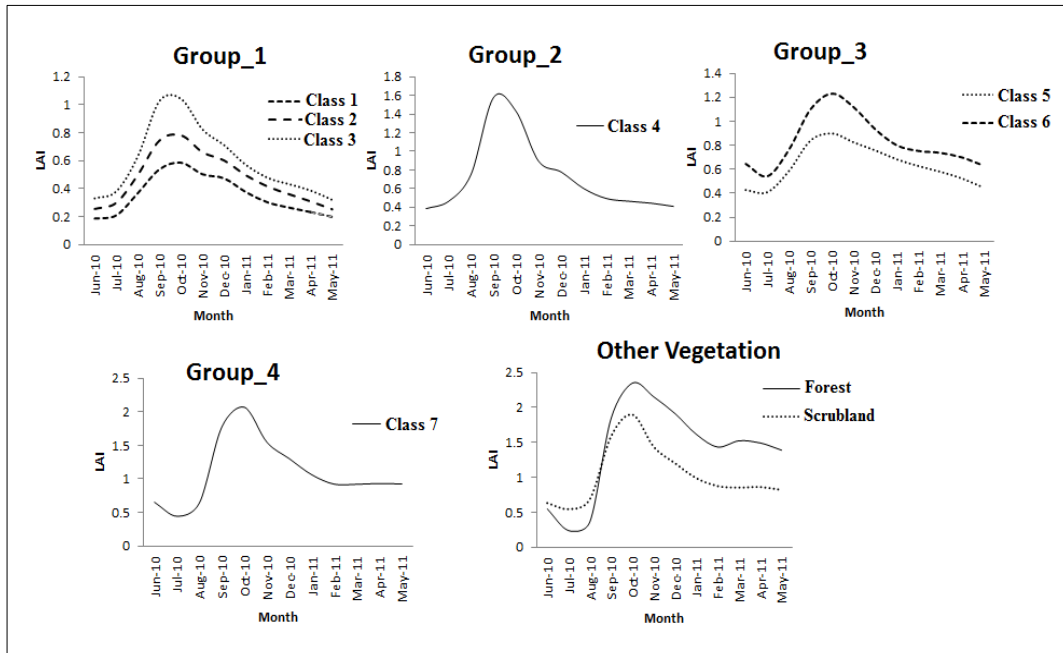


Figure 4.6 Temporal LAI profiles of the vegetation classes for the year 2010-11

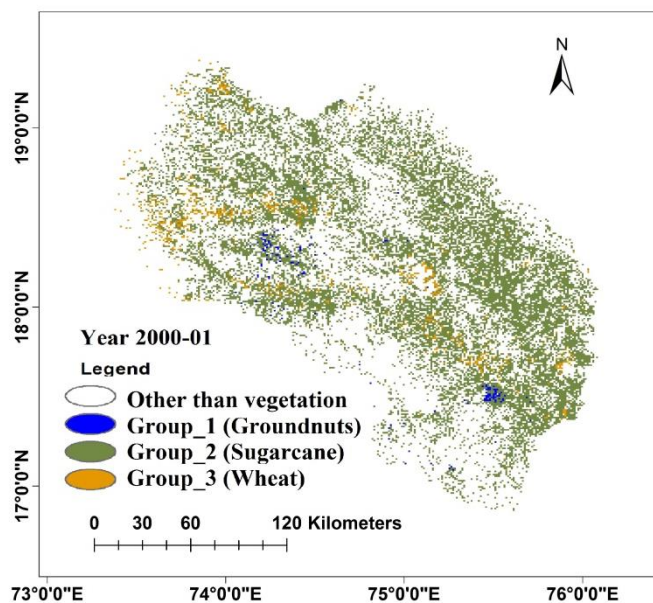


Figure 4.7 Spatial location of LAI groups for the year 2000–2001

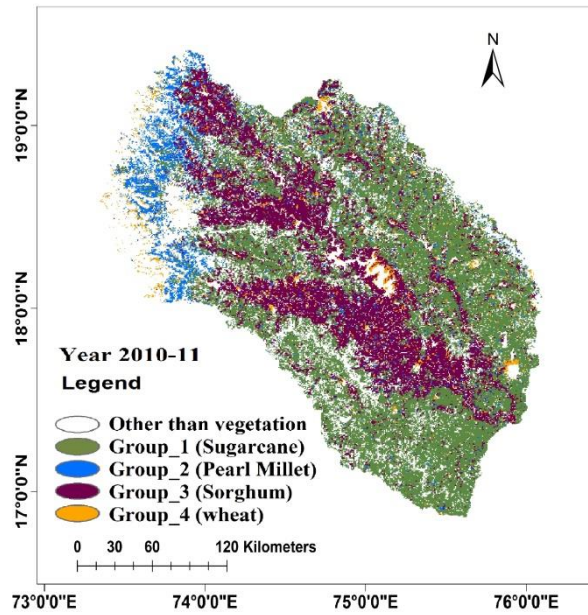


Figure 4.8 Spatial location of LAI groups for the year 2000–2001

Grid No	No. of land cover classes in that grid	Soil depth	Root distribution
①	4		
4	0.01521 0.100 0.200 0.450 0.400 1.000 0.400		
5	0.36407 0.100 0.400 0.450 0.500 1.000 0.100		
6	0.61850 0.100 0.000 0.450 0.000 1.000 0.000		
8	0.00222 0.100 0.000 0.450 0.000 1.000 0.000		
△	5		
5	0.11893 0.100 0.400 0.450 0.500 1.000 0.100		
6	0.88107 0.100 0.000 0.450 0.000 1.000 0.000		
3	5		
4	0.39270 0.100 0.200 0.450 0.400 1.000 0.400		
5	0.32049 0.100 0.400 0.450 0.500 1.000 0.100		
6	0.27546 0.100 0.000 0.450 0.000 1.000 0.000		
7	0.00284 0.100 0.000 0.450 0.000 1.000 0.000		
8	0.00852 0.100 0.000 0.450 0.000 1.000 0.000		
4	5		
4	0.23885 0.100 0.200 0.450 0.400 1.000 0.400		
5	0.32453 0.100 0.400 0.450 0.500 1.000 0.100		
6	0.41344 0.100 0.000 0.450 0.000 1.000 0.000		
7	0.00616 0.100 0.000 0.450 0.000 1.000 0.000		
8	0.01702 0.100 0.000 0.450 0.000 1.000 0.000		
5	6		
3	0.00241 0.100 0.600 0.450 0.300 1.000 0.100		
4	0.14581 0.100 0.200 0.450 0.400 1.000 0.400		
5	0.44850 0.100 0.400 0.450 0.500 1.000 0.100		
6	0.40287 0.100 0.000 0.450 0.000 1.000 0.000		
7	0.00010 0.100 0.000 0.450 0.000 1.000 0.000		
8	0.00031 0.100 0.000 0.450 0.000 1.000 0.000		

Figure 4.9 Typical vegetation parameter file for the LULC 2000 (Initial five grids are shown)

Table 4.3 Rooting depth information adopted for vegetation parameter with LULC 2000

Class-Index	Classes	1 st layer depth	Root distribution	2 nd layer depth	Root distribution	3 rd layer Depth	Root distribution
1	Groundnuts	0.1	0.95	0.45	0.05	1	0
2	Sugarcane	0.1	0.85	0.45	0.15	1	0
3	wheat	0.1	0.6	0.45	0.3	1	0.1
4	Forest	0.1	0.2	0.45	0.4	1	0.4
5	Scrubland	0.1	0.4	0.45	0.5	1	0.1
6	Barren Land	0.1	0	0.45	0	1	0
7	Water Bodies	0.1	0	0.45	0	1	0
8	Built-Up	0.1	0	0.45	0	1	0

Table 4.4 Rooting depth information adopted for vegetation parameter with LULC 2010

Class-Index	Classes	1 st layer depth	Root distribution	2 nd layer depth	Root distribution	3 rd layer Depth	Root distribution
1	Sugarcane	0.1	0.85	0.45	0.15	1	0
2	Pearl millet	0.1	0.7	0.45	0.25	1	0.05
3	Sorghum	0.1	0.8	0.45	0.15	1	0.05
4	wheat	0.1	0.6	0.45	0.3	1	0.1
5	Forest	0.1	0.2	0.45	0.4	1	0.4
6	Scrubland	0.1	0.4	0.45	0.5	1	0.1
7	Barren Land	0.1	0	0.45	0	1	0
8	Water Bodies	0.1	0	0.45	0	1	0
9	Built-Up	0.1	0	0.45	0	1	0

Vegetation library file defines the dynamic vegetation parameters such as stomatal resistance (~ 100 s/m), albedo, minimum architectural resistance (~ 2 s/m (grassland): ~ 50 s/m (evergreen forest)), LAI, vegetation height (H) roughness length ($0.123 \times H$) and displacement height ($0.67 \times H$) for each land cover classes (Fig. 4.10) (<https://vic.readthedocs.io/en/master/Documentation/Drivers/Classic/VegLib/>)

4.3.7 Elevation band file

The basin elevation band information was included in the model simulation, in order to represent more realistic hydrology in the Western Ghats region. Elevation band file was prepared using STRM-DEM, which was classified into four different elevation classes with the interval of 300 m (Fig. 4.11). The elevation band file defines the area fraction of each class within a grid cell, mean elevation and precipitation factor (fraction of cell precipitation) for each grid cell to the model (Fig. 4.12). The mean elevation of each band is used in the model to lapse the grid average pressure, temperature and precipitation. The values of area fraction itself were set as the precipitation factor, since the fraction of cell precipitation is hard to measure.

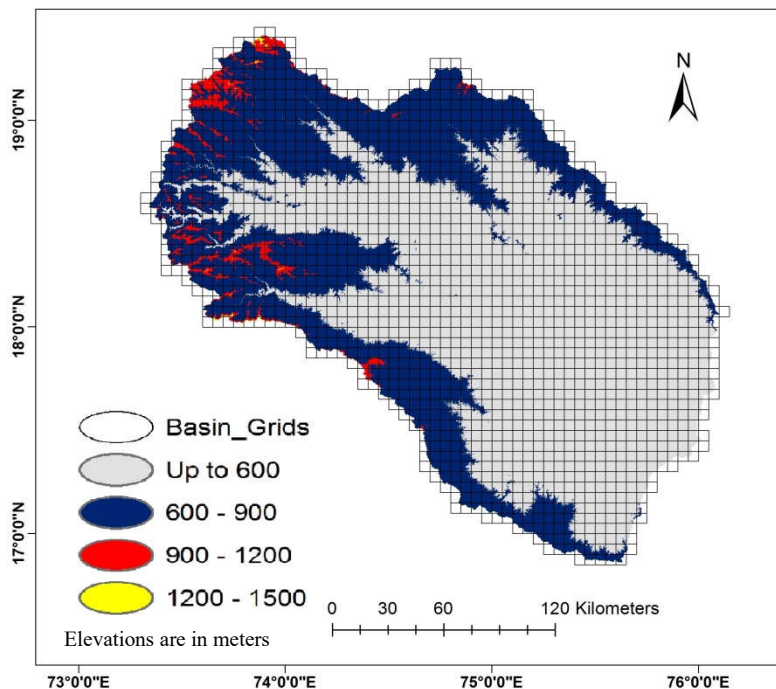


Figure 4.11 Classification of the basin elevation

1	0.00	0.68	0.24	0.07	0.00	818.21	922.93	1253.83	0.00	0.68	0.24	0.07
2	0.00	0.83	0.17	0.00	0.00	862.87	927.18	0.00	0.00	0.83	0.17	0.00
3	0.36	0.29	0.20	0.14	342.16	739.86	1014.57	1251.23	0.36	0.29	0.20	0.14
4	0.00	0.53	0.29	0.17	0.00	725.44	1048.04	1231.80	0.00	0.53	0.29	0.17
5	0.00	0.01	0.68	0.31	0.00	832.20	1076.23	1248.75	0.00	0.01	0.68	0.31
6	0.00	0.08	0.86	0.06	0.00	889.79	1017.91	1227.17	0.00	0.08	0.86	0.06
7	0.00	0.27	0.73	0.00	0.00	880.67	946.66	0.00	0.00	0.27	0.73	0.00
8	0.00	0.57	0.43	0.00	0.00	865.22	928.23	0.00	0.00	0.57	0.43	0.00
9	0.76	0.24	0.00	0.00	350.79	744.51	924.25	0.00	0.76	0.24	0.00	0.00
10	0.34	0.34	0.29	0.02	416.95	696.21	1041.25	1224.37	0.34	0.34	0.29	0.02
11	0.18	0.69	0.12	0.00	436.08	765.82	951.11	1214.64	0.18	0.69	0.12	0.00
12	0.00	0.98	0.02	0.00	0.00	701.03	953.63	0.00	0.00	0.98	0.02	0.00
13	0.00	0.67	0.32	0.01	0.00	835.09	1026.04	1209.66	0.00	0.67	0.32	0.01
14	0.00	0.61	0.39	0.00	0.00	776.71	937.91	0.00	0.00	0.61	0.39	0.00
15	0.00	0.86	0.14	0.00	0.00	760.00	942.52	1203.00	0.00	0.86	0.14	0.00
16	0.00	0.76	0.24	0.00	0.00	889.08	904.18	0.00	0.00	0.76	0.24	0.00
17	0.37	0.49	0.14	0.00	352.86	770.20	991.64	0.00	0.37	0.49	0.14	0.00
18	0.00	0.91	0.09	0.00	0.00	759.65	1013.28	1214.67	0.00	0.91	0.09	0.00
19	0.00	0.82	0.17	0.01	0.00	834.70	1009.57	1217.18	0.00	0.82	0.17	0.01
20	0.00	0.83	0.16	0.00	0.00	762.48	1010.81	1208.35	0.00	0.83	0.16	0.00

Figure 4.12 Typical Elevation band file (Initial 20 grids are shown)

4.4 ROUTING MODEL INPUT PARAMETERIZATION

The output fluxes from the VIC model are given as the input to the routing model. The required input parameters to the routing model are flow direction, flow fraction, flow velocity (set as 1.5 m/s) and grid cell impulse response (UH file). The directory/locations of all the parameter files and length of the model simulation are defined in a routing control file (Fig. 4.13).

```

# INPUT FILE FOR THE UPPER BHIMA BASIN.
# NAME OF FLOW DIRECTION FILE
./direction.txt
# NAME OF VELOCITY FILE
.false.
1.5
# NAME OF DIFF FILE
.false.
800
# NAME OF XMASK FILE
.false.
5500
# NAME OF FRACTION FILE
.true.
./fraction.txt
# NAME OF STATION FILE
./station.txt
# PATH OF INPUT FILES AND PRECISION
./Test/fluxes_
3
# PATH OF OUTPUT FILES
./Rout_Out/
# YEAR AND MONTH OF VIC OUTPUT TO ROUTE & ROUTED OUTPUT TO WRITE
1996 6 2005 5
1996 6 2005 5
# NAME OF UNIT HYDROGRAPH FILE
./UB_UHfile.txt

```

Figure 4.13 Typical routing control file

4.4.1 Flow direction file

The flow direction for the basin grids are defined in this file. The flow direction of a grid is indicated by a value ranging from 1 to 8. The mean elevation of each grid was calculated, and the flow direction values were assigned in a way that the direction of the deepest descent from that grid, considering the mean elevation of the surrounding grids (Fig. 4.14). The flow direction file is supplied to the routing model as an arc/info ASCII grid format.

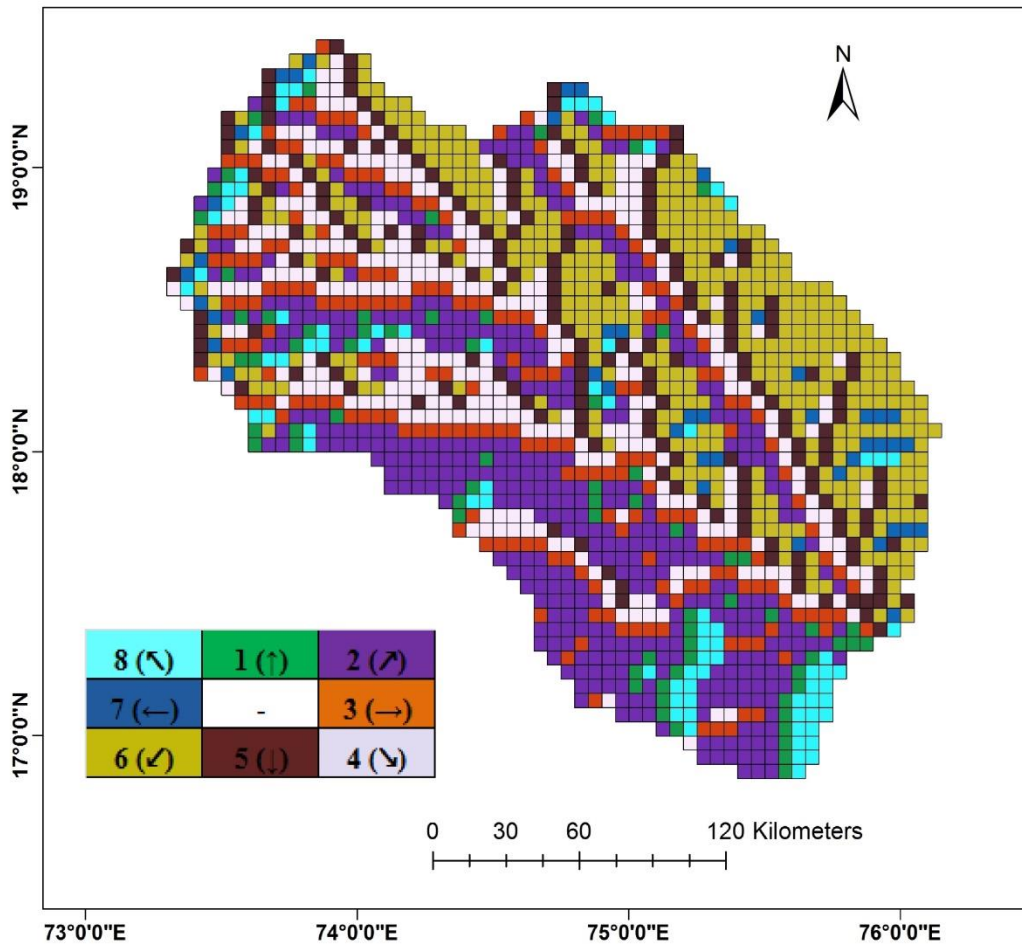


Figure 4.14 Flow directions of the basin grids

4.4.2 Flow fraction file

Flow fraction defines the fraction of each grid that flows into the catchment. The grids that are fully contributing their runoff and baseflow components to the catchment

were assigned the value as one, for the boundary grids, a fraction of the contributed area was calculated and assigned to the model (Fig. 4.15). The flow direction file is also supplied to the routing model as an arc/info ASCII grid format.

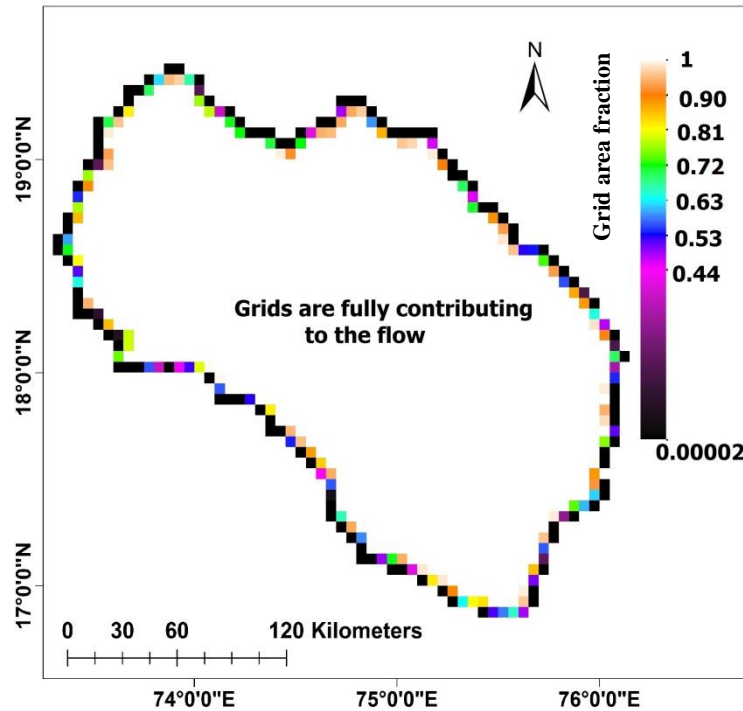


Figure 4.15 Basin grid flow fraction

4.4.3 Station location and UH files

The outlet grid of the basin is generally defined in the station location file. Multiple numbers of grid locations can be defined within the basin. Grid locations are indicated by rows (from bottom) and columns numbers (from left). The grid locations of two stations (Takli and Wadakbal) are shown in figure 4.16a. The grid cell impulse response function is defined in UH file (Fig. 4.16b). [b]

[a]

```
1 WADAK      52 14 -9999
NONE
1 TAKLI     51 12 -9999
NONE
```

```
0 0.01
1 0.24
2 0.33
3 0.18
4 0.24
5 0.00
6 0.00
7 0.00
8 0.00
9 0.00
10 0.00
11 0.00
```

Figure 4.16 Typical station location file [a] and UH file [b]

MODEL PERFORMANCE AND HYDROLOGICAL IMPACTS OF LU/LC CHANGE

In this chapter, a detailed discussion about the model parameters, calibration strategy and performance of the model is presented. In general, the catchment characteristics are approximated in the hydrological models, either in lumped or distributed manners through mathematical equations. Therefore, it is essential to calibrate the model parameters through input/output observed values for simulating the catchment responses. During the calibration, the model parameters are adjusted so as to closely approximate the process. A detailed assessment of LU/LC change impacts on the flow regime of the Upper Bhima basin is also presented in this chapter.

5.1 MODEL CALIBRATION AND VALIDATION

The model was calibrated and validated using the observed streamflow at two locations in the study area (Takli and Wadakbal stations) for the period of June 1994 – May 1999 and June 1999 – May 2001, respectively. The initial two years (1994 – 1996) were considered as the model spin-up period. The model simulation was carried out at daily time step, however, the monthly accumulated flows were utilised during the calibration and validation. The reason for evaluating with monthly flows is mainly the presence of discontinuity in the daily observed flow, which in turn might introduce difficulty while estimating reasonable parameter valued in the calibration. The model performance was evaluated using the coefficient of determination (R^2) and Nash-Sutcliffe Efficiency (NSE) (Nash and Sutcliffe 1970).

The parameters used in the calibration were: D_{smax} [Range: 0 – 30 mm/day]-fraction of maximum baseflow velocity and it has been assigned to each grid based on the grid slope and saturated hydraulic conductivity (K_{sat}); D_s [Range: 0 – 1] – fraction of D_{smax} , and higher the values of D_s will increase the baseflow in the simulation; W_s [Range: 0 - 1] - fraction of maximum soil moisture, and higher the values of W_s will

raise the water content required for rapidly increasing non-linear baseflow, which will tend to delay runoff peaks; b_{inf} [Range: 0 – 0.4] - exponent of infiltration capacity curve, and higher value of b_{inf} gives lower infiltration and yields higher surface runoff in the simulation. The parameters were calibrated at each grid level based on the individual grid K_{sat} values by trial and error method, considering the above model behaviour related to the parameters values. Thus, this approach adds physical meaning for assigning the parameter to the model simulation. The calibration parameter, range and their calibrated values are listed in Table 5.1

Table 5.1 Calibration parameter, range and calibrated value

If grid cell Avg K_{sat} (cm/hr)	Calibrated Values					Range
	>3.5	>3	>2.5	>2	<1.5	
b_{inf}	0.0125	0.025	0.05	0.075	0.1	10^{-5} - 0.4
D_s	0.0125	0.025	0.025	0.025	0.05	0 - 1
D_{smax} (mm/day)	Calculated for each grid based on K_{sat} and slope					0 - 30
W_s	0.6	0.7	0.7	0.7	0.65	0 – 1

5.2 MODEL PERFORMANCE

The model performance was found to be reasonably good in calibration and hence the simulated values were very close to observed discharge (Fig. 5.1). The model resulted with R^2 of 0.83 and 0.91 for the stations Takli and Wadakbal respectively. Similarly, the NSE values were also reasonable for the selected stations (NSE: 0.78 and 0.87). Very consistent results were found in the validation with R^2 [0.79, 0.89] and NSE [0.55, 0.71] (Fig. 5.2). Overall, the performance of the model for the data collected at the Wadakbal station was better than Takli station, both in calibration and validation. This is due to no large storage structures in the upstream of the station location (Sina catchment), compared to the Takli station. Though the short period of datasets was

used during the calibration and validation, the results showed support for the model capability to reproduce the annual and seasonal variation in streamflow in the Upper Bhima basin.

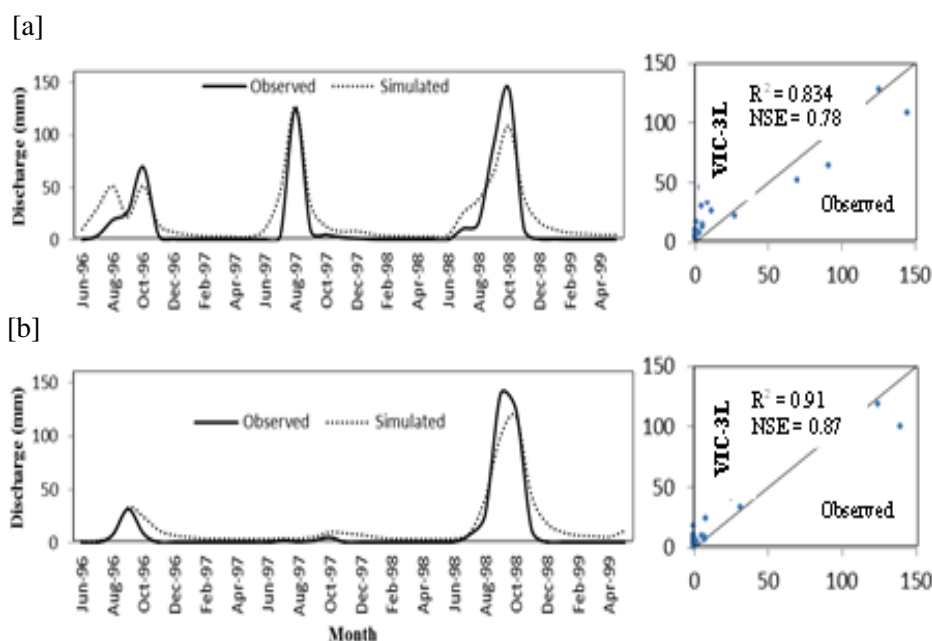


Figure 5.1 Observed and simulated discharge during calibration: a) Takli b) Wadakbal

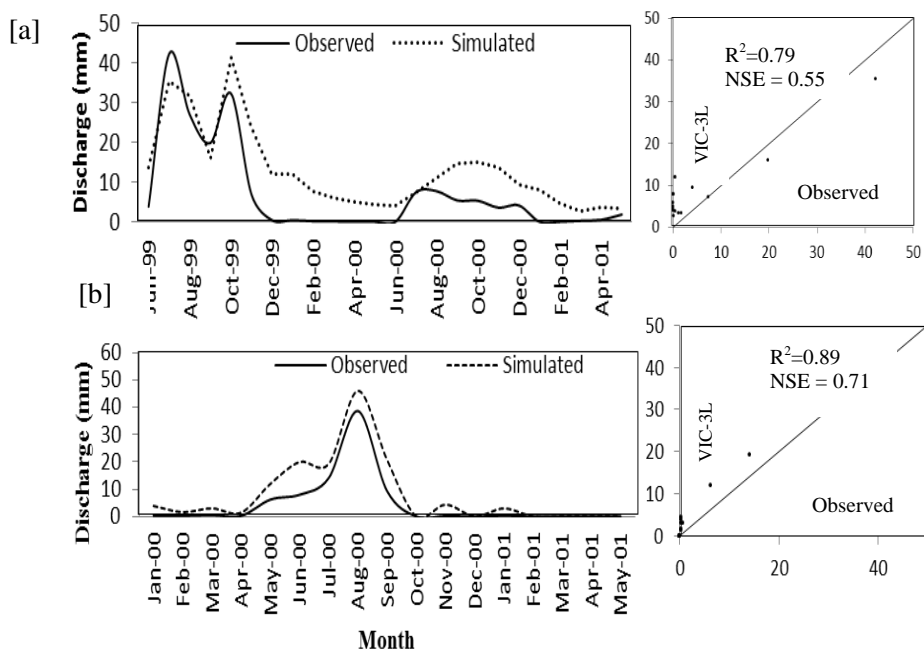


Figure 5.2 Observed and simulated discharge during validation: [a] Takli [b] Wadakbal

5.2.1 Inter comparison of ET estimation

The calibrated and validated model was used to simulate the ET with a resolution of $0.05^\circ \times 0.05^\circ$ (Model resolution: about 5.5km). The model simulated and Moderate Resolution Imaging Spectroradiometer (MODIS) derived ET was compared, and evaluated with ET estimate based on FAO-56 Penman-Monteith (PM) approach during water year June 2001 – May 2005. The observed meteorological variables (T_{\max} , T_{\min} , relative humidity, wind speed, and sunshine hours) at the Pune station were collected from IMD- Agromet station for the estimation of ET using FAO-56 PM method.

The FAO-56 PM model is recognized as a standard model for estimating reference evapotranspiration and being used for evaluating other models worldwide. The equation being used for estimating ET_0 is described as (Allen et al. 1998):

$$ET_0 = \frac{0.408\Delta(Rn - G) + \gamma \frac{37}{T_a + 275} u_2 [e^o(T_a)(1 - Rh)]}{\Delta + \gamma(1 + 0.34u_2)} \quad (5.1)$$

Where,

R_n - Net solar radiation at the reference grass surface ($\text{MJ m}^{-2} \text{h}^{-1}$)

G - Soil heat flux density ($\text{MJ m}^{-2} \text{h}^{-1}$)

T_a - Mean hourly air temperature ($^\circ\text{C}$)

Δ - Saturation slope of vapor pressure curve ($\text{kPa } ^\circ\text{C}^{-1}$)

$e^o(T_a)$ - Saturation vapor pressure at air temperature T_a (kPa)

u_2 - Average hourly wind speed at 2 m height (ms^{-1})

Rh - Relative humidity

γ - psychrometric constant ($\text{kPa } ^\circ\text{C}^{-1}$)

The ET estimation from model and MODIS (the grid covered the station location) was evaluated with observed (FAO-56 PM). The ET estimation from MODIS showed

an under prediction with observed [RMSE of 7.51 mm/8-days and R^2 of 0.57], whereas VIC simulated ET has a good agreement with R^2 of 0.745 and RMSE of 5.62 mm/8-days (Fig. 5.3). However, the MODIS-derived ET was reasonably good in dry months (March, April and May). These results are consistent with similar earlier studies (Ruhoff et al. 2013; Srivastava et al. 2017).

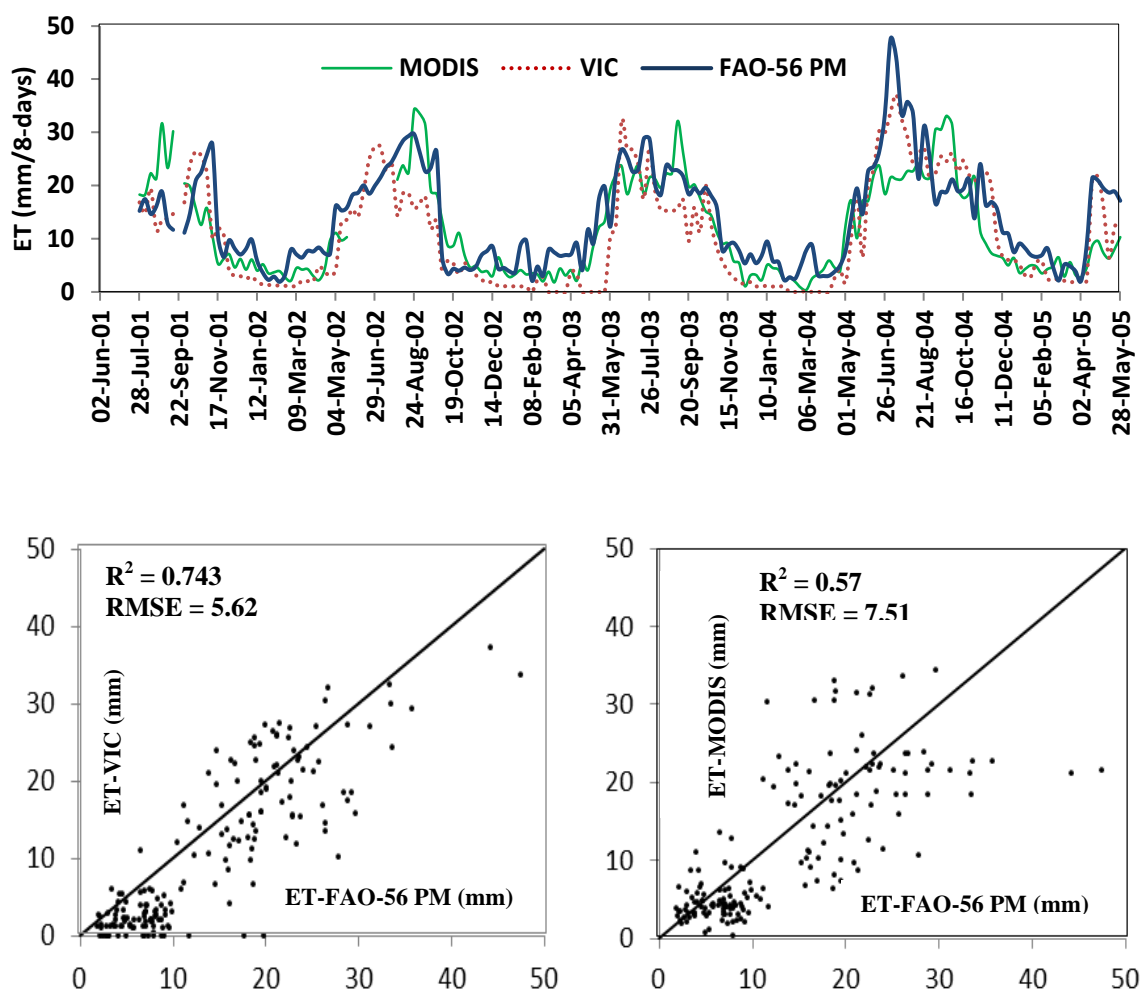


Figure 5.3 Comparison of 8-days ET estimation from VIC, MODIS and FAO-56PM during the period June 2001 – May 2005

It was observed that the annual average ET estimates from VIC-3L, MODIS and FAO-56 PM at the selected grid were 465, 602 and 613 mm, respectively. It is noted that the LU/LC patterns of the selected grid were mainly of sugarcane (36%),

sorghum (12%), scrubland (39%), barren land (12%), built-up (30%). Further, the basin average of 8-day and monthly ET from VIC model and MODIS was compared. It was observed that the average monthly ET loss in the basin ranges from about 6 – 98 mm during the year 2001 – 05 (Fig 5.4).

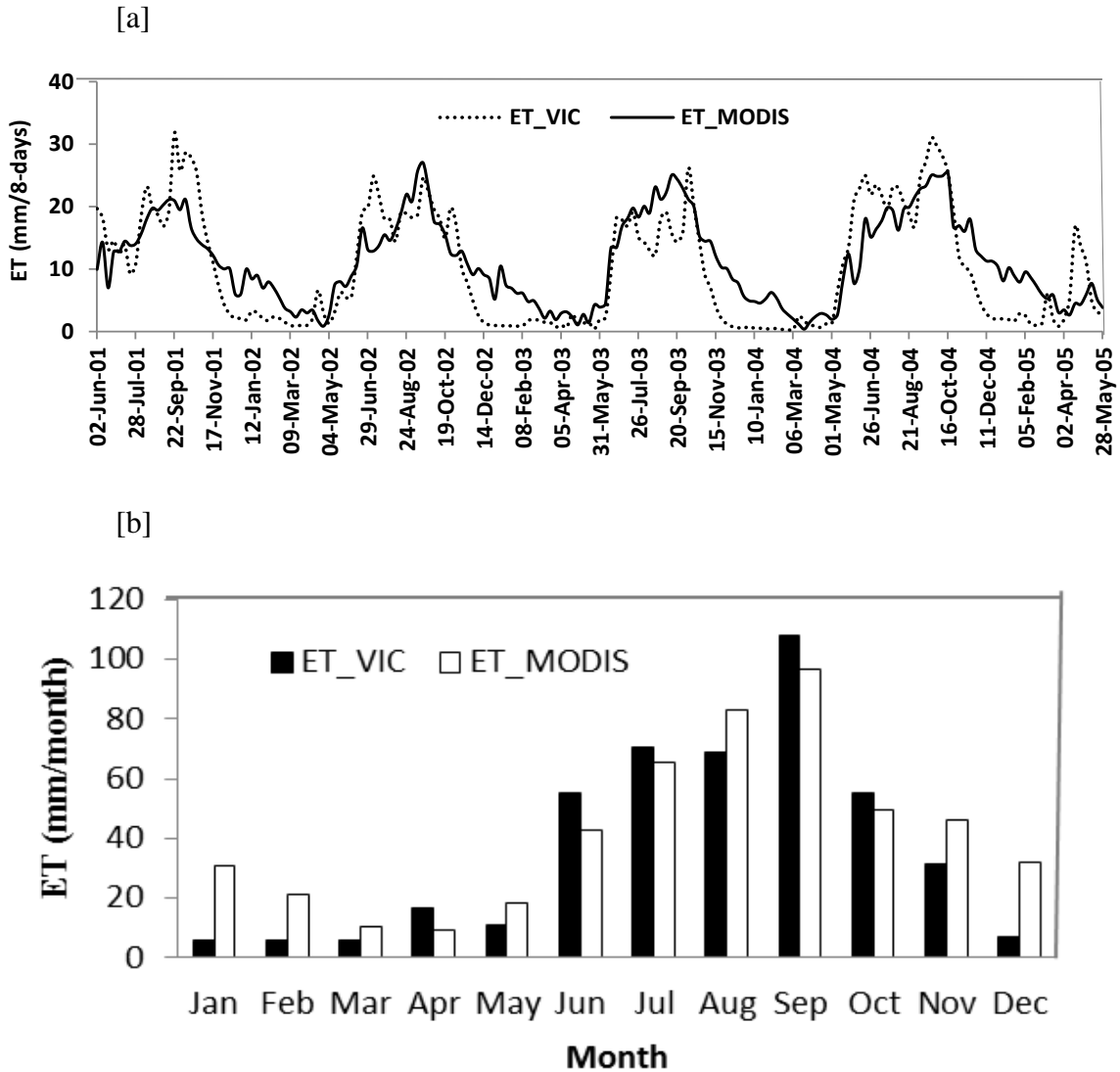


Figure 5.4 Comparison of basin average ET during the period 2001-05: [a] 8-day [b] month-wise

5.2.2 Validation of soil moisture

The model was used to simulate the soil moisture (about 5.5 km resolution) at different soil depth (0 – 10 cm, 10 – 45 cm and 45 – 100 cm). The simulated soil moisture at 10 cm and 45 cm were evaluated with field observed soil moisture at Pune

station. A comparison of VIC simulated soil moisture (the model grid covering Pune station) with field observation indicated that the model is able to capture soil moisture dynamics reasonably good (Fig. 5.5). However, the simulated soil moisture at 45 cm showed relatively poor results (R^2 of 0.432 and NSE of 0.498). This may be due to the fact that the crop-covered agricultural land was assumed in the grid for the hydrological modelling as it was indicated by LULC information, while the field observation mostly from the bare soil. Further, it is noted that point measurements are compared with model grid average (about 5.5km)

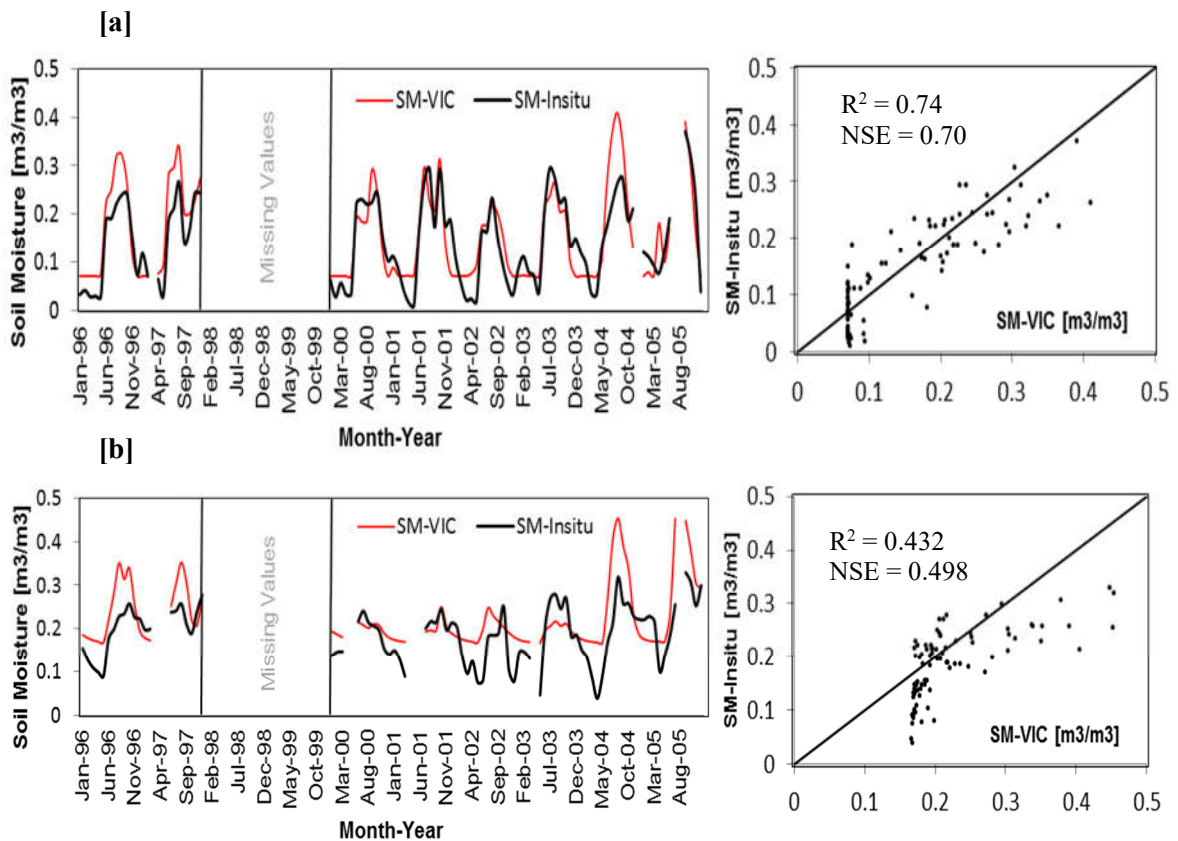


Figure 5.5 Validation of model simulated soil moisture with field observed soil moisture at [a] 10 cm and [b] 45 cm soil depth

Further, the simulated soil moisture (at layer 1) was also compared with the published soil moisture data ($0.5^{\circ} \times 0.5^{\circ}$ resolution) (Das and Maity, 2015), referred as SM-DM15 hereafter). The modelled soil moisture was averaged to the resolution of SM-DM15, and the comparison showed a good correlation (Fig. 5.6). The correlation coefficient values were ranging from 0.45 – 0.763, and more than 50% of the grid showed the values of above 0.55 during the simulation period 1996 - 2005.

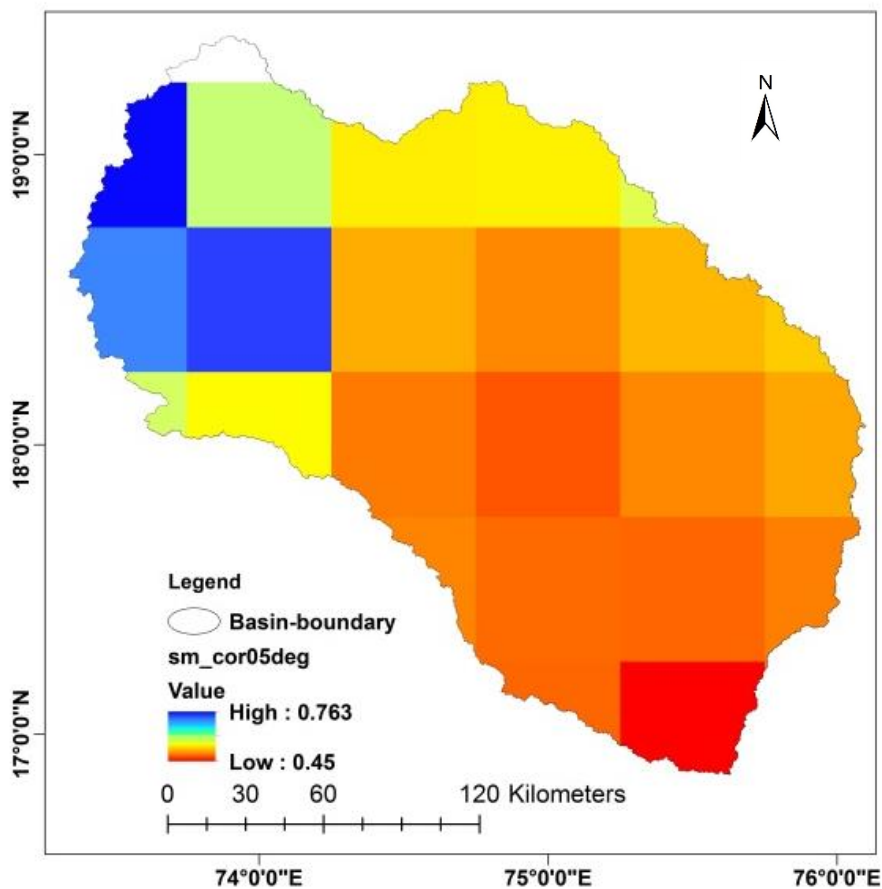


Figure 5.6 Correlation coefficient of VIC-soil moisture with SM-DM15

5.3 LU/LC CHANGE AND WATER BALANCE

The model was run using LU/LC information acquired in the year 2000 and 2010 separately with observed meteorological forcing from 1996 to 2001, and soil datasets have been kept constant. As the land cover scenario changed from 2000 to 2010, the total area enclosed by agricultural land, water bodies and built-up increased from 37 to 73%, 1.13 to 3.3% and 0.66 to 2.79%, respectively. Similarly, the total area enclosed by forest land, scrubland and barren/sparse vegetation land decreased from 1.99 to 1.09%, 17.76 to 4.10% and 41.4 to 15.68%, respectively (see Fig. 3.4 in Chapter 3). The results support the most evident changes occurred in the agricultural land, barren/sparse vegetation land, scrubland and built-up when comparing the LU/LC 2000 and 2010. The model predicted average monthly surface runoff, baseflow and evapotranspiration (ET) were evaluated for different land cover

parameterization during period (1996-2001) (Table 5.2). It was observed that basin receives rainfall only in the south-west monsoon (June – September). The average annual rainfall during the period (1996 – 2001) was calculated as 826.49 mm, which resulted in an average annual surface runoff of 157.51 mm (19.05%) (Table 5.3). The average annual surface runoff and baseflow over the basin have decreased from 157.41 to 127.72 mm and 82.58 to 77.76 mm respectively (Table 5.3). The low runoff during the year 2000-01 is probably due to excessive ET (i.e. about 80% of the total rainfall). Further, this can be confirmed with a low ET (i.e. about 59% of total rainfall) during the year 1998 – 99 with high runoff (Table 5.3). The average annual evapotranspiration over the basin increased from 562.36 to 606.25 mm, which is the major sink in the hydrological balance (about 60 – 80% of rainfall and 40% occurred only in monsoon season) predominantly used by the agricultural crops (Tables 5.2 & 5.3). These changes can be attributed to LU/LC by increased agricultural land, while a decrease in barren/sparse vegetation land and scrubland due to demanding irrigation development in the study area.

The results from average monthly water balance statistics are consistent with the different earlier studies reported in the Upper Bhima basin (Immerzeel and Droogers 2008; Immerzeel et al. 2008; Garg et al. 2012). Those studies used Soil Water Assessment Tool (SWAT) to characterize the hydrological processes in the basin and sub-basin level, while the present study assessed the LU/LC change impact on water balance at finer grid level in the basin (about 5.5 km resolution) with improved vegetation parameterization incorporating region specific condition. It was observed that the changes due to LU/LC impacts on hydrology are balancing over the basin level (Table 5.3). Thus, the spatial variation in each component was further analysed at grid level. Such detailed assessment at a finer scale provides important information to decision makers, for framing the mitigation and adaptation policies under changing LU/LC scenarios. The spatial variation of each component for both LU/LU scenarios was assessed for the water year 2000-01 (1 June 2000 – 31 May 2001), because the annual average rainfall in the year 2000-01 (about 610 mm) (Table 5.3) is proximate to long-term average annual rainfall (about 650 mm) observed and reported in the Upper Bhima basin (Gartley et al. 2009; Garg et al. 2012).

Table 5.2 Average monthly statistics for water balance components during period (1996 – 2000)

Month	Avg_Rainfall (mm)	ET (mm)		Change (mm)	Baseflow (mm)		Change (mm)	Runoff (mm)		Change (mm)
		Lulc2000	Lulc2010		Lulc2000	Lulc2010		Lulc2000	Lulc2010	
Jan	0.98	14.75	25.33	10.58	0.01	0.01	0.00	6.59	4.73	-1.86
Feb	1.07	7.32	16.94	9.62	0.01	0.01	0.00	4.74	3.46	-1.27
Mar	0.94	4.95	10.81	5.86	0.01	0.00	0.00	4.51	3.33	-1.17
Apr	4.16	5.53	7.64	2.10	0.04	0.03	-0.01	3.94	2.94	-1.00
May	22.79	19.12	19.35	0.23	0.53	0.31	-0.23	3.68	2.76	-0.92
Jun	143.70	74.58	68.92	-5.66	7.08	6.55	-0.53	5.20	3.95	-1.25
Jul	166.17	86.91	77.93	-8.99	22.69	22.98	0.29	16.26	14.75	-1.51
Aug	147.07	73.53	80.44	6.90	22.22	21.84	-0.38	26.08	23.31	-2.77
Sep	173.30	89.79	95.38	5.59	15.13	13.40	-1.73	26.13	21.25	-4.88
Oct	136.11	99.64	104.70	5.06	14.21	12.05	-2.16	33.31	27.00	-6.31
Nov	21.80	56.89	60.81	3.92	0.46	0.41	-0.06	17.37	13.33	-4.04
Dec	6.95	29.34	38.00	8.66	0.19	0.16	-0.03	9.61	6.90	-2.71

Table 5.3 Annual sums of water balance components during the period (1996 – 2000)

year	Ranifall (mm)	lulc 2000			lulc 2010		
		ET(mm)	Baseflow(mm)	Runoff(mm)	ET(mm)	Baseflow(mm)	Runoff(mm)
1996-97	884.87	592.37	74.67	126.59	636.80	72.64	110.45
1997-98	768.61	523.67	118.24	124.48	558.75	118.24	107.35
1998-99	1,099.80	655.62	102.65	260.44	712.66	86.05	210.89
1999-00	769.58	547.26	90.31	168.55	596.80	86.18	133.85
2000-01	609.58	496.13	27.06	107.50	529.34	25.71	76.46
Average	826.49	563.01	82.59	157.51	606.87	77.76	127.80

Further, it was observed that 80% of the basin grids showed an increase in ET (maximum of about 292 mm) with respect to change in LULC (Fig. 5.7). The variability in surface runoff in some parts of the basin attributed to LULC change increased by a maximum of 202.80 mm and decreased by a maximum of 166.2 mm, while baseflow increased by a maximum of 63.75 mm and decreased by a maximum of 33.55 mm. Similarly, the maximum decrease in ET was observed about 289 mm (Table 5.4). Further, the grids having maximum change (decrease/increase in magnitude) in water balance components and rapid increase in urban sprawl were studied for better understanding (Fig. 5.8).

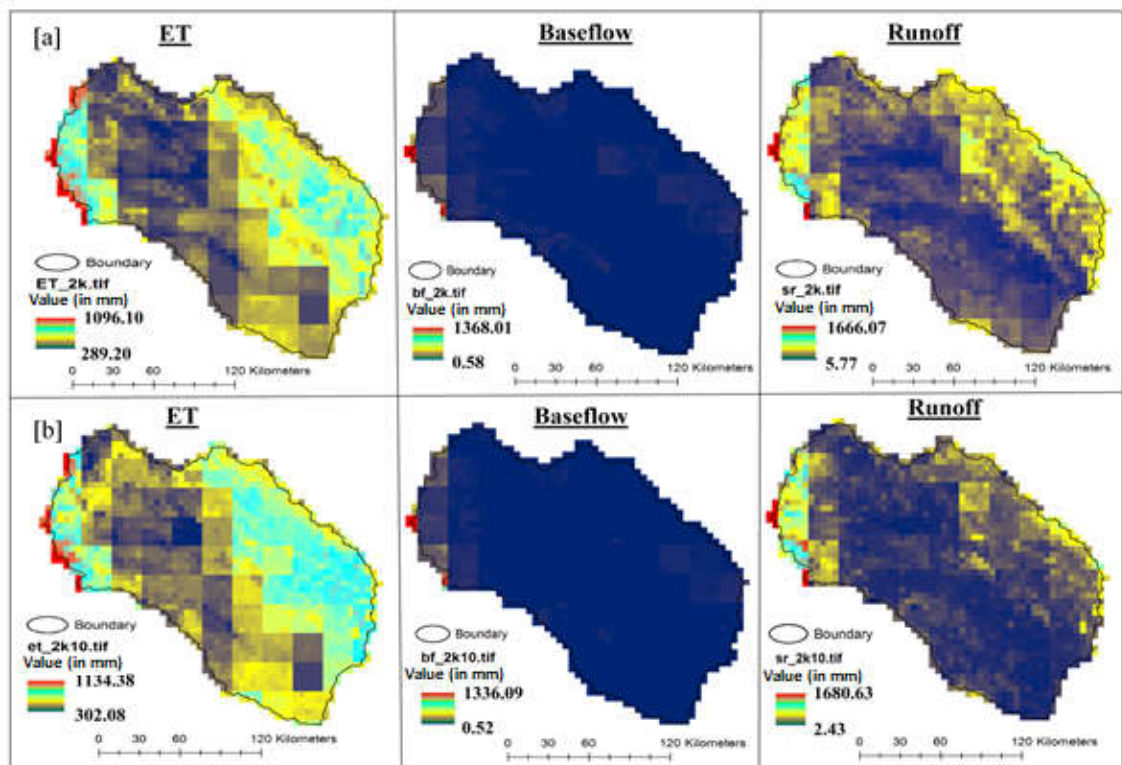


Figure 5.7 Spatial variation of estimated annual water balance components for the water year 2000 – 01 using both LULC period 2000 [a] and 2010 [b]

Table 5.4 Change in water balance component with respect to change in LULC

Grid No	Lat	Long	Vegetation class area fraction		Change (in mm)		
			lulc2000	lulc2010	Baseflow	ET	Runoff
26	18.825	73.625	SL-0.026; BL-0.974	SL-0.810; BL-0.190	-4.51	292.18	-169.00
287	19.275	74.725	F-0.098; SL- 0.556; BL-0.346	AL-0.107; F-0.026;SL-0.026;BL-0.731; WB-0.101	31.84	-289.10	202.80
487	18.625	74.975	AL-0.083; SL-0.144;BL-0.761	AL-0.831;SL-0.077;BL-0.070;WB-0.021	-33.55	176.92	-166.24
733	18.375	75.725	AG-0.469; SL-0.098; BL-0.434	AL-0.847; BL-0.128; WB-0.13	-2.15	41.90	-66.01
701	18.375	73.625	AG-0.02;SL-0.460;BL- 0.319;WB-0.10	AL-0.02;SL-0.182;BL-0.581;WB-0.19	63.75	-207.60	136.65
606	18.475	73.825	UB-0.236;SL-0.37;BL-0.-276	UB-0.852;SL-0.117;WB-0.031;	10.64	-99.93	6.48
1361	17.675	75.925	BL-0.168;SL-0.43;UB-0.402	SL-0.050;BL-0.015;UB-0.935	5.96	-14.91	1.81
463	18.625	73.775	BL-0.359;SL-0.386; UB-0.255	SL-0.027;WB-0.039;UB-0.935	12.36	6.12	12.86
89	19.125	74.725	AL-0.027;SL-0.573;BL- 0.227;UB-0.172	AL-0.393;SL-0.094;UB-0.513	1.53	-51.86	22.14

Note: F – Forest; SL – Scrubland; BL – Barren/sparse vegetation land; AL – Agricultural/crop land; WB- Water bodies; UB – Urban/built-up

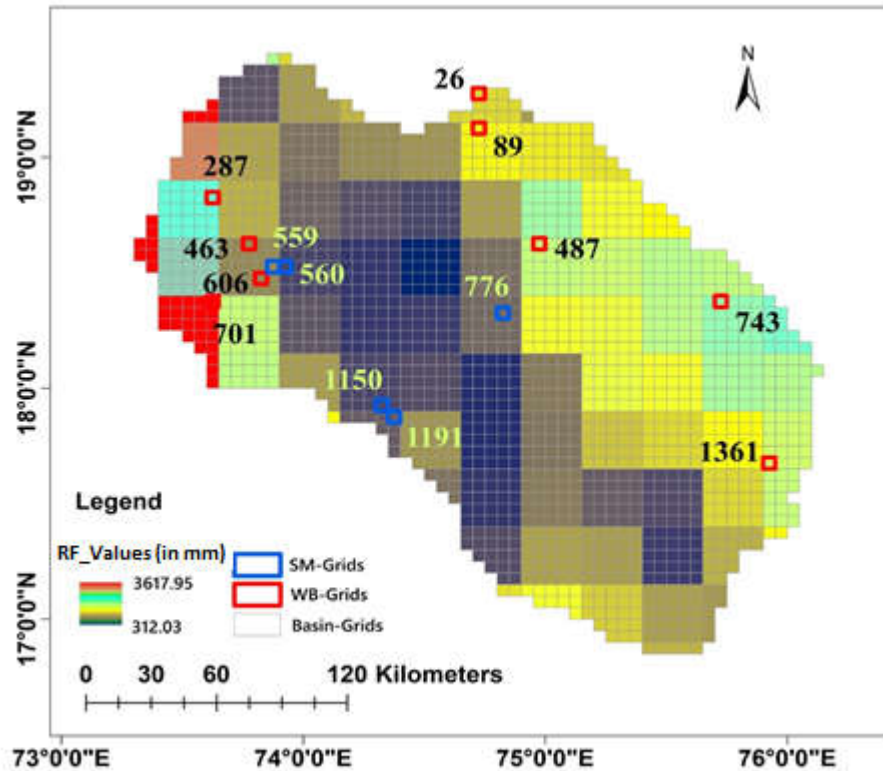


Figure 5.8 Spatial variation of observed annual rainfall for the water year 2000 - 01 along with basin grids and grid showing a maximum change in water balance

It was observed that the maximum increase in ET (292 mm) in the grid 26, because of a dense growth of scrubland over the barren/sparse vegetation land (Table 5.4). In the grids 487 and 733, agricultural/cropland has increased and subsequently scrubland and barren land reduced due to irrigation development. The growth of vegetative land further raises transpiration, which has been exhibited by an increase in overall ET in the above grids. Even though forest/scrubland and cropland have increased in the grids 287 and 701, the increase in surface runoff and baseflow was observed because these grids are located in the higher altitude having steep slopes (Table 5.4). In the grids 606, 1361 and 463, the intensification in built-up and subsequently diminution in scrubland has happened; a common trend of increase in runoff was witnessed because of extended impervious area with a decrease in the vegetative surface. Further, the increase in agricultural/cropland and built-up, subsequently reduced scrub/forest land made the reduction in ET and slightly increase in surface runoff (Table 5.4).

5.3.1 Impacts of LU/LC change on soil moisture

Similarly, the model simulated average monthly soil moisture was evaluated for both LULC condition. It was observed that the impacts of LULC changes on soil moisture were more evident in the deeper layers (45 cm and 100 cm) (Table 5.5). The soil moisture decreased by an average of 14.43 and 18.21% (percentage change), particularly in dry periods at second and third layers, respectively. It can be attributed to the increase in crop-covered agricultural land. As a result, the moisture available in the deeper layers was utilised by the vegetation root systems. Overall, the variation in soil moisture attributed to LU/LC change at different soil layer was observed either an increase or a decrease in space, and it was influenced by types of vegetation, land use and soil depth. The soil moisture decreased by a maximum of 13.55% and increased by a maximum of 21.32% at the top layer (70% of top layer grids showed an increase). Similarly, in the second and third layer, it was observed a maximum decrease of 48.01 and 65.7%, and a maximum increase of 55.8 and 79.19%, respectively. However, it was observed that more than 75% of the basin grid showed a decrease in soil moisture in the deeper layers. Thus, the grids that are showing a maximum change in soil moisture were studied in detail for better understanding.

To show the spatial soil moisture variability at different depth, Table 5.6 presents the results of grids showing maximum change. For instance the grid 26 showed decrease in soil moisture at layer 2 and 3. This can be attributed to more loss of soil moisture through transpiration from roots, due to the dense growth of scrubs over barren land. As a result of rapid urbanization and subsequent decrease in the crop-covered agricultural land and scrubs in the grids 559 and 560, a more amount of evaporation from the bare soil caused decrease in soil moisture in layer 1. Thus, the deeper soil layers showed a maximum increase in soil moisture due to no transpiration loss. In the grid 776, the increase in soil moisture in the deeper layer might be attributed to infiltrated water from increased water bodies (Table 5.6). A maximum decrease in the deeper layers was found in the grid 1150 and 1191. This can be due to high transpiration loss from increased crop-covered agricultural land. However, in the above grids, the increase in soil moisture at top layer might be the result of intercepted water from the surface vegetative cover.

Table 5.5 Average monthly statistics for soil moisture at multiple layers during the period (1996-2005)

Month	Avg_Rainfall (mm)	SM-Layer 1 (m ³ /m ³)			SM-Layer 2 (m ³ /m ³)			SM-Layer 3 (m ³ /m ³)		
		Lulc2000	Lulc2010	Change (%)	Lulc2000	Lulc2010	Change (%)	Lulc2000	Lulc2010	Change (%)
Jan	1.04	0.082	0.086	4.70	0.244	0.226	-7.22	0.253	0.211	-16.90
Feb	1.429	0.083	0.087	4.78	0.235	0.208	-11.74	0.246	0.202	-17.94
Mar	2.91	0.083	0.087	5.03	0.231	0.197	-14.94	0.241	0.196	-18.51
Apr	9.58	0.087	0.092	5.40	0.228	0.191	-16.45	0.236	0.192	-18.61
May	24.23	0.105	0.114	8.35	0.228	0.189	-16.90	0.232	0.189	-18.58
Jun	179.43	0.220	0.235	6.85	0.252	0.221	-12.14	0.235	0.191	-18.77
Jul	214.62	0.218	0.239	9.38	0.280	0.267	-4.80	0.254	0.208	-18.24
Aug	210.41	0.229	0.228	-0.35	0.294	0.287	-2.28	0.268	0.221	-17.32
Sep	169.69	0.239	0.233	-2.56	0.301	0.293	-2.63	0.279	0.234	-16.08
Oct	102.91	0.227	0.217	-4.19	0.281	0.288	0.02	0.287	0.254	-11.43
Nov	15.35	0.116	0.113	-2.51	0.281	0.280	-0.52	0.287	0.244	-14.94
Dec	2.96	0.094	0.096	2.56	0.258	0.250	-3.13	0.274	0.229	-16.27

Table 5.6 Grids showing maximum change in soil moisture with respect to LULC change

Grid No	Lat	Long	Land cover area fraction		%Change		
			lulc2000	lulc2010	SM-Layer 1	SM-Layer 2	SM-Layer 3
26	18.825	73.625	SL-0.026;BL-0.974	SL-0.810-BL-0.190	13.10	-48.02	-48.81
559	18.525	73.875	AG-0.163; F-0.05;SL-0.4; BL-0.12; WB-0.01; UB-0.30	SL-0.05; BL-0.01; WB-0.05; UB-0.89	-13.55	34.28	44.89
560	18.525	73.925	AG-0.25; SL-0.38; BL-0.2; UB-0.17	AG-0.04; SL-0.03; BL-0.02; WB-0.03; UB-0.88	-11.88	46.65	79.16
776	18.325	74.825	AG-0.15; SL-0.56; BL-0.03; WB-0.26; UB-0.01	AG-0.243; BL-0.02; WB-0.72; UB-0.02	-3.93	55.79	50.24
1150	17.925	74.325	AG-0.12; F- 0.003; SL-0.07;BL-0.81	AG-0.80; SL-0.1;BL-0.05;WB-0.04;UB-0.01	21.32	-32.06	-44.03
1191	17.875	74.375	F-0.02; SL-0.31; BL-0.67	AG-0.80; SL-0.1;BL-0.05;WB-0.04	11.29	-18.27	-65.70

Note: F – Forest; SL – Scrubland; BL – Barren/sparse vegetation land; AL – Agricultural/crop land; WB- Water bodies; UB – Urban/built-up

SPATIO-TEMPORAL ANALYSIS OF SOIL MOISTURE

6.1 GENERAL

In this chapter, a detailed assessment of spatio-temporal variability of the soil moisture in the basin is presented. The VIC model simulated soil moisture at multiple depths (0-10 cm, 10-45 cm and 45-100 cm) considering with LU/LC change, and three different satellite-derived surface soil moisture products (SM-CCI, SM-TRMM and SM-AMSRE) were utilized for the analysis. The soil moisture at multiple depths was derived as an output fluxes from the hydrological modeling with a resolution of $0.05^{\circ} \times 0.05^{\circ}$ (about 5.5 km). The soil moisture was simulated at daily time step; however, the monthly average values were utilized for the analysis. The spatio-temporal variability of modeled and satellite derived soil moisture was assessed using the first and second statistical moments along with temporal stability analysis. Further, the representative grid locations were identified in order to estimate spatial mean soil moisture temporal pattern of the entire basin. The schematic representation of the workflow is represented in the Figure 6.1.

6.2 TEMPORAL VARIATION OF SOIL MOISTURE

Initially, the temporal variation of spatial mean soil moisture for the modelled and satellite based products was evaluated. Though the range of values resulted from satellite products as well as model were different, it was found a very similar trend (Fig. 6.2). The seasonality of the precipitation and with that of soil moisture is clearly visible. It was also observed that the deeper soil layers were wetter than the top layer. It was observed that soil moisture decreased in the deeper layers as a result of change in LU/LC. However, similar temporal patterns were observed in both LU/LC conditions.

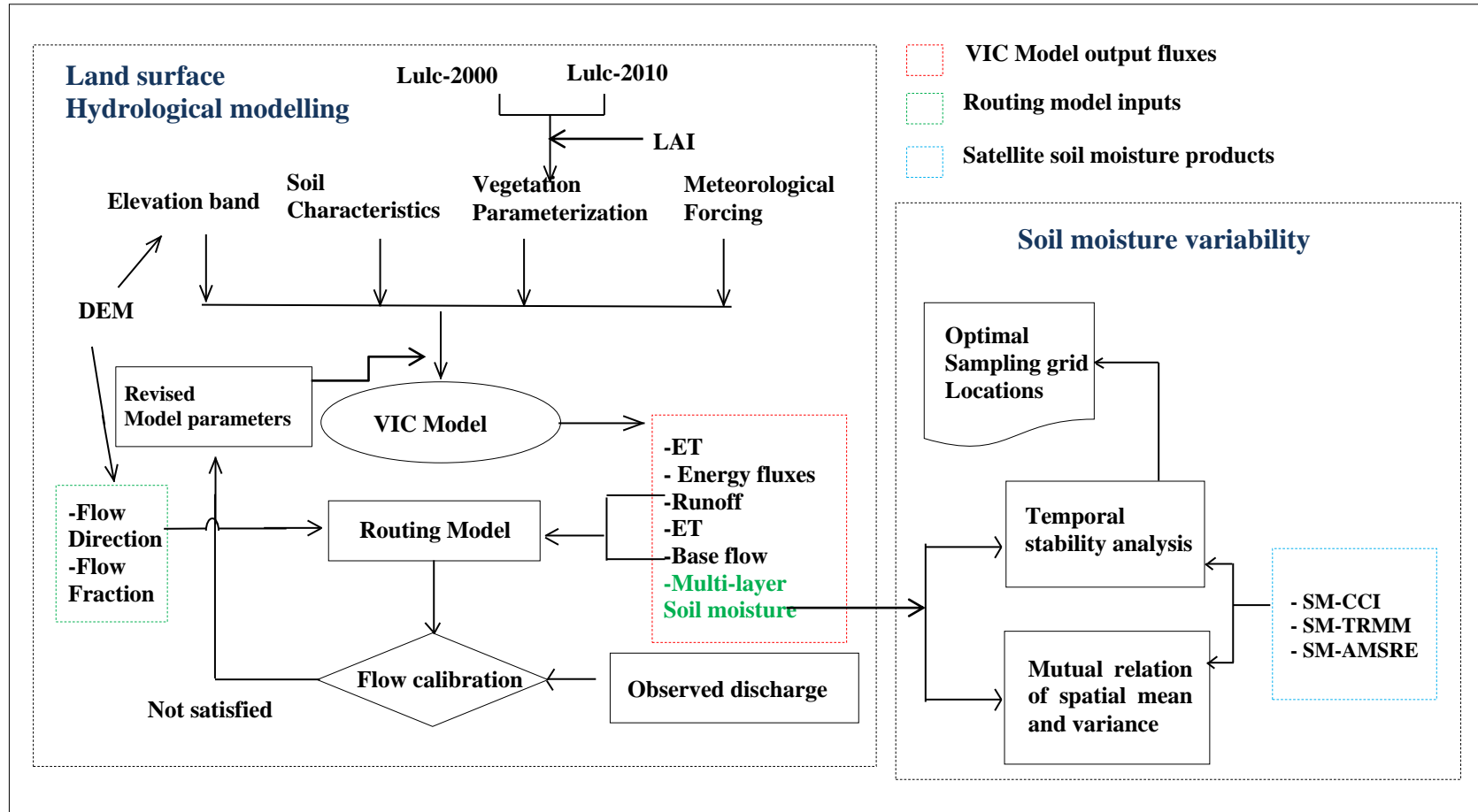


Figure 6.1 Schematic representation of the workflow

Further analysis was conducted to examine the temporal stability of modeled and satellite soil moisture. This began with the temporal persistence analysis for all the soil moisture products using spatial correlation (r) among the soil moisture of different time steps (monthly) during the period (the year 1996 – 2005). Figure 6.3 to 6.7 show the correlation matrix for the modelled and satellite-derived soil moisture during the year 1996 – 2005. It was observed that during the summer and winter seasons, the mean soil moisture was almost constant, and observed high correlation ($r > 0.8$). Interestingly, the soil moisture during the winter was significantly correlated (p -value < 0.001), even the lag was eight months. As anticipated, the transition period (monsoon period; June – September), particularly dry to wet condition the correlation values strongly decreased ($r < 0.2$).

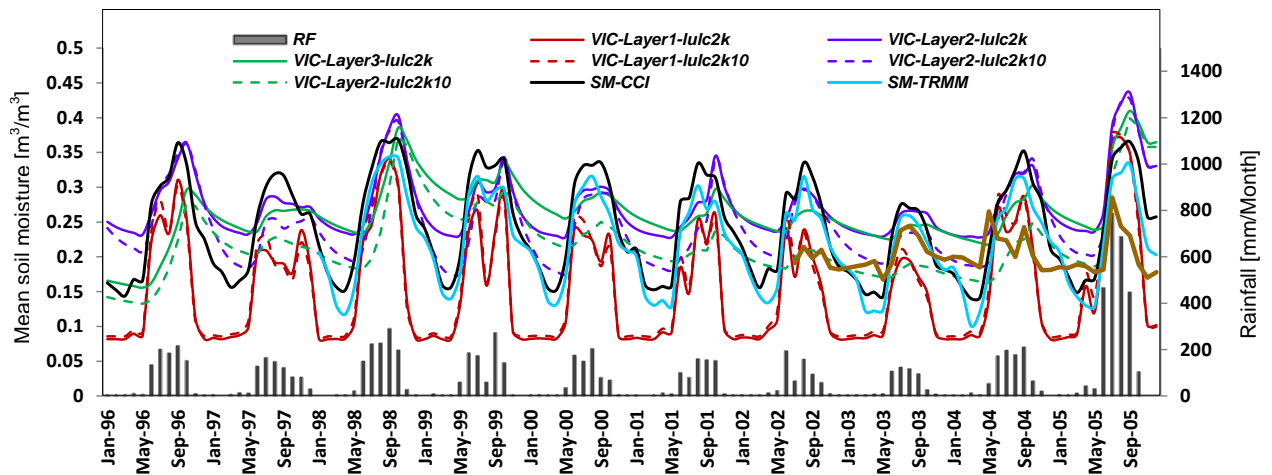


Figure 6.2 Time series of spatial mean soil moisture

The correlation values were quite high in the deeper layers with LU/LC-2000 condition, while it relatively reduced with LU/LC-2010 condition especially during the transition period. It is noted that the cropping pattern in the basin predominantly includes sugarcane and sorghum, and their sowing season is generally during the month of June – August. Thus, the decrease in the correlation values can be the result of increased crop-covered agricultural land in the LU/LC-2010 condition. This analysis showed that the temporal variation of soil moisture is high in the top layer compared to the deeper layers.

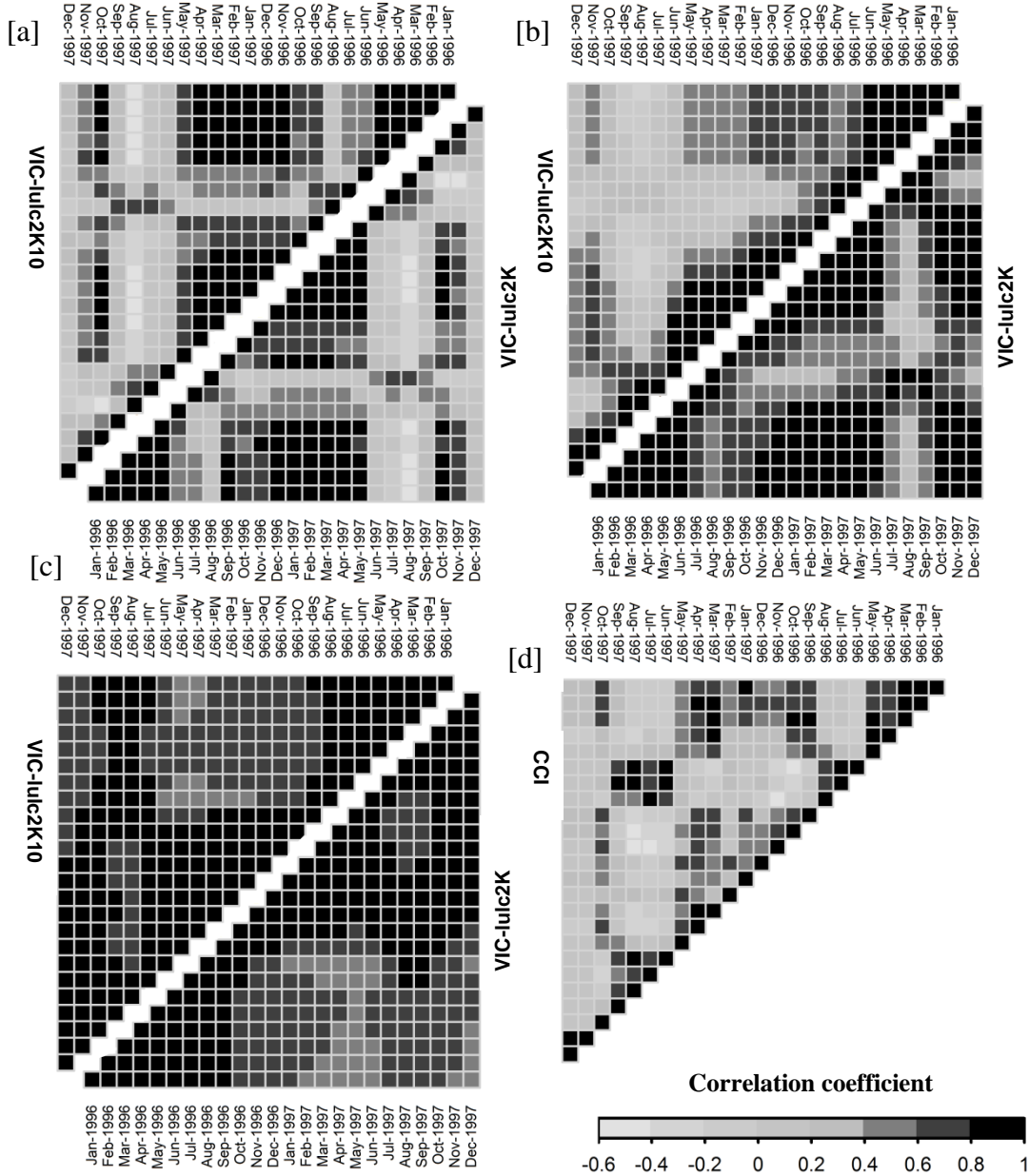


Figure 6.3 Spatial correlation coefficient matrix between the soil moisture during different time step for the modelled and satellite soil moisture data in the year 1996-97 [a] VIC-Layer1 [b] VIC-Layer 2 [c] VIC-Layer 3 (LU/LC-2000, lower triangle; LU/LC-2010, upper triangle) [d] satellite soil moisture.

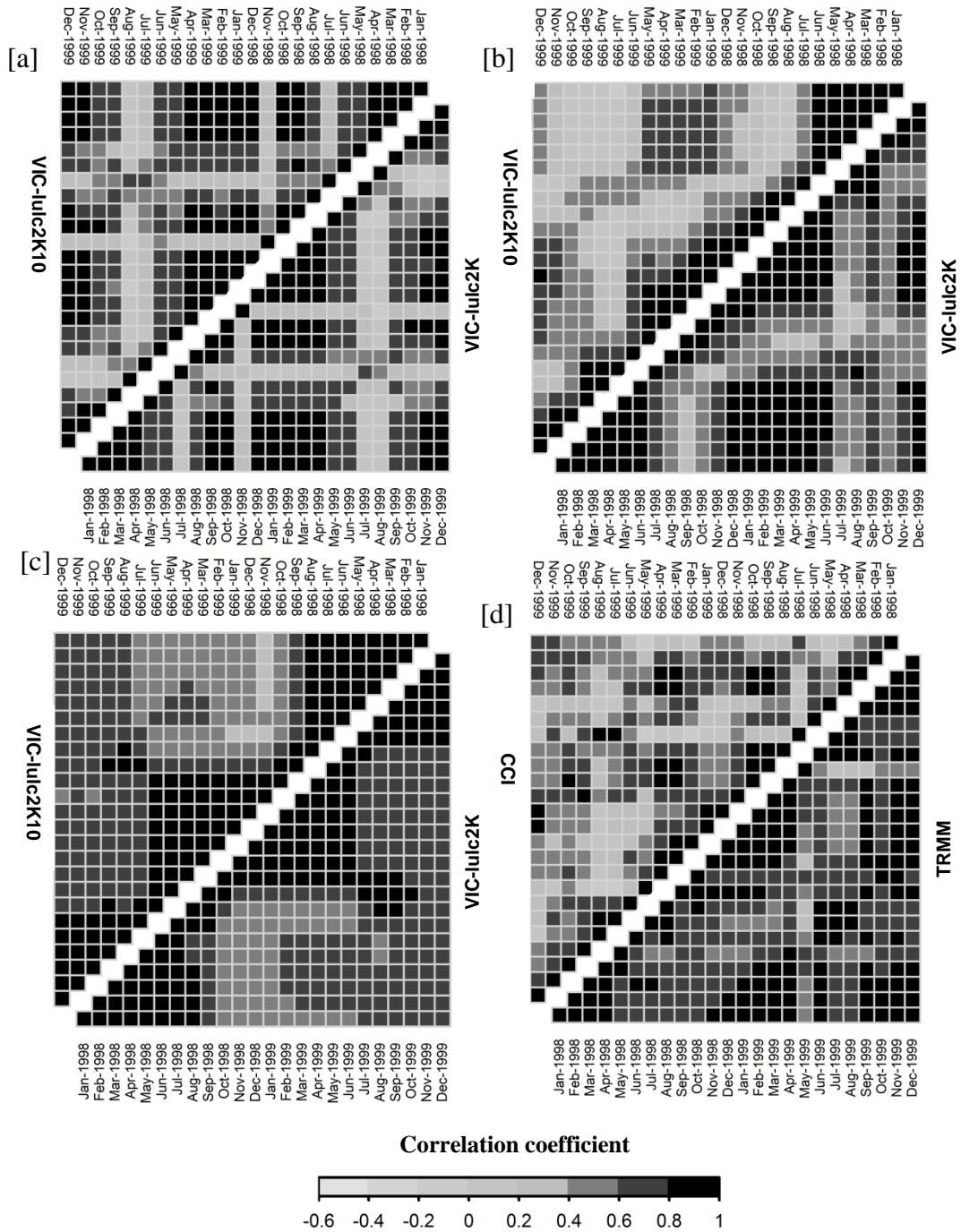


Figure 6.4 Spatial correlation coefficient matrix between the soil moisture during different time step for the modelled and satellite soil moisture data in the year 1998-99 [a] VIC-Layer1 [b] VIC-Layer 2 [c] VIC-Layer 3 (LU/LC-2000, lower triangle; LU/LC-2010, upper triangle) [d] satellite soil moisture (

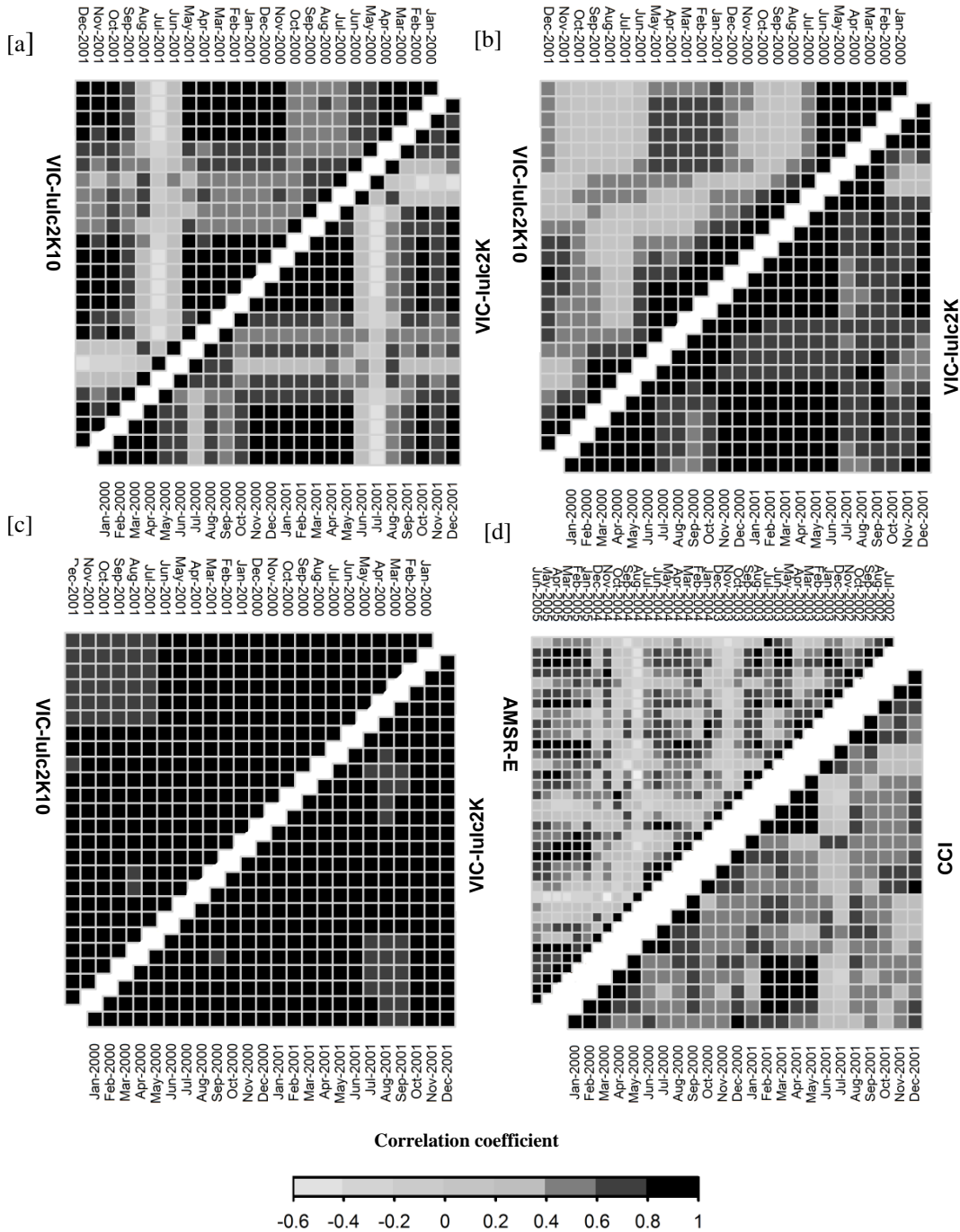


Figure 6.5 Spatial correlation coefficient matrix between the soil moisture during different time step for the modelled and satellite soil moisture data [a] VIC-Layer1 [b] VIC-Layer 2 [c] VIC-Layer 3 (LU/LC-2000, lower triangle; LU/LC-2010, upper triangle) [d] satellite soil moisture

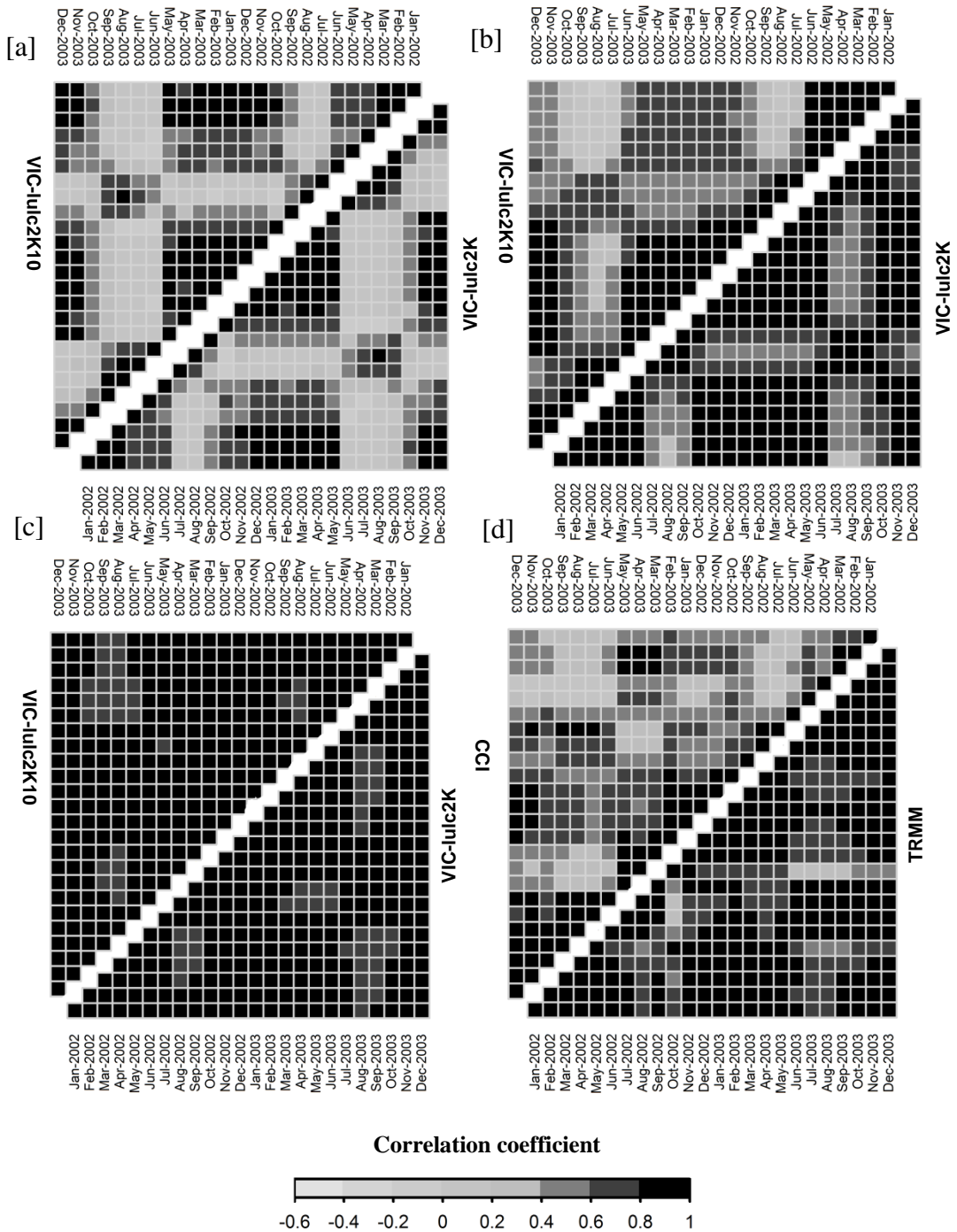


Figure 6.6 Spatial correlation coefficient matrix between the soil moisture during different time step for the modelled and satellite soil moisture data in the year 2002-03 [a] VIC-Layer1 [b] VIC-Layer 2 [c] VIC-Layer 3 (LU/LC-2000, lower triangle; LU/LC-2010, upper triangle) [d] satellite soil moisture.

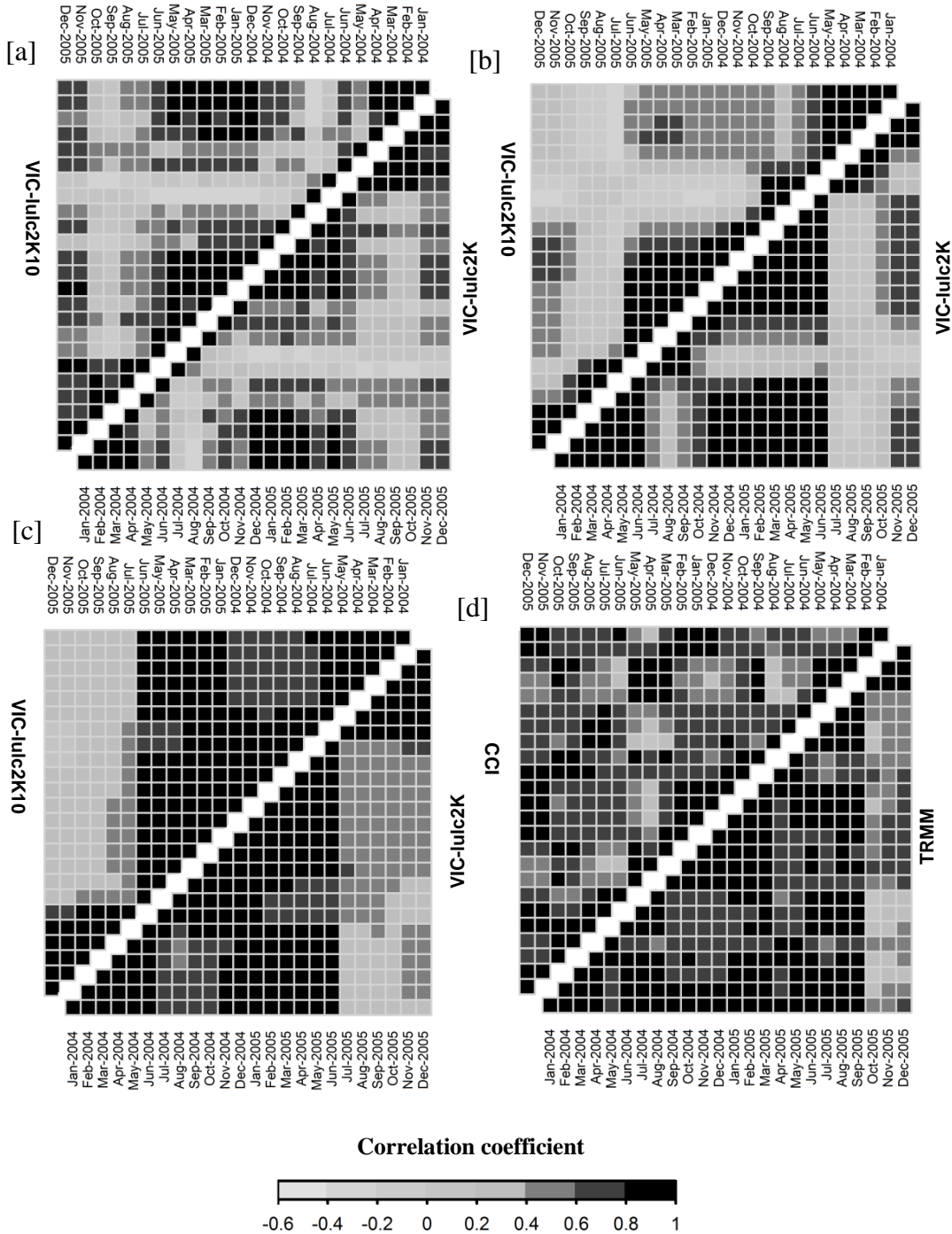


Figure 6.7 Spatial correlation coefficient matrix between the soil moisture during different time step for the modelled and satellite soil moisture data in the year 2004-05 [a] VIC-Layer1 [b] VIC-Layer 2 [c] VIC-Layer 3 (LU/LC-2000, lower triangle; LU/LC-2010, upper triangle) [d] satellite soil moisture.

6.3 SPATIAL MEAN AND VARIANCE

Let θ_i be the soil moisture at grid i , and the spatial mean for one time step (monthly),

$\bar{\theta}_t$ is given by:

$$\bar{\theta}_t = \frac{1}{N_g} \sum_{i=1}^{N_g} \theta_{i,t} \quad (6.1)$$

where N_g is the number of grids.

$$\sigma_t^2 = \frac{1}{N_g-1} \sum_{i=1}^{N_g} (\bar{\theta}_t - \theta_i)^2 \quad (6.2)$$

where σ_t^2 is the spatial variance of each month.

The mutual relation of spatial mean ($\bar{\theta}_t$) and variance (σ_t^2) of the modelled and satellite soil moisture were investigated (Fig. 6.8). It showed mostly a similar convex upward relationship, which indicates that the basin showed high variation in soil moisture during the intermediate wetness condition. This relationship was also reported in the earlier studies with different extent scales (Famiglietti et al., 2008; Brocca et al., 2012b; Li and Rodell, 2013; Rötzer et al., 2015).

This relationship is mainly influenced by precipitation and evapotranspiration in the large extent scales, however, it is also influenced by soil characteristics, topography, vegetation and land use (Li and Rodell, 2013; Rötzer et al., 2015). In this study region, the relationship can be the result of seasonality of precipitation with that of soil moisture (see Fig. 6.2). During the post monsoon season (September – October), the basin was wet and thus showed high $\bar{\theta}_t$ and low σ_t^2 . When the monsoon started, $\bar{\theta}_t$ and σ_t^2 were rising. During the wetting period (June – August), σ_t^2 was observed higher compared to the drying period (December - February), which indicates the occurring of homogeneous drying. It was observed that the deeper layer showed high spatial variability (high σ_t^2) than the top layer.

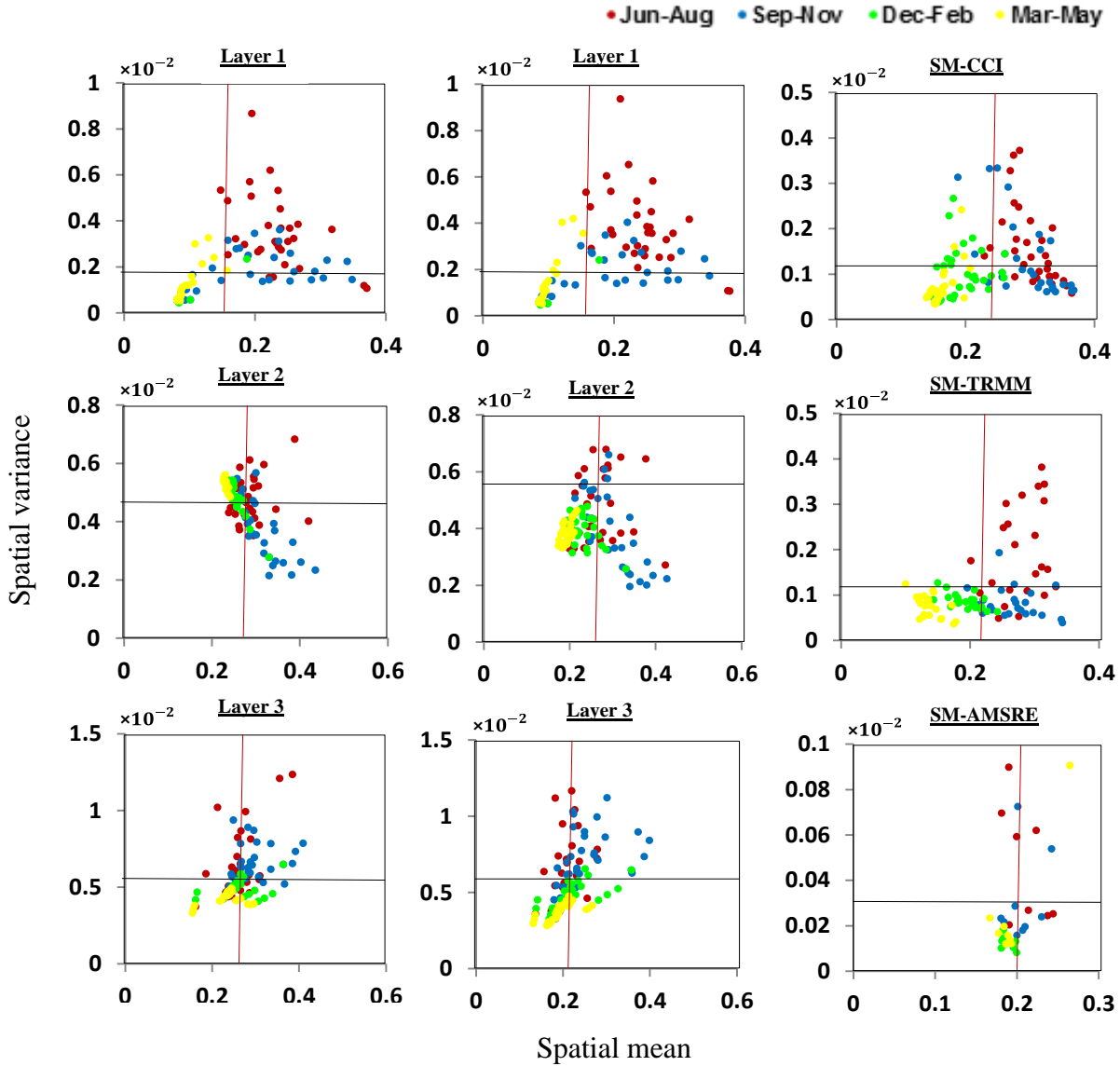


Figure 6.8 Relationship between $\bar{\theta}_t$ and σ_t^2 of modelled and satellite soil moisture. Left side column shows VIC-lulc2000, middle VIC-lulc2010 and right satellite soil moisture. The red and black lines indicate the means of $\bar{\theta}_t$ and σ_t^2 , respectively

The convexity was less pronounced in the second layer for the LULC-2000 condition. It can be seen that mean soil moisture values during dry and transition period (dry to wet) were centered at average with no trend, along with high variability. Further it decreases with increased wetness (Fig. 9). The increase in average σ_t^2 was also

observed in the second layers as a result of LULC change. The convexity is also less evident in SM-AMSRE, and it may be due to length of data is very less (July 2002 – June 2005). However, it showed a similar pattern of variability with other counter parts; while the mean soil moisture below the mid-range σ_t^2 increases with wetness.

6.4 TEMPORAL STABILITY ANALYSIS

Further, the temporal stability analysis based on the relative difference was performed. This method proposed by Vachaud et al. (1985), characterizes the spatial pattern of the temporal stability of the soil moisture. The relative difference, $RD_{i,t}$, at grid, i and time t is given by:

$$RD_{i,t} = \frac{\bar{\theta}_t - \theta_i}{\bar{\theta}_t} \quad (6.3)$$

The mean relative differences (MRDs) and their standard deviations (SRDs) were calculated over the entire time step for every grid:

$$MRD_i = \frac{1}{M} \sum_{t=1}^M RD_{i,t} \quad (6.4)$$

$$SRD_i = \sqrt{\frac{1}{M-1} \sum_{t=1}^M (RD_{i,t} - MRD_i)^2} \quad (6.5)$$

The MRDs and SRDs for the modeled and satellite soil moisture were investigated. The top layer from the modeled soil moisture had MRDs between -0.04 to 0.072, while second and third layer had MRDs between -0.140 to 0.144 and -0.308 to 0.147, respectively (Fig. 6.9). The SRDs for the modeled soil moisture in the deeper layers were quite high, and it ranged from 0.016 to 0.105 (layer 2) and 0.016 to 0.120 (layer 3) (Fig. 6.10). As discussed in the earlier sections, the impact of LU/LC change is more evident in the deeper layers. Further, it can be seen that the standard deviations of MRDs increased for the LU/LC-2010 scenario in the deeper layers. Hence, the temporal stability analysis showed that the soil moisture in the deeper layers exhibit

more dynamic in the spatial pattern of temporal variability. Compared to modeled soil moisture from top layer, the standard deviation of MRDs from the satellite observations were low and it ranged from 0.007 to 0.053. However, the SM-CCI showed a similar pattern with VIC model derived top layer soil moisture.

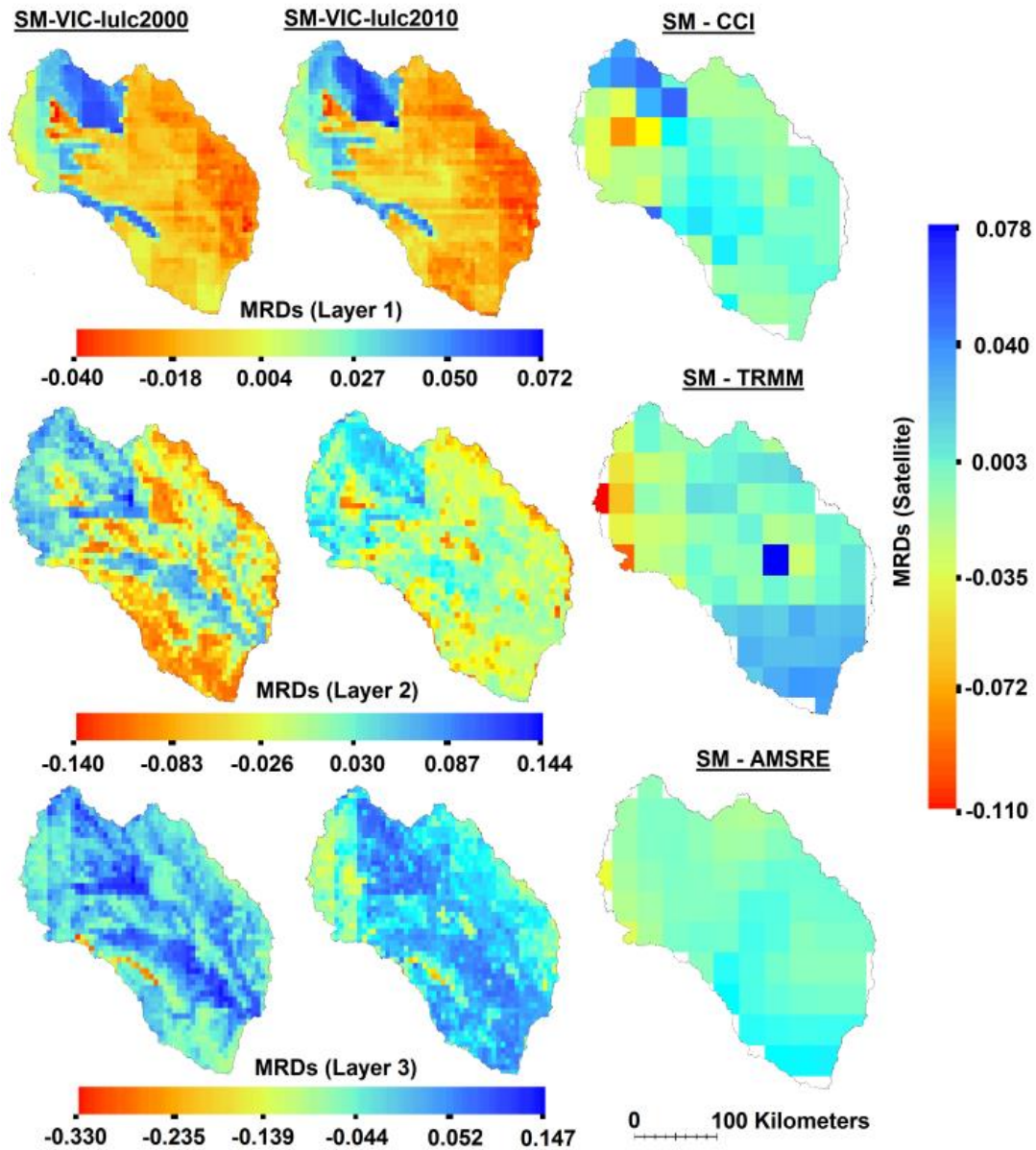


Figure 6.9 The Spatial maps of MRDs. Left side column shows VIC-lulc2000, middle VIC-lulc2010 and right satellite soil moisture

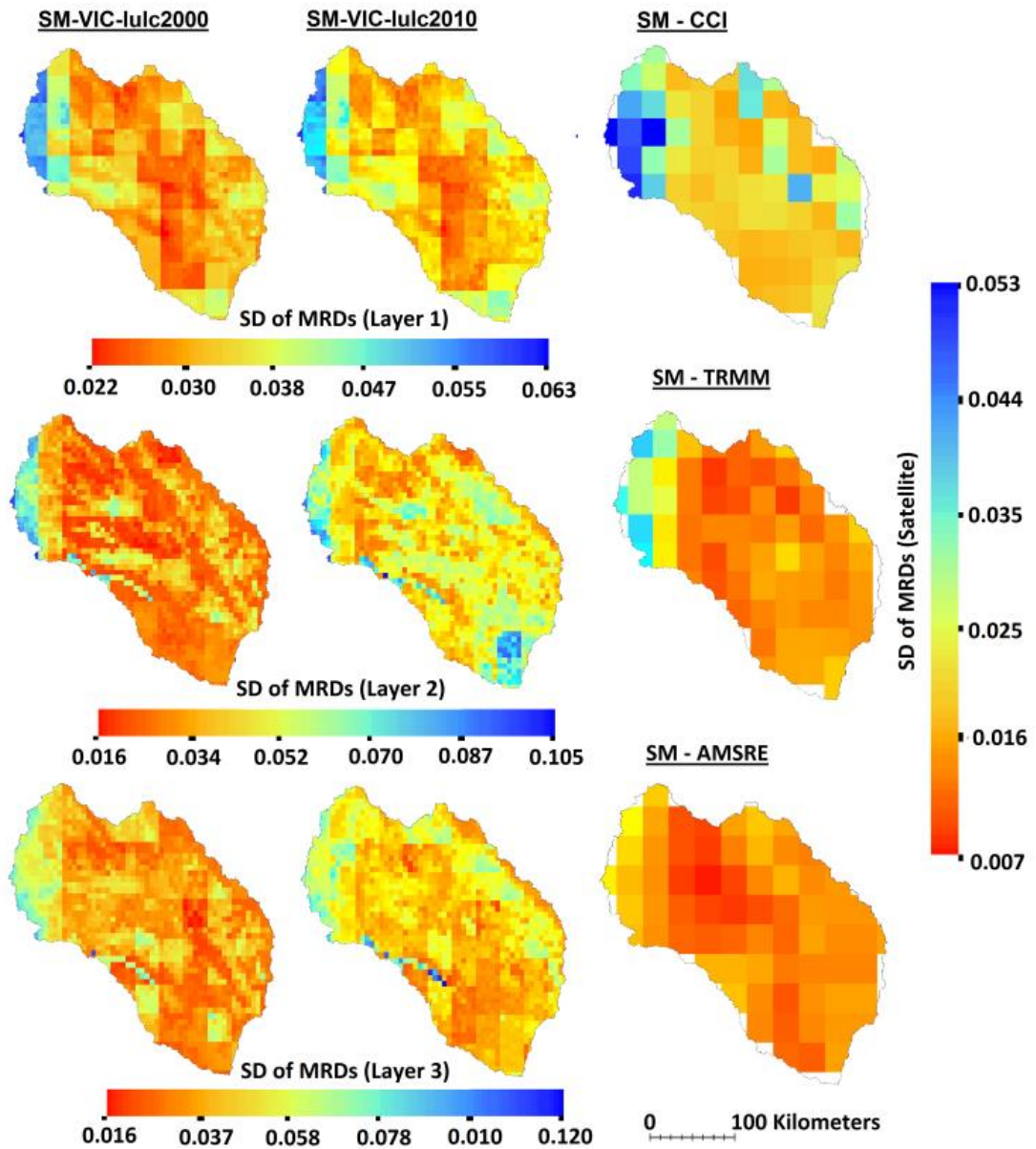


Figure 6.10 The Spatial maps of standard deviation of MRDs. Left side column shows VIC-lulc2000, middle VIC-lulc2010 and right satellite soil moisture

The modeled soil moisture for the top layer was averaged to the pixel resolution (about 25 km) of the satellite products, and the rank ordered MRDs were compared (Fig. 6.11). It is further confirmed that the SM-CCI showed a similar pattern with modeled soil moisture. Thus, the temporal stability analysis can also be used as a validation method, and it was also reported by Rötzer et al., (2014). It also aims to

identify the representative locations for the spatial mean soil moisture temporal pattern, which are considered by low values of MRDs and its standard deviations (.Brocca et al., 2012b).

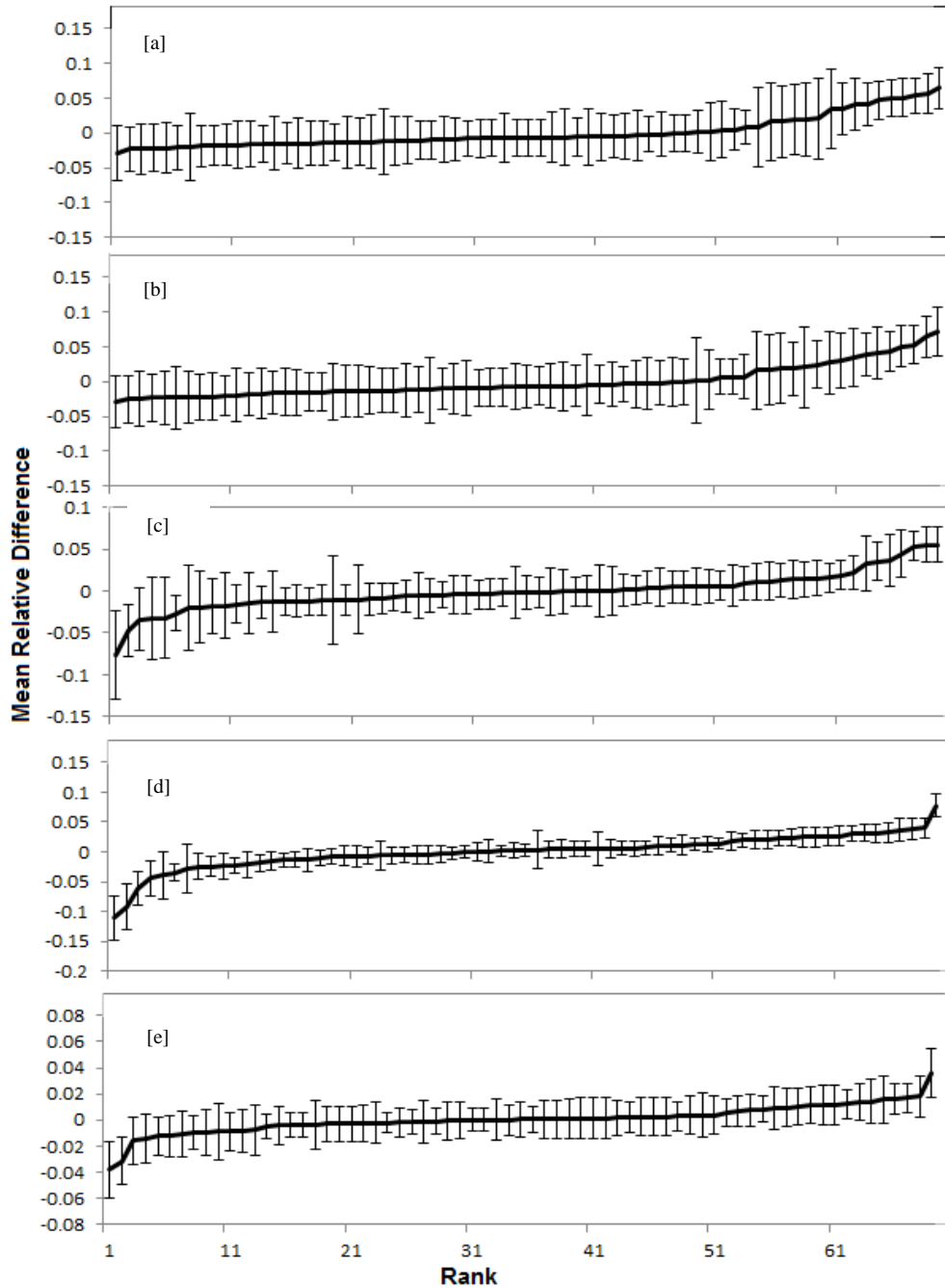


Figure 6.11 Rank ordered mean relative difference for [a] VIC-lulc2000 [b] VIC-lulc2010 [c] SM-CCI [d] SM-TRMM [e] SM-AMSRE (Error bar indicates ± 1 std. deviation)

6.5 REPRESENTATIVE GRID LOCATIONS

The second and third layer soil moisture statistics were considered for identifying the representative locations, since these layers showed more dynamics in spatial pattern of temporal variability. The individual grid soil moisture time series was compared with the time series of areal mean soil moisture (as the benchmark) from the all basin grids. In Table 6.1, for modeled and satellite observations the mean, maximum and minimum values of both coefficient of determination (R^2) and root mean square error (RMSE) between the benchmark time series and that of each grid are presented.

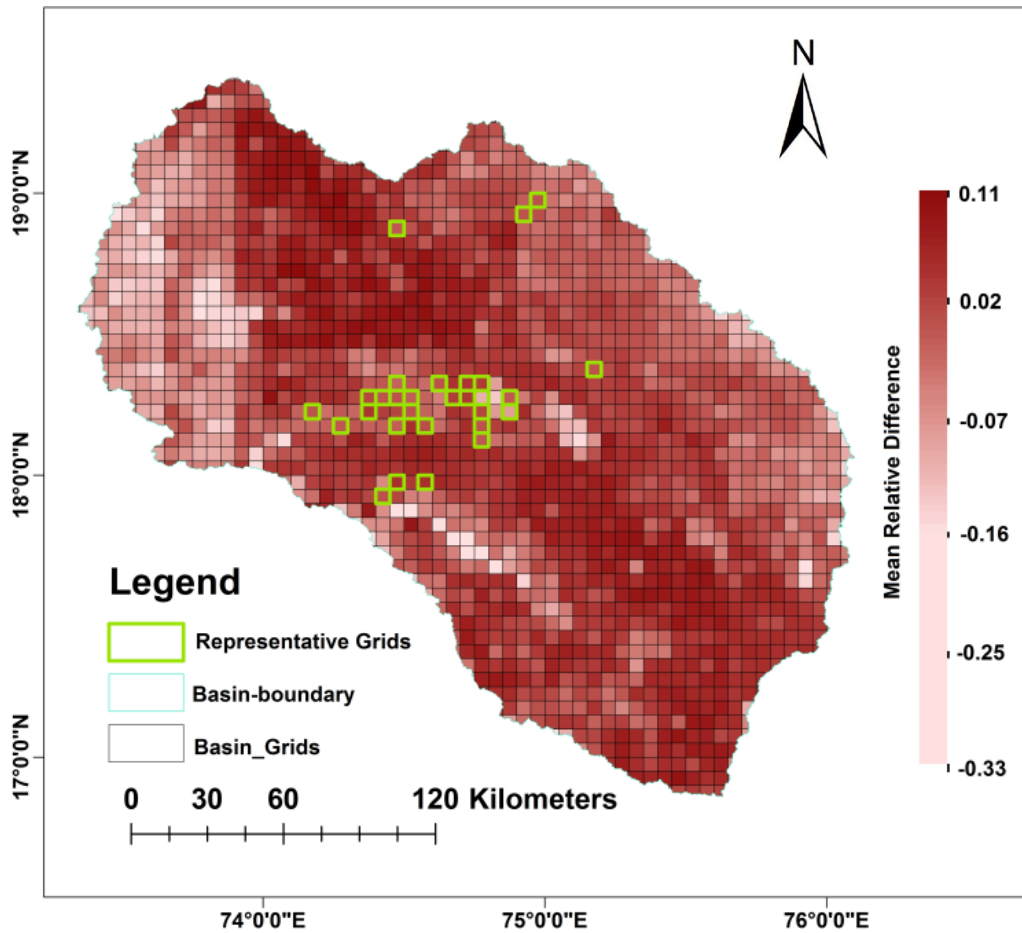


Figure 6.12 Spatial maps of “Representative” grid locations along with the MRDs of third layer

Table 6.1 R² and RMSE between the bench mark time series and time series at each grid

Data	R2			RMSE (% vol/vol)		
	Mean	Max	Min	Mean	Max	Min
SM-VICL1-lulc2k	0.860	0.941	0.729	3.235	5.968	1.851
SM-VICL2-lulc2k	0.708	0.866	0.371	2.725	8.735	0.684
SM-VICL3-lulc2k	0.592	0.924	0.212	3.770	9.896	1.255
SM-CCI	0.914	0.958	0.703	2.099	5.064	1.562
SM-TRMM	0.943	0.982	0.787	1.564	3.870	0.854
SM-AMSRE	0.754	0.924	0.186	1.371	2.238	0.891
SM-VICL1-lulc2k10	0.851	0.927	0.700	3.359	9.621	1.881
SM-VICL2-lulc2k10	0.633	0.858	0.148	4.434	9.621	1.814
SM-VICL3-lulc2k10	0.586	0.922	0.199	4.284	10.601	1.814

Table 6.2 Representative grids and its location

Grid_No	Lat	Long
198	18.975	74.975
234	18.925	74.925
264	18.875	74.475
732	18.375	75.175
769	18.325	74.475
772	18.325	74.625
774	18.325	74.725
775	18.325	74.775
819	18.275	74.375
820	18.275	74.425
821	18.275	74.475
822	18.275	74.525
825	18.275	74.675

826	18.275	74.725
827	18.275	74.775
829	18.275	74.875
865	18.225	74.175
869	18.225	74.375
872	18.225	74.525
877	18.225	74.775
879	18.225	74.875
917	18.175	74.275
921	18.175	74.475
923	18.175	74.575
927	18.175	74.775
977	18.125	74.775
1113	17.975	74.475
1115	17.975	74.575
1152	17.925	74.425

The representative grids were identified by the combination of grids that are having low MRDs (less than ± 0.003), low standard deviation (less than 0.02), RMSE of less than 3% vol/vol and R^2 of higher than 0.85. Hence, in the study area, 29 grid locations were identified, and it can be sufficient to estimate the spatial mean temporal pattern of the entire study area (Fig. 6.12).

SUMMARY AND CONCLUSIONS

7.1 GENERAL

Hydrological models are popular, and often consider as an efficient tool to study the long term behavior of the hydrologic system. In general, these models vary from simple empirical relation to complex distributed models. However, these models have its own effectiveness depending upon the study objective, degree of complexity of the problem and preferred accuracy. The physically-based distributed hydrological models are efficient and providing suitable framework for assessing the hydrological impacts driven by LU/LC change. Remote sensing capability fosters the applications of these complex distributed hydrologic models especially in the assessment LU/LC impacts on water resources. In the case of LU/LC impact assessment, various researchers focused the impacts on agricultural management, runoff potential, ground water assessment and sediment yield by scenario analysis. However, the hydrologic impacts of LU/LC on water resources are usually region specific, as each region is characterized by its own hydrology, terrain, climate and also anthropogenic factors.

The role of soil moisture is well recognized in the hydrological application (e.g., runoff modelling and flood forecasting, agricultural monitoring and drought monitoring). Hence, the characterization of soil moisture variability is more essential. Though several studies were dedicated, the magnitude of soil moisture variability often under estimated and the spatial pattern of soil moisture is not consistent, and it is largely varying across the site and climate with the influence of static and dynamic factors. The primary focus of the present thesis is to characterize the hydrological processes, and analyzing the spatio-temporal variation of soil moisture in the Upper Bhima basin, considering with LU/LC change at finer spatial scale.

In this chapter, the work elaborated is summarized, and the specific conclusions drawn from this study are recalled.

7.2 SUMMARY

In this study, the VIC model was used to simulate the different hydrological components of the basin with a resolution of $0.05^{\circ} \times 0.05^{\circ}$ (about 5.5 km) under two different LU/LC conditions (the year 2000 and 2010). Initially, the basin boundary was delineated using DEM. Further, total drainage area of the basin was discretized into number of model grids (5.5 km resolution: totally 1694 grids), and the input parameterization of the model was made at each grid level. As mentioned in the earlier chapters, the major input parameters to the model are meteorological forcing (Precipitation, T_{\max} , T_{\min}), soil characteristics, land surface vegetation classes (vegetation parameter & library) and topography. The soil parameters were derived based on USDA soil texture using FAO-HWSD global soil map to the model with three layers parameterization (0 - 10 cm, 10 – 45 cm and 45 – 100 cm). For each soil, the hydraulic properties (adopted from Cosby et al., 1984; Rawls et al., 1998; Reynolds et al., 2000) were derived by their area-weighted average based on the textural class for each model grid. The elevation band file is an optional input parameter to the model. However, it was prepared and included in the model simulation, in order to represent more realistic hydrology in the Western Ghats region.

This study demonstrated a methodological frame work for improved vegetation parameterization to the model simulation. The model vegetation parameterization was carried out by iso-clustering approach, using temporal information of LAI and LU/LC maps (the year 2000 and 2010). MODIS-derived 8-day LAI time-series data was used to sub-group agricultural dominant areas into major crop groups and corresponding monthly vegetation phenology in terms of LAI, albedo, height, root distribution were arrived. This exercise enabled improved definition of vegetation parameterization for the study area, incorporating the region specific conditions.

The model was calibrated and validated using the observed stream flow data collected at two different locations for the period 1994 – 2001. Further, the model simulated and MODIS-derived ET was compared, and evaluated with ET estimation based on FAO-56 PM approach using observed meteorological variables collected at the Pune station. The model simulated soil moisture at multiple layers was evaluated with field observed soil moisture at Pune station. The simulated soil moisture at the top layer (0-10 cm) was

averaged to $0.5^{\circ} \times 0.5^{\circ}$, and it was compared with published surface soil moisture data (SM-DM15).

To assess the hydrological impacts of LU/LC change on the flow regime of the basin, the model was run using the two LULC conditions separately with the same observed meteorological forcing and soil data. Further, the variability in hydrological components and the spatial variation of each component attributed to LU/LC change was assessed at the basin grid level. The spatio-temporal variation of soil moisture was assessed using the model simulated soil moisture along with three different satellite derived surface soil moisture products (SM-CCI, SM-TRMM and SM-AMSRE). Based on the temporal stability analysis, the optimal locations were identified for setting up the soil moisture observational network in the study region.

7.3 CONCLUSIONS

The specific conclusions drawn from the study includes:

1. As the LULC scenario changed from 2000 to 2010, the most evident changes occurred in agricultural land. The total area covered by agricultural land increased from 37 to 73%. Hence, the changes attributed to LU/LC at basin level indicate that the surface runoff and baseflow decreased by 18.86 and 5.83% respectively. The evapotranspiration increased by 7.8%, mainly because of the agricultural crops.
2. The majority of the basin grids showed an increase in evapotranspiration (80 % of basin grids) and subsequent decrease in runoff and baseflow (79 and 85% of basin grids, respectively) with respect to LU/LC change. A slight change in LU/LC can largely impact the hydrology of the basin, so there is a need to investigate such variability in finer spatial scale than basin as a whole.
3. LAI information indirectly represents the vegetation phenology. Thus, the framework based on MODIS-derived temporal LAI information and LU/LC maps (iso-clustering approach) along with the site specific condition can improve the

model vegetation parameterization. However, it can be applicable for large-scale application, since the spatial resolution of data is moderate (500 – 1000 m).

4. The deeper soil layers (10 – 45 cm and 45 -100 cm) showed a decrease in soil moisture, particularly during the dry period with response to the LU/LC change (applicable to vegetation class).
5. Though the range of values resulted from satellite products as well as model were different, a similar trend was observed for the spatial mean soil moisture from the modelled and satellite observations with strong seasonality of precipitation. The soil moisture in the surface layer (up to 10 cm) showed high temporal variations. However, the mean soil moisture was almost constant during the summer and winter seasons.
6. Mutual relationship of soil moisture spatial mean and variance showed the convex upward relation indicating that the basin shows high variability during intermediate wetness [0.2 to 0.25 m³/m³] condition. The spatial variability in soil moisture during the wetting period was high compared to drying period. Thus the basin exhibits homogeneous drying.
7. The surface soil moisture from satellite observations showed less variability with the standard deviation of MRDs ranged from 0.007 – 0.53 compared to modelled soil moisture. However, the SM-CCI showed a similar pattern with modelled surface layer soil moisture.
8. Overall, 29 representative grid locations were identified in the basin. It can be sufficient to estimate the spatial mean temporal pattern of the basin with RMSE of less than 3% vol/vol and R² of higher than 0.85.
9. The results obtained from this study can be used to design soil moisture observational network operating in near real-time to this data scarce region for agricultural monitoring.

7.4 LIMITATIONS

1. Monthly average LAI value was utilized for the study since the model structure only incorporates the month-wise vegetation dynamic parameter such as minimum stomatal resistance, LAI, architectural resistance, vegetation height roughness length, albedo and displacement height for each land cover classes. However, in reality, these parameters should be allowed to vary at shorter time scale which in turn would elevate model structural uncertainty specific to this study.
2. The historic satellite images used for the LU/LC classification were only from the month of February/March as the availability of the cloud-free images is very limited.

7.5 SCOPE FOR THE FUTURE WORK

1. In order to handle the inherent model uncertainty related to defining the vegetation dynamic parameters, the source code can be modified to incorporate daily-wise parameters.
2. The effects of heterogeneities in topography and soil properties on soil moisture variability can be analysed further.
3. The procedure developed in this study could be extended to other such hydrological models for improving the model parameterization using remotely sensed Earth Observation (EO) data.
4. The framework based on MODIS-derived temporal LAI information and LU/LC maps (iso-clustering approach) can be explore further to improve LULC classification from satellite imageries.

REFERENCES

- Abdulla, F. A., Lettenmaier, D. P., Wood, E. F., and Smith, J. A. (1996). "Application of a macroscale hydrologic model to estimate the water balance of the Arkansas-Red River Basin." *J. Geophys. Res. Atmos.*, 101(D3), 7449–7459.
- Aggarwal, S. P., Garg, V., Gupta, P. K., Nikam, B. R., and Thakur, P. K. (2012). "Climate and Lulc Change Scenarios To Study Its Impact on Hydrological Regime." *ISPRS - Int. Arch. Photogramm. Remote Sens. Spat. Inf. Sci.*, XXXIX-B8(September), 147–152.
- Allen, R. G., Pereira, L. S., Raes, D., and Smith, M. (1998) Crop evapotranspiration: Guidelines for computing crop water requirements, FAO Irrigation and Drainage Paper No. 56, Food and Agriculture Organization of the United Nations, Rome.
- Al-Shrafany, D., Rico-Ramirez, M. A., Han, D., and Bray, M. (2014). "Comparative assessment of soil moisture estimation from land surface model and satellite remote sensing based on catchment water balance." *Meteorol. Appl.*, 21(3), 521–534.
- Andreadis, K. M., and Lettenmaier, D. P. (2006). "Trends in 20th century drought over the continental United States." *Geophys. Res. Lett.*, 33(10).
- Arnell, N. W. (1999). "The effect of climate change on hydrological regimes in Europe: a continental perspective." *Glob. Environ. Chang.*, 9(1), 5–23.
- Bergstrom, S., Forsman, A. (1973). Development of a conceptual deterministic rainfall-runoff model. *Nordic Hydrology*, 4, 147-170.
- Betts, A. K. (2004). "Understanding Hydrometeorology Using Global Models." *Bull. Am. Meteorol. Soc.*, 85(11), 1673–1688.
- Bevan, K. J., and Kirkby, M. J. (1979). "A physically based, variable contributing area model of basin hydrology / Un modèle à base physique de zone d'appel variable de l'hydrologie du bassin versant." *Hydrol. Sci. Bull.*, 24(1), 43–69.
- Biggs, T. W., Gaur, A., Scott, C. a., Thenkabail, P. S., Rao, P. G., Gumma, M. K.,

- Acharya, S., and Turrall, H. N. (2007). *Closing of the Krishna Basin: Irrigation, Streamflow Depletion and Macroscale Hydrology*.
- Bindlish, R., Jackson, T. J., Wood, E., Gao, H., Starks, P., Bosch, D., and Lakshmi, V. (2003). "Soil moisture estimates from TRMM Microwave Imager observations over the Southern United States." *Remote Sens. Environ.*, 85(4), 507–515.
- Blinn, J. C., Quade, J. G. (1972). Microwave properties of geological materials: Studies of penetration depth and moisture effects. In, 4th Annual Earth Resources Program Review, NASA.
- Bogena, H. R., Huisman, J. A., Baatz, R., Hendricks Franssen, H.-J., and Vereecken, H. (2013). "Accuracy of the cosmic-ray soil water content probe in humid forest ecosystems: The worst case scenario." *Water Resour. Res.*, 49(9), 5778–5791.
- Bogena, H. R., Huisman, J. A., Oberdörster, C., and Vereecken, H. (2007). "Evaluation of a low-cost soil water content sensor for wireless network applications." *J. Hydrol.*, 344(1–2), 32–42.
- Bormann, H., and Elfert, S. (2010). "Application of WaSiM-ETH model to Northern German lowland catchments: model performance in relation to catchment characteristics and sensitivity to land use change." *Adv. Geosci.*, 27, 1–10.
- Bowling, L. C., and Lettenmaier, D. P. (2010). "Modeling the Effects of Lakes and Wetlands on the Water Balance of Arctic Environments." *J. Hydrometeorol.*, 11(2), 276–295.
- Bowling, L. C., Pomeroy, J. W., and Lettenmaier, D. P. (2004). "Parameterization of Blowing-Snow Sublimation in a Macroscale Hydrology Model." *J. Hydrometeorol.*, 5(5), 745–762.
- Brocca, L., Hasenauer, S., Lacava, T., Melone, F., Moramarco, T., Wagner, W., Dorigo, W., Matgen, P., Martínez-Fernández, J., Llorens, P., Latron, J., Martin, C., and Bittelli, M. (2011). "Soil moisture estimation through ASCAT and AMSR-E sensors: An intercomparison and validation study across Europe." *Remote Sens.*

-
- Environ.*, 115(12), 3390–3408.
- Brocca, L., Melone, F., Moramarco, T., Wagner, W., Naeimi, V., Bartalis, Z., and Hasenauer, S. (2010). “Improving runoff prediction through the assimilation of the ASCAT soil moisture product.” *Hydrol. Earth Syst. Sci.*, 14(10), 1881–1893.
- Brocca, L., Morbidelli, R., Melone, F., and Moramarco, T. (2007). “Soil moisture spatial variability in experimental areas of central Italy.” *J. Hydrol.*, 333(2–4), 356–373.
- Brocca, L., Ponziani, F., Moramarco, T., Melone, F., Berni, N., and Wagner, W. (2012a). “Improving Landslide Forecasting Using ASCAT-Derived Soil Moisture Data: A Case Study of the Torgiovannetto Landslide in Central Italy.” *Remote Sens.*, 4(5), 1232–1244.
- Brocca, L., Tullo, T., Melone, F., Moramarco, T., and Morbidelli, R. (2012b). “Catchment scale soil moisture spatial – temporal variability.” *J. Hydrol.*, 422–423, 63–75.
- Burnash, RJC, Ferral, R. L., McGuire, R. A. (1973). A generalized streamflow simulation system – conceptual modelling for digital computers. US Department of Commerce, National Weather Service of California, Department of Water resources.
- Chan, S. K., Bindlish, R., O’Neill, P. E., Njoku, E., Jackson, T., Colliander, A., Chen, F., Burgin, M., Dunbar, S., Piepmeier, J., Yueh, S., Entekhabi, D., Cosh, M. H., Caldwell, T., Walker, J., Wu, X., Berg, A., Rowlandson, T., Pacheco, A., McNairn, H., Thibeault, M., Martinez-Fernandez, J., Gonzalez-Zamora, A., Seyfried, M., Bosch, D., Starks, P., Goodrich, D., Prueger, J., Palecki, M., Small, E. E., Zreda, M., Calvet, J., Crow, W. T., and Kerr, Y. (2016). “Assessment of the SMAP Passive Soil Moisture Product.” *IEEE Trans. Geosci. Remote Sens.*, 54(8), 4994–5007.
- Chawla, I., and Mujumdar, P. P. (2015). “Isolating the impacts of land use and climate change on streamflow.” *Hydrol. Earth Syst. Sci.*, 19(8), 3633–3651.
- Chen, F., Crow, W. T., Bindlish, R., Colliander, A., Burgin, M. S., Asanuma, J., and Aida, K. (2018). “Global-scale evaluation of SMAP, SMOS and ASCAT soil

- moisture products using triple collocation.” *Remote Sens. Environ.*, 214, 1–13.
- Chen, Y., Li, J., and Xu, H. (2016). “Improving flood forecasting capability of physically based distributed hydrological models by parameter optimization.” *Hydrol. Earth Syst. Sci.*, 20(1), 375–392.
- Chen, Y., Xu, Y., and Yin, Y. (2009). “Impacts of land use change scenarios on storm-runoff generation in Xitiaoxi basin, China.” *Quat. Int.*, 208(1–2), 121–128.
- Cherkauer, K. A., Bowling, L. C., and Lettenmaier, D. P. (2003). “Variable infiltration capacity cold land process model updates.” *Glob. Planet. Change*, 38(1–2), 151–159.
- Cherkauer, K. A., and Lettenmaier, D. P. (1999). “Hydrologic effects of frozen soils in the upper Mississippi River basin.” *J. Geophys. Res. Atmos.*, 104(D16), 19599–19610.
- Choudhury, B., Schmugge, T. J., Chang, A., Newton, R. (1979). Effect of surface roughness on the microwave emission from soils. *J. Geophys. Res. Oceans* 84, 5699–5706
- Chow. V.T., Maidment. D. R, and Mays. L. W (1988), “Applied Hydrology”, Mc Graw Hill, Singapore.
- Christensen, N., and Lettenmaier, D. P. (2007). “A multimodel ensemble approach to assessment of climate change impacts on the hydrology and water resources of the Colorado River Basin.” *Hydrol. Earth Syst. Sci.*, 11(4), 1417–1434.
- Congalton, R. G. (1991). “A review of assessing the accuracy of classifications of remotely sensed data.” *Remote Sens. Environ.*, 37(1), 35–46.
- Cosby, B. J., Hornberger, G. M., Clapp, R. B., and Ginn, T. R. (1984). “Exploration of the Relationships of Soil Moisture Characteristics to the Physical Properties of Soils.” *Water Resour. Res.*, 20(6), 682–690.
- Cosh, M. H., Jackson, T. J., Moran, S., and Bindlish, R. (2008). “Temporal persistence and stability of surface soil moisture in a semi-arid watershed.” *Remote Sens.*

-
- Environ.*, 112(2), 304–313.
- Crow, W. T., Berg, A. A., Cosh, M. H., Loew, A., Mohanty, B. P., Panciera, R., de Rosnay, P., Ryu, D., and Walker, J. P. (2012). “Upscaling sparse ground-based soil moisture observations for the validation of coarse-resolution satellite soil moisture products.” *Rev. Geophys.*, 50(2), 2746–2763.
- Das, S. K., and Maity, R. (2015). “Potential of Probabilistic Hydrometeorological Approach for Precipitation-Based Soil Moisture Estimation.” *J. Hydrol. Eng.*, 20(4), 04014056.
- DeFries, R., and Eshleman, K. N. (2004). “Land-use change and hydrologic processes: a major focus for the future.” *Hydrol. Process.*, 18(11), 2183–2186.
- Desilets, D., Zreda, M., and Ferré, T. P. A. (2010). “Nature’s neutron probe: Land surface hydrology at an elusive scale with cosmic rays.” *Water Resour. Res.*, 46(11), 1–7.
- Dharssi, I., Bovis, K. J., Macpherson, B., and Jones, C. P. (2011). “Operational assimilation of ASCAT surface soil wetness at the Met Office.” *Hydrol. Earth Syst. Sci.*, 15(8), 2729–2746.
- Dorigo, W. A., Gruber, A., De Jeu, R. A. M., Wagner, W., Stacke, T., Loew, A., Albergel, C., Brocca, L., Chung, D., Parinussa, R. M., and Kidd, R. (2015). “Evaluation of the ESA CCI soil moisture product using ground-based observations.” *Remote Sens. Environ.*, 162, 380–395.
- Drusch, M. (2007). “Initializing numerical weather prediction models with satellite-derived surface soil moisture: Data assimilation experiments with ECMWF’s Integrated Forecast System and the TMI soil moisture data set.” *J. Geophys. Res.*, 112(D3), D03102.
- Duband, D., Obléd, C., and Rodriguez, J. Y. (1993). “Unit hydrograph revisited: an alternate iterative approach to UH and effective precipitation identification.” *J. Hydrol.*, 150(1), 115–149.
- Dwarakish, G. S., and Ganasri, B. P. (2015). “Impact of land use change on hydrological

- systems: A review of current modeling approaches.” *Cogent Geosci.*, 1(1), 1–18.
- Eagleman, J. R., and Lin, W. C. (1976). “Remote sensing of soil moisture by a 21-cm passive radiometer.” *J. Geophys. Res.*, 81(21), 3660–3666.
- Enenkel, M., Steiner, C., Mistelbauer, T., Dorigo, W., Wagner, W., See, L., Atzberger, C., Schneider, S., and Roggenhofer, E. (2016). “A Combined Satellite-Derived Drought Indicator to Support Humanitarian Aid Organizations.” *Remote Sens.*, 8(4), 340.
- Famiglietti, J. S., Ryu, D., Berg, A. A., Rodell, M., and Jackson, T. J. (2008a). “Field observations of soil moisture variability across scales.” *Water Resour. Res.*, 44(1), 1–16.
- Famiglietti, J. S., Ryu, D., Berg, A. A., Rodell, M., and Jackson, T. J. (2008b). “Field observations of soil moisture variability across scales.” *Water Resour. Res.*, 44(1), 1–16.
- Fang, X., Ren, L., Li, Q., Zhu, Q., Shi, P., and Zhu, Y. (2013). “Hydrologic Response to Land Use and Land Cover Changes within the Context of Catchment-Scale Spatial Information.” *J. Hydrol. Eng.*, 18(November), 1539–1548.
- Fischer, G, F, Nachtergaele, S, Prieler, H, T, van Velthuisen, L, Verelst, D, Wiberg (2008) Global Agro-ecological Zones Assessment for Agriculture (GAEZ 2008).IIASA, Laxenburg, Austria and FAO, Rome, Italy. <http://www.fao.org/soils-portal/soil-survey/soil-maps-and-databases/harmonized-world-soil-database-v12/en/> Accessed 01 November 2019.
- Franchini, M., and Pacciani, M. (1991). “Comparative analysis of several conceptual rainfall-runoff models.” *J. Hydrol.*, 122(1–4), 161–219.
- Franz, T. E., Zreda, M., Ferre, T. P. A., Rosolem, R., Zweck, C., Stillman, S., Zeng, X., and Shuttleworth, W. J. (2012). “Measurement depth of the cosmic ray soil moisture probe affected by hydrogen from various sources.” *Water Resour. Res.*, 48(8), 1–9.
- Fry, J. E., and Guber, A. K. (2020). “Temporal stability of field-scale patterns in soil

- water content across topographically diverse agricultural landscapes.” *J. Hydrol.*, 580, 124260.
- Gao, H., Tang, Q., Shi, X., Zhu, C., Bohn, T., and Su, F. (2009). “Water Budget Record from Variable Infiltration Capacity (VIC) Model Algorithm Theoretical Basis Document.”
- Gao, H., Wood, E. F., Drusch, M., and McCabe, M. F. (2007). “Copula-Derived Observation Operators for Assimilating TMI and AMSR-E Retrieved Soil Moisture into Land Surface Models.” *J. Hydrometeorol.*, 8(3), 413–429.
- Gao, H., Wood, E. F., Jackson, T. J., Drusch, M., and Bindlish, R. (2006). “Using TRMM/TMI to Retrieve Surface Soil Moisture over the Southern United States from 1998 to 2002.” *J. Hydrometeorol.*, 7(1), 23–38.
- Gao, L., Shao, M., Peng, X., and She, D. (2015). “Spatio-temporal variability and temporal stability of water contents distributed within soil profiles at a hillslope scale.” *CATENA*, 132, 29–36.
- Gao, L., Wang, Y., Geris, J., Hallett, P. D., and Peng, X. (2019). “The role of sampling strategy on apparent temporal stability of soil moisture under subtropical hydroclimatic conditions.” *J. Hydrol. Hydromechanics*, 67(3), 260–270.
- Garg, K. K., Bharati, L., Gaur, A., George, B., Acharya, S., Jella, K., and Narasimhan, B. (2012). “Spatial Mapping Of Agricultural Water Productivity Using The Swat Model In Upper Bhima Catchment, India.” *Irrig. Drain.*, 61(1), 60–79.
- Garg, V., Aggarwal, S. P., Gupta, P. K., Nikam, B. R., Thakur, P. K., Srivastav, S. K., and Senthil Kumar, A. (2017). “Assessment of land use land cover change impact on hydrological regime of a basin.” *Environ. Earth Sci.*, 76(18), 635.
- Garg, V., Nikam, B. R., Thakur, P. K., Aggarwal, S. P., Gupta, P. K., and Srivastav, S. K. (2019). “Human-induced land use land cover change and its impact on hydrology.” *HydroResearch*, 1, 48–56.
- Gartley, M. L., George, B., Davidson, B., Malano, H. M., and Garg, K. K. (2009).

- “Hydro-economic modelling of the Upper Bhima.” *18th World IMACS / MODSIM Congr. Cairns, Aust.*, (July), 3831–3837.
- Gashaw, T., Tulu, T., Argaw, M., and Worqlul, A. W. (2018). “Modeling the hydrological impacts of land use/land cover changes in the Andassa watershed, Blue Nile Basin, Ethiopia.” *Sci. Total Environ.*, 619–620, 1394–1408.
- Ghaffari, G., Keesstra, S., Ghodousi, J., and Ahmadi, H. (2010). “SWAT-simulated hydrological impact of land-use change in the Zanzanrood Basin, Northwest Iran.” *Hydrol. Process.*, 24(7), 892–903.
- Githui, F., Mutua, F., and Bauwens, W. (2009). “Estimating the impacts of land-cover change on runoff using the soil and water assessment tool (SWAT): case study of Nzoia catchment, Kenya / Estimation des impacts du changement d’occupation du sol sur l’écoulement à l’aide de SWAT: étude du cas du bassin.” *Hydrol. Sci. J.*, 54(5), 899–908.
- Gómez-Plaza, A., Alvarez-Rogel, J., Albaladejo, J., and Castillo, V. M. (2000). “Spatial patterns and temporal stability of soil moisture across a range of scales in a semi-arid environment.” *Hydrol. Process.*, 14(7), 1261–1277.
- González-Zamora, Á., Sánchez, N., Pablos, M., and Martínez-Fernández, J. (2019). “CCI soil moisture assessment with SMOS soil moisture and in situ data under different environmental conditions and spatial scales in Spain.” *Remote Sens. Environ.*, 225, 469–482.
- Gosain, A. K., Rao, S., and Arora, A. (2011). “Climate change impact assessment of water resources of India.” *Curr. Sci.*, 101(3), 356–371.
- Crawford, N. H. and Linsley, R. K. (1966). *Digital Simulation on Hydrology: Stanford Watershed Model IV*. Stanford University Technical Report No. 39, Stanford University, Palo Alto, CA.
- Gruhier, C., de Rosnay, P., Kerr, Y., Mougin, E., Ceschia, E., Calvet, J.-C., and Richaume, P. (2008). “Evaluation of AMSR-E soil moisture product based on

- ground measurements over temperate and semi-arid regions.” *Geophys. Res. Lett.*, 35(10), 2–7.
- Haddeland, I., Skaugen, T., and Lettenmaier, D. P. (2006). “Anthropogenic impacts on continental surface water fluxes.” *Geophys. Res. Lett.*, 33(8), L08406.
- Haddeland, I., Skaugen, T., and Lettenmaier, D. P. (2007). “Hydrologic effects of land and water management in North America and Asia: 1700 -1992.” *Hydrol. Earth Syst. Sci.*, 11(2), 1035–1045.
- He, Z.-B., Zhao, M.-M., Zhu, X., Du, J., Chen, L.-F., Lin, P.-F., and Li, J. (2019). “Temporal stability of soil water storage in multiple soil layers in high-elevation forests.” *J. Hydrol.*, 569(December 2018), 532–545.
- Hébrard, O., Voltz, M., Andrieux, P., and Moussa, R. (2006). “Spatio-temporal distribution of soil surface moisture in a heterogeneously farmed Mediterranean catchment.” *J. Hydrol.*, 329(1–2), 110–121.
- Horton, R. E. (1933). The role of infiltration in the hydrologic cycle. Transactions, American Geophysical Union, 14: 446–460.
- Hu, W., Shao, M., Han, F., Reichardt, K., and Tan, J. (2010). “Watershed scale temporal stability of soil water content.” *Geoderma*, 158(3–4), 181–198.
- Hu, W., and Si, B. C. (2016). “Estimating spatially distributed soil water content at small watershed scales based on decomposition of temporal anomaly and time stability analysis.” *Hydrol. Earth Syst. Sci.*, 20(1), 571–587.
- Hydrology project, Goveenment of India. <http://hydrology-project.gov.in> Accessed 01 November 2019
- Immerzeel, W. W., Gaur, A., and Zwart, S. J. (2008). “Integrating remote sensing and a process-based hydrological model to evaluate water use and productivity in a south Indian catchment.” *Agric. Water Manag.*, 95(1), 11–24.
- Jackson, T. J., Cosh, M. H., Bindlish, R., Starks, P. J., Bosch, D. D., Seyfried, M.,

- Goodrich, D. C., Moran, M. S., and Du, J. (2010). "Validation of Advanced Microwave Scanning Radiometer Soil Moisture Products." *IEEE Trans. Geosci. Remote Sens.*, 48(12), 4256–4272.
- Karthikeyan, L., Pan, M., Wanders, N., Kumar, D. N., and Wood, E. F. (2017a). "Four decades of microwave satellite soil moisture observations: Part 1. A review of retrieval algorithms." *Adv. Water Resour.*, 109, 106–120.
- Karthikeyan, L., Pan, M., Wanders, N., Kumar, D. N., and Wood, E. F. (2017b). "Four decades of microwave satellite soil moisture observations: Part 2. Product validation and inter-satellite comparisons." *Adv. Water Resour.*, 109, 236–252.
- Keith A. Cherkauer and Dennis P. Lettenmaier. (2003). "Simulation of spatial variability in snow and frozen soil." *J. Geophys. Res.*, 108(D22), 8858.
- Kerr, Y. H., Waldteufel, P., Wigneron, J. P., Martinuzzi, J. M., Font, J., and Berger, M. (2001). "Soil moisture retrieval from space: The Soil Moisture and Ocean Salinity (SMOS) mission." *IEEE Trans. Geosci. Remote Sens.*, 39(8), 1729–1735.
- Koster, R. D., Mahanama, S. P. P., Livneh, B., Lettenmaier, D. P., and Reichle, R. H. (2010). "Skill in streamflow forecasts derived from large-scale estimates of soil moisture and snow." *Nat. Geosci.*, 3(9), 613–616.
- Li, B., and Rodell, M. (2013). "Spatial variability and its scale dependency of observed and modeled soil moisture over different climate regions." *Hydrol. Earth Syst. Sci.*, 17(3), 1177–1188.
- Li, J., Gao, X., and Sorooshian, S. (2007). "Modeling and Analysis of the Variability of the Water Cycle in the Upper Rio Grande Basin at High Resolution." *J. Hydrometeorol.*, 8(4), 805–824.
- Li, Z., Liu, W. zhao, Zhang, X. chang, and Zheng, F. li. (2009). "Impacts of land use change and climate variability on hydrology in an agricultural catchment on the Loess Plateau of China." *J. Hydrol.*, 377(1–2), 35–42.
- Liang, X., Lettenmaier, D. P., Wood, E. F., and Burges, S. J. (1994). "A simple

- hydrologically based model of land surface water and energy fluxes for general circulation models.” *J. Geophys. Res.*, 99(D7), 14415.
- Liang, X., Wood, E. F., and Lettenmaier, D. P. (1996). “Surface soil moisture parameterization of the VIC-2L model: Evaluation and modification.” *Glob. Planet. Change*, 13(1–4), 195–206.
- Loew, A., and Schlenz, F. (2011). “A dynamic approach for evaluating coarse scale satellite soil moisture products.” *Hydrol. Earth Syst. Sci.*, 15(1), 75–90.
- Lohmann, D., Nolte-Holube, R., and Raschke, E. (1996). “A large-scale horizontal routing model to be coupled to land surface parametrization schemes.” *Tellus A*, 48(5), 708–721.
- Lohmann, D., Raschke, E., Nijssen, B., and Lettenmaier, D. P. (1998). “Regional scale hydrology: I. Formulation of the VIC-2L model coupled to a routing model.” *Hydrol. Sci. J.*, 43(1), 131–141.
- Lørup, J. K., Refsgaard, J. C., and Mazvimavi, D. (1998). “Assessing the effect of land use change on catchment runoff by combined use of statistical tests and hydrological modelling: Case studies from Zimbabwe.” *J. Hydrol.*, 205(3–4), 147–163.
- Luo, L., and Wood, E. F. (2007). “Monitoring and predicting the 2007 U.S. drought.” *Geophys. Res. Lett.*, 34(22), L22702.
- Mahrt, L., and Pan, H. (1984). “A two-layer model of soil hydrology.” *Boundary-Layer Meteorol.*, 29(1), 1–20.
- Martínez-Fernández, J., and Ceballos, A. (2003). “Temporal Stability of Soil Moisture in a Large-Field Experiment in Spain.” *Soil Sci. Soc. Am. J.*, 67(6), 1647.
- Matheussen, B., Kirschbaum, R. L., Goodman, I. A., O ’donnell, G. M., Lettenmaier, D. P., and Lettenmaier, D. P. (2000). “Effects of land cover change on streamflow in the interior Columbia River Basin (USA and Canada).” *Hydrol. Process.*, 14, 867–885.

- Maurer, E. P., O'Donnell, G. M., Lettenmaier, D. P., and Roads, J. O. (2001). "Evaluation of NCEP/NCAR reanalysis water and energy budgets using macroscale hydrologic model simulations." *L. Surf. Hydrol. Meteorol. Clim. Obs. Model.*, 137–158.
- Meng, L., and Quiring, S. M. (2008). "A Comparison of Soil Moisture Models Using Soil Climate Analysis Network Observations." *J. Hydrometeorol.*, 9(4), 641–659.
- Merta, M., Seidler, C., Bianchin, S., Heilmeyer, H., and Richert, E. (2008). "Analysis of land use change in the Eastern Erzgebirge regarding both nature protection and flood prevention." *Soil Water Res.*, 3(Special Issue No. 1), S105–S115.
- Micovic, Z., and Quick, M. C. (1999). "A rainfall and snowmelt runoff modelling approach to flow estimation at ungauged sites in British Columbia." *J. Hydrol.*, 226(1–2), 101–120.
- Mishra, A., Kar, S., and Singh, V. P. (2007). "Prioritizing structural management by quantifying the effect of land use and land cover on watershed runoff and sediment yield." *Water Resour. Manag.*, 21(11), 1899–1913.
- Mishra, V., Shah, R., and Thrasher, B. (2014). "Soil Moisture Droughts under the Retrospective and Projected Climate in India*." *J. Hydrometeorol.*, 15(6), 2267–2292.
- Mittelbach, H., and Seneviratne, S. I. (2012). "A new perspective on the spatio-temporal variability of soil moisture: temporal dynamics versus time-invariant contributions." *Hydrol. Earth Syst. Sci.*, 16(7), 2169–2179.
- Mo, T., Choudhury, B. J., Schmutge, T. J., Wang, J. R., and Jackson, T. J. (1982). "A model for microwave emission from vegetation-covered fields." *J. Geophys. Res.*, 87(C13), 11229–11237.
- Mohanty, B. ., and Skaggs, T. . (2001). "Spatio-temporal evolution and time-stable characteristics of soil moisture within remote sensing footprints with varying soil, slope, and vegetation." *Adv. Water Resour.*, 24(9–10), 1051–1067.

- Mohanty, B. P., Skaggs, T. H., and Famiglietti, J. S. (2000). “Analysis and mapping of field-scale soil moisture variability using high-resolution, ground-based data during the Southern Great Plains 1997 (SGP97) Hydrology Experiment.” *Water Resour. Res.*, 36(4), 1023–1031.
- Montenegro, A. A. A., Lopes, I., de Carvalho, A. A., de Lima, J. L. M. P., de Souza, T. E. M. S., Araújo, H. L., Lins, F. A. C., Almeida, T. A. B., and Montenegro, H. G. L. A. (2019). “Spatio Temporal Soil Moisture Dynamics and Runoff under Different Soil Cover Conditions in a Semiarid Representative Basin in Brazil.” *Adv. Geosci.*, 48(2008), 19–30.
- Naha, S., Thakur, P. K., and Aggarwal, S. P. (2016). “Hydrological Modelling and data assimilation of Satellite Snow Cover Area using a Land Surface Model, VIC.” *ISPRS - Int. Arch. Photogramm. Remote Sens. Spat. Inf. Sci.*, XLI-B8, 353–360.
- NASA JPL (2013) NASA Shuttle Radar Topography Mission Global 1 arc-second DEM. NASA LP DAAC. <https://doi.org/10.5067/measures/srtm/srtmg11.003>. Accessed 01 November 2019
- Nash, J. E., and Sutcliffe, J. V. (1970). “River flow forecasting through conceptual models part I - A discussion of principles.” *J. Hydrol.*, 10(3), 282–290.
- Niehoff, D., Fritsch, U., and Bronstert, A. (2002). “Land-use impacts on storm-runoff generation: scenarios of land-use change and simulation of hydrological response in a meso-scale catchment in SW-Germany.” *J. Hydrol.*, 267(1–2), 80–93.
- Nijssen, B., Lettenmaier, D. P., Liang, X., Wetzel, S. W., and Wood, E. F. (1997). “Streamflow simulation for continental-scale river basins.” *Water Resour. Res.*, 33(4), 711–724.
- Nijssen, B., Schnur, R., and Lettenmaier, D. P. (2001). “Global Retrospective Estimation of Soil Moisture Using the Variable Infiltration Capacity Land Surface Model, 1980–93.” *J. Clim.*, 14(8), 1790–1808.
- NRSC (2011) National Land Use and Land Cover Mapping Using Multi-Temporal Awifs

Data.Interim report Seventh Cycle (2010-11).
<http://bhuvannoeda.nrsc.gov.in/gis/thematic/tools/document/LULC250/1011.pdf>.

Accessed 01 November 2019

Open Government Data (OGD) Platform India. <https://data.gov.in/resources/district-wise-season-wise-crop-production-statistics-1997> Accessed 01 November 2019

Pai, D. S., Sridhar, L., Rajeevan, M., Sreejith, O. P., Satbhai, N. S., and Mukhopadhyay, B. (2014). “Development of a new high spatial resolution ($0.25^\circ \times 0.25^\circ$) Long Period (1901-2010) daily gridded rainfall data set over India and its comparison with existing data sets over the region.” *Mausam*, 65(1), 1–18.

Pan, F., and Peters-Lidard, C. D. (2008). “On the Relationship Between Mean and Variance of Soil Moisture Fields 1.” *JAWRA J. Am. Water Resour. Assoc.*, 44(1), 235–242.

Pan, M., and Wood, E. F. (2006). “Data Assimilation for Estimating the Terrestrial Water Budget Using a Constrained Ensemble Kalman Filter.” *J. Hydrometeorol.*, 7(3), 534–547.

Porporato, A., D’Odorco, P., Laio, F., Ridolfi, L., and Rodriguez-Iturbe, I. (2002). “Ecohydrology of water-controlled ecosystems.” *Adv. Water Resour.*, 25, 1335–1348.

Reynolds, C. A., Jackson, T. J., and Rawls, W. J. (2000). “Estimating soil water-holding capacities by linking the Food and Agriculture Organization Soil map of the world with global pedon databases and continuous pedotransfer functions.” *Water Resour. Res.*, 36(12), 3653–3662.

Rivera Villarreyes, C. A., Baroni, G., and Oswald, S. E. (2011). “Integral quantification of seasonal soil moisture changes in farmland by cosmic-ray neutrons.” *Hydrol. Earth Syst. Sci.*, 15(12), 3843–3859.

Robinson, D. A., Jones, S. B., Wraith, J. M., Or, D., and Friedman, S. P. (2003). “A Review of Advances in Dielectric and Electrical Conductivity Measurement in Soils

-
- Using Time Domain Reflectometry.” *Vadose Zo. J.*, 2(4), 444–475.
- Rosnay, P., Balsamo, G., Albergel, C., Muñoz-Sabater, J., and Isaksen, L. (2014). “Initialisation of Land Surface Variables for Numerical Weather Prediction.” *Surv. Geophys.*, 35(3), 607–621.
- Rötzer, K., Montzka, C., Bogena, H., Wagner, W., Kerr, Y. H., Kidd, R., and Vereecken, H. (2014). “Catchment scale validation of SMOS and ASCAT soil moisture products using hydrological modeling and temporal stability analysis.” *J. Hydrol.*, 519, 934–946.
- Rötzer, K., Montzka, C., and Vereecken, H. (2015). “Spatio-temporal variability of global soil moisture products.” *J. Hydrol.*, 522, 187–202.
- Ruhoff, A. L., Paz, A. R., Aragao, L. E. O. C., Mu, Q., Malhi, Y., Collischonn, W., Rocha, H. R., and Running, S. W. (2013). “Assessment of the MODIS global evapotranspiration algorithm using eddy covariance measurements and hydrological modelling in the Rio Grande basin.” *Hydrol. Sci. J.*, 58(8), 1658–1676.
- Sánchez, N., González-Zamora, Á., Piles, M., and Martínez-Fernández, J. (2016). “A New Soil Moisture Agricultural Drought Index (SMADI) Integrating MODIS and SMOS Products: A Case of Study over the Iberian Peninsula.” *Remote Sens.*, 8(4), 287.
- Schilling, K. E., Jha, M. K., Zhang, Y.-K., Gassman, P. W., and Wolter, C. F. (2008). “Impact of land use and land cover change on the water balance of a large agricultural watershed: Historical effects and future directions.” *Water Resour. Res.*, 44(7), 1–12.
- Schneider, K., Huisman, J. A., Breuer, L., Zhao, Y., and Frede, H.-G. (2008). “Temporal stability of soil moisture in various semi-arid steppe ecosystems and its application in remote sensing.” *J. Hydrol.*, 359(1–2), 16–29.
- Seneviratne, S. I., Corti, T., Davin, E. L., Hirschi, M., Jaeger, E. B., Lehner, I., Orlowsky, B., and Teuling, A. J. (2010). “Investigating soil moisture–climate interactions in a

- changing climate: A review.” *Earth-Science Rev.*, 99(3–4), 125–161.
- Shah, R. D., and Mishra, V. (2015). “Development of an Experimental Near-Real-Time Drought Monitor for India*.” *J. Hydrometeorol.*, 16(1), 327–345.
- Sharma, T., Kiran, P. V. S., Singh, T. P., Trivedi, A. V., and Navalgund, R. R. (2001). “Hydrologic response of a watershed to land use changes: A remote sensing and GIS approach.” *Int. J. Remote Sens.*, 22(11), 2095–2108.
- Sheffield, J., Goteti, G., Wen, F., and Wood1, E. F. (2004). “A simulated soil moisture based drought analysis for the United States.” *J. Geophys. Res.*, 109(D24), D24108.
- Sherman, L. K. (1932). Streamflow from rainfall by the unit-graph method. *Engineering News Record*, 108, 501-505.
- Shukla, S., Steinemann, A. C., and Lettenmaier, D. P. (2011). “Drought Monitoring for Washington State: Indicators and Applications.” *J. Hydrometeorol.*, 12(1), 66–83.
- Singh, H. V., Kalin, L., Morrison, A., Srivastava, P., Lockaby, G., and Pan, S. (2015). “Post-validation of SWAT model in a coastal watershed for predicting land use/cover change impacts.” *Hydrol. Res.*, 46(6), 837–853.
- Sivapalan, M., and Woods, R. A. (1995). “Evaluation of the effects of general circulation models’ subgrid variability and patchiness of rainfall and soil moisture on land surface water balance fluxes.” *Hydrol. Process.*, 9(5–6), 697–717.
- Srivastava, A., Rajeevan, M., and Kshirsagar, S. (2009). “Development of a high resolution daily gridded temperature data set (1969 – 2005) for the Indian region.” *Atmos. Sci. Lett.*, 10, 249–254.
- Srivastava, A., Sahoo, B., Raghuwanshi, N. S., and Singh, R. (2017). “Evaluation of Variable-Infiltration Capacity Model and MODIS-Terra Satellite-Derived Grid-Scale Evapotranspiration Estimates in a River Basin with Tropical Monsoon-Type Climatology.” *J. Irrig. Drain. Eng.*, 143(8), 04017028.
- Storck, P., Bowling, L., Wetherbee, P., and Lettenmaier, D. (1998). “Application of a

- GIS-based distributed hydrology model for prediction of forest harvest effects on peak stream flow in the Pacific Northwest.” *Hydrol. Process.*, 12(6), 889–904.
- Topp, G. C., Davis, J. L., and Annan, A. P. (1980). “Electromagnetic determination of soil water content: Measurements in coaxial transmission lines.” *Water Resour. Res.*, 16(3), 574–582.
- Ulaby, F., Moore, R., Fung, A. (1982). *Microwave remote sensing: Active and Passive, 2-Radar Remote Sensing and Surface Scattering and Emission Theory* .
- Vachaud, G., Passerat De Silans, A., Balabanis, P., and Vauclin, M. (1985). “Temporal Stability of Spatially Measured Soil Water Probability Density Function.” *Soil Sci. Soc. Am. J.*, 49(4), 822.
- Variable Infiltration Capacity (VIC) Model, Department of Civil and Environmental Engineering University of Washington Seattle, WA 98195. <https://vic.readthedocs.io/en/master/Overview/ModelOverview/> Accessed 01 November 2019.
- Verbunt, M., Zwaafink, M. G., and Gurtz, J. (2005). “The hydrologic impact of land cover changes and hydropower stations in the Alpine Rhine basin.” *Ecol. Modell.*, 187(1), 71–84.
- Vereecken, H., Huisman, J. A., Bogaen, H., Vanderborght, J., Vrugt, J. A., and Hopmans, J. W. (2008). “On the value of soil moisture measurements in vadose zone hydrology: A review.” *Water Resour. Res.*, 44(4), 1–21.
- Vereecken, H., Huisman, J. A., Pachepsky, Y., Montzka, C., van der Kruk, J., Bogaen, H., Weihermüller, L., Herbst, M., Martinez, G., and Vanderborght, J. (2014). “On the spatio-temporal dynamics of soil moisture at the field scale.” *J. Hydrol.*, 516(July 2015), 76–96.
- Vörösmarty, C. J., McIntyre, P. B., Gessner, M. O., Dudgeon, D., Prusevich, A., Green, P., Glidden, S., Bunn, S. E., Sullivan, C. A., Liermann, C. R., and Davies, P. M. (2010). “Global threats to human water security and river biodiversity.” *Nature*,

467(7315), 555–561.

- Vörösmarty, C. J., Moore, B., Grace, A. L., Gildea, M. P., Melillo, J. M., Peterson, B. J., Rastetter, E. B., and Steudler, P. a. (1989). “Continental scale models of water balance and fluvial transport: An application to South America.” *Global Biogeochem. Cycles*, 3(3), 241–265.
- Wagner, P. D., Bhallamudi, S. M., Narasimhan, B., Kantakumar, L. N., Sudheer, K. P., Kumar, S., Schneider, K., and Fiener, P. (2016). “Dynamic integration of land use changes in a hydrologic assessment of a rapidly developing Indian catchment.” *Sci. Total Environ.*, 539, 153–164.
- Wagner, P. D., Kumar, S., and Schneider, K. (2013). “An assessment of land use change impacts on the water resources of the Mula and Mutha Rivers catchment upstream of Pune, India.” *Hydrol. Earth Syst. Sci.*, 17(6), 2233–2246.
- Wagner, W., Blöschl, G., Pampaloni, P., Calvet, J.-C., Bizzarri, B., Wigneron, J.-P., and Kerr, Y. (2007). “Operational readiness of microwave remote sensing of soil moisture for hydrologic applications.” *Hydrol. Res.*, 38(1), 1–20.
- Wang, G. Q., Zhang, J. Y., Jin, J. L., Pagano, T. C., Calow, R., Bao, Z. X., Liu, C. S., Liu, Y. L., and Yan, X. L. (2012). “Assessing water resources in China using PRECIS projections and a VIC model.” *Hydrol. Earth Syst. Sci.*, 16(1), 231–240.
- Wang, G., Yu, J., Shrestha, S., Ishidaira, H., and Takeuchi, K. (2010). “Application of a distributed erosion model for the assessment of spatial erosion patterns in the Lushi catchment, China.” *Environ. Earth Sci.*, 61(4), 787–797.
- Wang, S., Kang, S., Zhang, L., and Li, F. (2008). “Modelling hydrological response to different land-use and climate change scenarios in the Zamu River basin of northwest China.” *Hydrol. Process.*, 22(14), 2502–2510.
- Wang, T., Wedin, D. A., Franz, T. E., and Hiller, J. (2015). “Effect of vegetation on the temporal stability of soil moisture in grass-stabilized semi-arid sand dunes.” *J. Hydrol.*, 521, 447–459.

- Western, A. W., Zhou, S., Grayson, R. B., McMahon, T. A., Blöschl, G., and Wilson, D. J. (2004). "Spatial correlation of soil moisture in small catchments and its relationship to dominant spatial hydrological processes." *J. Hydrol.*, 286(1–4), 113–134.
- Wigmosta, M. S., Vail, L. W., and Lettenmaier, D. P. (1994). "A distributed hydrology-vegetation model for complex terrain." *Water Resour. Res.*, 30(6), 1665–1679.
- Wilk, J., and Hughes, D. A. (2002). "Simulating the impacts of land-use and climate change on water resource availability for a large south Indian catchment." *Hydrol. Sci. J.*, 47(1), 19–30.
- WMO (1975). Inter comparison of conceptual models used in operational hydrological forecasting. Operational hydrology, Report 7, WMO No 429, Geneva.
- Wood, E. F., Lettenmaier, D. P., and Zartarian, V. G. (1992). "A land-surface hydrology parameterization with subgrid variability for general circulation models." *J. Geophys. Res.*, 97(D3), 2717–2728.
- Wu, Z., Lu, G., Wen, L., Lin, C. A., Zhang, J., and Yang, Y. (2007). "Thirty-five year (1971–2005) simulation of daily soil moisture using the variable infiltration capacity model over China." *Atmosphere-Ocean*, 45(1), 37–45.
- Yang, H., Wang, G., Yang, Y., Xue, B., and Wu, B. (2014). "Assessment of the Impacts of Land Use Changes on Nonpoint Source Pollution Inputs Upstream of the Three Gorges Reservoir." *Sci. World J.*, 2014, 1–15.
- Yin, J., He, F., Jiu Xiong, Y., and Yu Qiu, G. (2017). "Effects of land use/land cover and climate changes on surface runoff in a semi-humid and semi-arid transition zone in northwest China." *Hydrol. Earth Syst. Sci.*, 21(1), 183–196.
- Zhang, X., Zhang, T., Zhou, P., Shao, Y., and Gao, S. (2017). "Validation Analysis of SMAP and AMSR2 Soil Moisture Products over the United States Using Ground-Based Measurements." *Remote Sens.*, 9(2), 104.
- Zhang, Y.-K., and Schilling, K. E. (2006). "Effects of land cover on water table, soil

- moisture, evapotranspiration, and groundwater recharge: A Field observation and analysis.” *J. Hydrol.*, 319(1–4), 328–338.
- Zhao, R., Zuang, Y., Fang, L., Liu, X., and Zhang, Q. (1980). “The Xinanjiang model.” *Hydrol. Forecast. — Prévisions Hydrol.*, (129), 351–356.
- Zhou, J., Fu, B., Gao, G., Lü, N., Lü, Y., and Wang, S. (2015). “Temporal stability of surface soil moisture of different vegetation types in the Loess Plateau of China.” *CATENA*, 128, 1–15.
- Zhou, X., Lin, H., and Zhu, Q. (2007). “Temporal stability of soil moisture spatial variability at two scales and its implication for optimal field monitoring.” *Hydrol. Earth Syst. Sci. Discuss.*, 4(3), 1185–1214.
- Zreda, M., Desilets, D., Ferré, T. P. A., and Scott, R. L. (2008). “Measuring soil moisture content non-invasively at intermediate spatial scale using cosmic-ray neutrons.” *Geophys. Res. Lett.*, 35(21), L21402.

LIST OF PUBLICATIONS

Refereed journals:

- 1) **Mohaideen, M.M.D.,** and Varija, K. (2018). “Improved vegetation parameterization for hydrological model and assessment of land cover change impacts on flow regime of the Upper Bhima basin, India.” *Acta Geophys.* 66:697. doi:10.1007/s11600-018-0161-y
- 2) **Mohaideen, M.M.D.,** Varija, K., Kasiviswanathan K. S. “Impacts of Land Cover Change on Spatio-temporal Variability of Soil Moisture: Modelling and Satellite Observations.” *Journal of Hydrology* (Under review: Manuscript revised)

International conferences:

- 3) **Mohaideen, M.M.D.,** and Varija, K (2018) Understanding the Soil Moisture Variability: Modelling and Satellite Observation, AGU Fall Meeting, Dec 10- 14, Washington, D.C., USA (**Awarded student grant from AGU**).
- 4) **Mohaideen, M.M.D.,** and Varija K. (2018). Evaluation of model and satellitederived estimation of evapotranspiration in a semi-arid catchment, International Conference on Sustainable Water Resources – Innovations and Impacts, 6 - 8 Sep 2018, VIT, Vellore, INDIA
- 5) **Mohaideen, M.M.D.,** and Varija K. (2017). Assessment of LULC and Improved Vegetation parameter for hydrological modelling, International Conference on the Status and Future of the World's Large Rivers, 17 – 21 April, 2017, India Habitat Centre, New Delhi, INDIA

CURRICULAM VITAE

Name : Diwan Mohaideen M M

Date of Birth : 24/03/1990



EDUCATIONAL QUALIFICATIONS

2011 Bachelor of Engineering

Specialization : Civil Engineering

Institution : Noorul Islam College of Engineering,
Nagercoil, Tamil Nadu, INDIA

2014 Master of Engineering

Specialization : Integrated Water Resources Management

Institution : Centre for Water Resources,
College of Engineering Guind,
Anna University, Chennai

2020 Doctor of Philosophy

Specialization : Water Resources Engineering and Management

Institution : National Institute of Technology Karnataka

Date of Registration: 21 July 2014.